AD_____

Award Number: DAMD17-03-1-0363

TITLE: Therapeutic Vascular Targeting and Irradiation:
        Correlation of MRI and Tissue Changes at Cellular and
        Molecular Levels to Optimizing Outcome

PRINCIPAL INVESTIGATOR: Dawen Zhao, M.D., Ph.D.

CONTRACTING ORGANIZATION: University of Texas Southwestern Medical
                           Center
                           Dallas, TX   75390

REPORT DATE: June 2005

TYPE OF REPORT: Annual

PREPARED FOR: U.S. Army Medical Research and Materiel Command
               Fort Detrick, Maryland   21702-5012

DISTRIBUTION STATEMENT: Approved for Public Release;
                        Distribution Unlimited

The views, opinions and/or findings contained in this report are
those of the author(s) and should not be construed as an official
Department of the Army position, policy or decision unless so
designated by other documentation.

REPORT DOCUMENTATION PAGE

1. REPORT DATE (DD-MM-YYYY)	2. REPORT TYPE	3. DATES COVERED (From - To)
01-06-2005	Annual	1 Jun 2004 – 31 May 2005

4. TITLE AND SUBTITLE
Therapeutic Vascular Targeting and Irradiation:

Correlation of MRI and Tissue Changes at Cellular and Molecular Levels to Optimizing Outcome

5a. CONTRACT NUMBER

5b. GRANT NUMBER
DAMD17-03-1-0363

5c. PROGRAM ELEMENT NUMBER

6. AUTHOR(S)
Dawen Zhao, M.D., Ph.D.

E-Mail: dawen.zhao@utsouthwestern.edu

5d. PROJECT NUMBER

5e. TASK NUMBER

5f. WORK UNIT NUMBER

7. PERFORMING ORGANIZATION NAME(S) AND ADDRESS(ES)
University of Texas Southwestern Medical Center
Dallas, TX 75390

8. PERFORMING ORGANIZATION REPORT NUMBER

9. SPONSORING / MONITORING AGENCY NAME(S) AND ADDRESS(ES)
U.S. Army Medical Research and Materiel Command
Fort Detrick, Maryland 21702-5012

10. SPONSOR/MONITOR'S ACRONYM(S)

11. SPONSOR/MONITOR'S REPORT NUMBER(S)

12. DISTRIBUTION / AVAILABILITY STATEMENT
Approved for Public Release; Distribution Unlimited

13. SUPPLEMENTARY NOTES

14. ABSTRACT
Abstract follows.

15. SUBJECT TERMS
Vascular targeting, magnetic resonance imaging (MRI), pO_2, perfusion, irradiation

16. SECURITY CLASSIFICATION OF:			17. LIMITATION OF ABSTRACT	18. NUMBER OF PAGES	19a. NAME OF RESPONSIBLE PERSON
a. REPORT	**b. ABSTRACT**	**c. THIS PAGE**	UU	77	**19b. TELEPHONE NUMBER** (include area code)
U	U	U			

ABSTRACT

Vascular targeting agents (VTA) are new types of anticancer drugs that act on existing tumor vasculature, causing vascular disruption, which ultimately leads to extensive ischemic tumor cell death. One major goal of this project is to assess physiological changes at different time points following VTA in breast tumors. Continuous studies of tumor vascular perfusion and tissue oxygenation by MRI confirmed our previous findings during Year 1. Complementary data during this annum showed that a significant drop in mean tumor pO_2 within 90 min after administration of combretastatin A4 phosphate (CA4P) and a further decrease was observed at 2 h. Intriguingly, the initial changes in pO_2 in central and peripheral regions were parallel, but by 24 h post treatment significant difference was apparent: pO_2 in the periphery improved significantly, while the center remained hypoxic. These data are consistent with DCE (dynamic contrast enhanced) MRI, which revealed a ~70% decrease in perfusion/permeability at 2 h, which recovered fully after 24 h in a thin peripheral region, but not the tumor center. Based on the imaging results, the radiation treatment has been designed and initiated. We believe that quantitative pO_2 measurements are potentially important for optimizing therapeutic combination of CA4P with irradiation.

Table of Contents

Background:

Tumor growth, survival and metastasis depend critically on the development of new blood vessels [1]. Therefore, extensive research has focused on developing strategies to attack tumor vasculature [1,2]. Tubulin binding agents, *e.g.*, combretastatin A-4-phosphate (CA4P) represent one kind of vascular targeting agent (VTA) [3,4]. Promising preclinical studies have shown that such agents selectively cause tumor vascular shutdown and subsequently trigger a cascade of tumor cell death in experimental tumors [4,5]. Although massive necrosis can be induced, tumors usually regrow from a thin viable rim. Thus, a combination of VTAs with additional conventional therapeutic approaches will be required [6,7]. Indeed, several studies involving the combination of the VTAs with irradiation or chemotherapeutic agents have shown enhanced tumor response [8-10]. To better understand the mode of action, and hence, optimize such combinations, *in vivo* imaging approaches have been initiated to monitor physiological changes resulting from VTA administration [11-13]. Dynamic contrast enhanced (DCE) MRI based on the transport properties of gadolinium-DTPA (Gd-DTPA) is the most commonly used imaging approach to study tumor vascular perfusion and permeability [14,15]. For combination with radiotherapy, measurement of tumor oxygen dynamics will be especially important since hypoxia affects radiation response. By applying [19]F *FREDOM* (Fluorocarbon Relaxometry using Echo planar imaging for Dynamic Oxygen Mapping) MRI [16], dynamic tumor oxygenation can be monitored following the treatment with CA4P.

Body:

Continuing from Year 1, tumor physiological changes after CA4P injection have been extensively studied in Year 2. Consistent with previous results of Year 1, DCE MRI showed a ~70% decrease, averaged over a group of 13762NF rat breast tumors (n = 5), in perfusion/permeability (initial area under signal-intensity curve (IAUC)) at 2 h. The IAUC recovered fully after 24 h in a thin peripheral region, but not the tumor center (Fig. 1 and Table 1) [17].
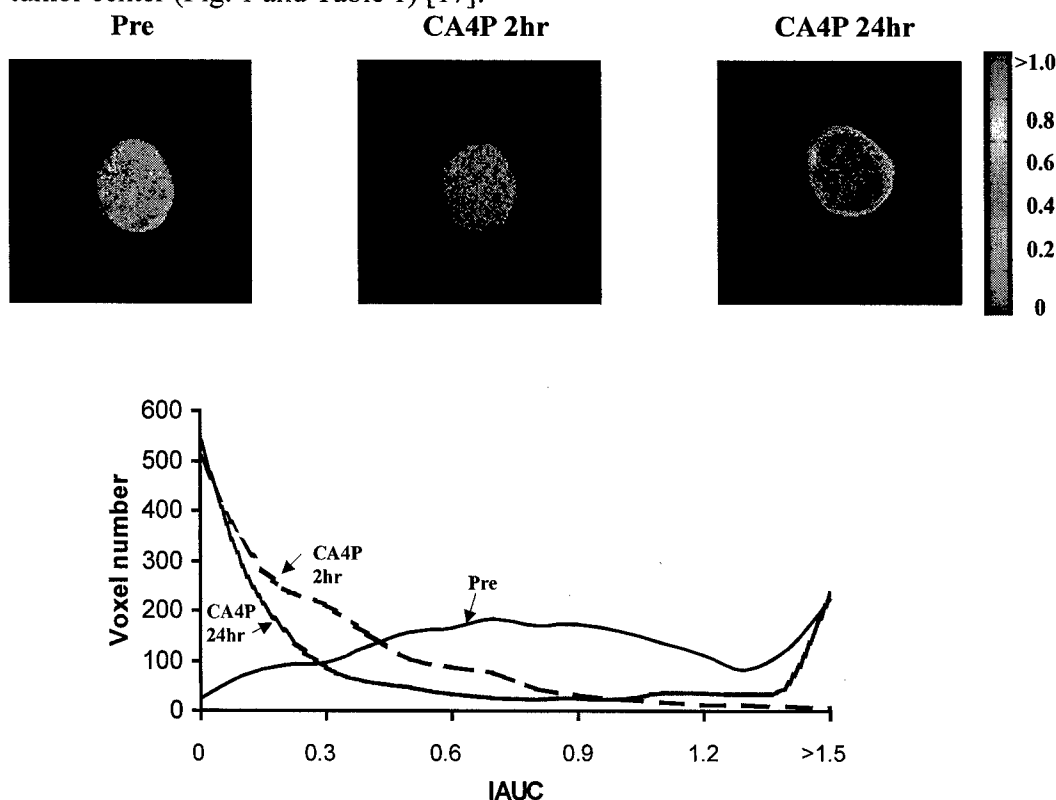

Pre   CA4P 2hr   CA4P 24hr

4

Figure 1. Dynamic contrast enhanced (DCE) MRI with respect to CA4P (30 mg/kg) treatment. A) Normalized T1-weighted contrast enhanced images were acquired 23 s after a bolus injection of contrast agent pre, and 2 h and 24 h after treatment. Significantly less signal enhancement was observed for the whole tumor region 2 h after treatment. A full recovery was apparent in the tumor rim 24 h post-treatment. B) IAUC frequency of DCE MRI on voxel by voxel basis obtained on the same tumor at pre, 2 h and 24 h after CA4P. Compared with pre, curves of 2 h and 24 h after showed a significant increase in the number of voxels with no signal enhancement (typically IAUC < 0.05). However, the frequency of highly enhancing voxels (IAUC > 1.5) at 24 h recovered to the pre-treatment level.

Table 1 Normalized IAUC by dynamic contrast enhanced MRI

Groups		Mean IAUC		
		baseline	2 h	24 h
CA4P (n = 6)	periphery	0.88 ± 0.06	$0.31 \pm 0.08^{*\ddagger}$	0.86 ± 0.06
(30 mg/kg)	center	$0.44 \pm 0.11^{+}$	$0.13 \pm 0.08^{*\ddagger}$	$0.12 \pm 0.05^{*+\ddagger}$
Control (n = 3)	periphery	1.09 ± 0.04	0.93 ± 0.13	0.86 ± 0.05
(saline)	center	$0.52 \pm 0.19^{+}$	$0.46 \pm 0.05^{+}$	$0.44 \pm 0.03^{+}$

IAUC: initial area under signal-intensity curve;

$^{*}p < 0.05$ from baseline; $^{+}p < 0.05$ from periphery; $^{\ddagger}p < 0.05$ from control.

^{19}F *FREDOM* MRI further demonstrated that a significant decrease in the mean pO_2 for the group of 7 tumors was found at 90 min after CA4P (23 ± 5 vs. 9 ± 3 torr; $p < 0.05$) and a further decrease at 2 h (2 ± 2 torr). The mean pO_2 increased to 15 ± 4 torr at 24 h, which was still significantly lower than pretreated baseline ($p < 0.05$). More interestingly, the initial changes in pO_2 in central and peripheral regions were parallel, but by 24 h post treatment significant difference was apparent: pO_2 in the periphery improved significantly, while the center remained hypoxic (Figs. 2 and 3) [17].
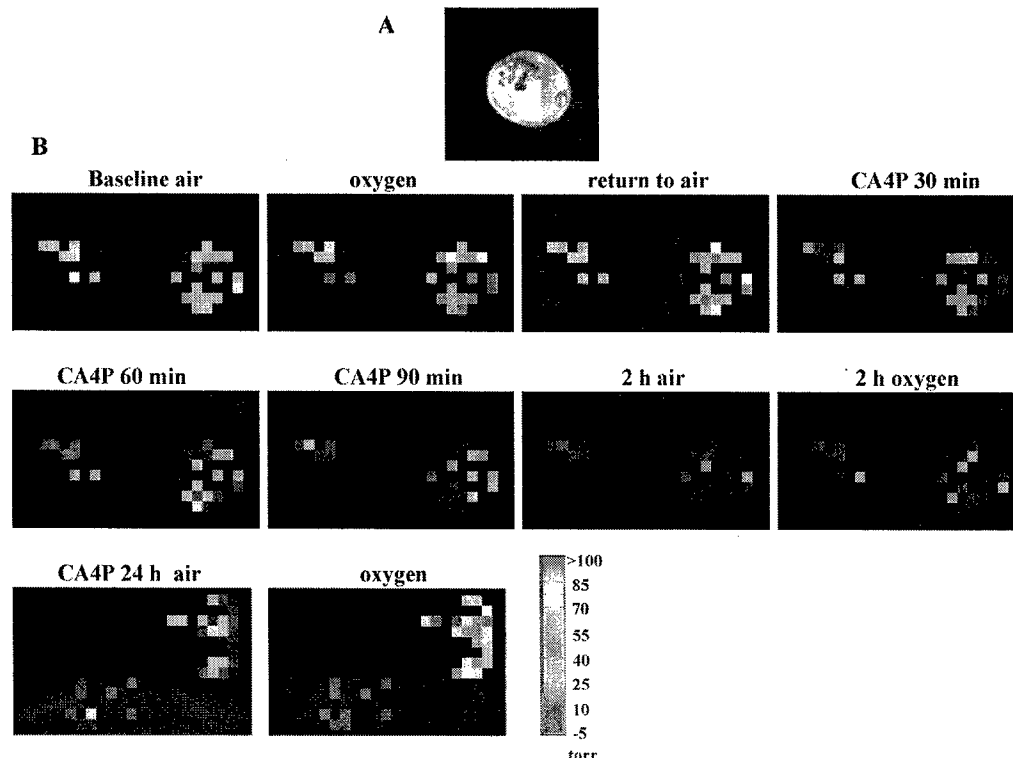

5

Figure 2 A) Distribution of hexafluorobenzene (HFB) in a representative tumor. An overlay of ^{19}F signal density on the anatomic image indicates HFB in both peripheral and central regions. B) pO_2 maps obtained from the same tumor comprise two separated groups of voxels, which correspond to the locations of HFB on the anatomic image. Twenty five individual voxels were traceable from the pretreated baseline to 2 h after CA4P with oxygen breathing. Thirty one voxels could be followed 24 h post-treatment. Significant decrease in pO_2 was evident for all the individual voxels after CA4P, and pO_2 did not respond to oxygen inhalation after 2 h. The 24 h maps showed improved pO_2 and significant response to oxygen breathing in the peripheral region (right), but not in the central region (left).
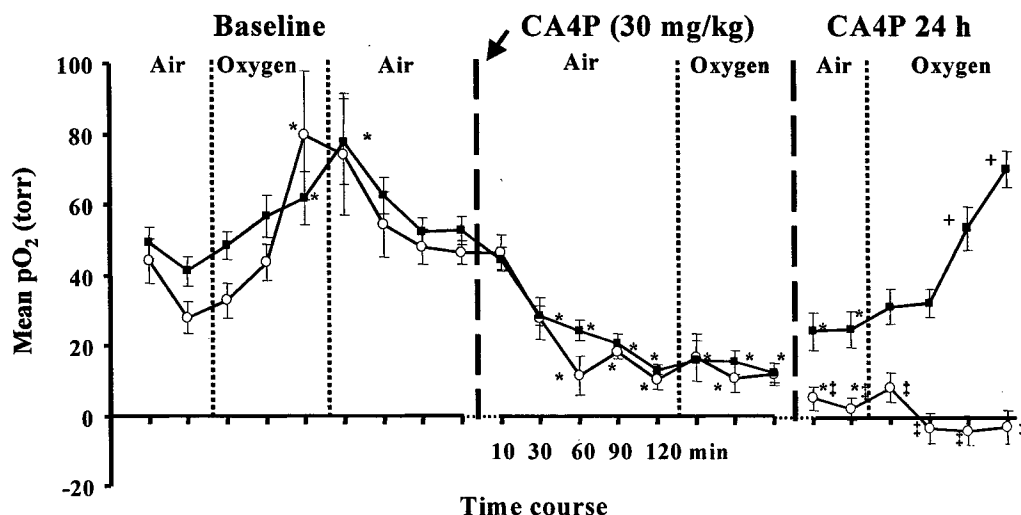

Figure 3 Mean pO_2 curves are shown for the peripheral (■) and central (○) voxels of the tumor shown in Fig. 2. Significant decrease in pO_2 was found as early as 30 min after CA4P (30 mg/kg) for both peripheral and central tumor. * $p < 0.05$ from baseline air, + $p <0.05$ from 24 h air, ‡ $p < 0.05$ from periphery.

As a normal tissue control, pO_2 in femoral muscle was also monitored before and after injection of CA4P. Unlike the tumor behavior, normal muscle showed no decreased pO_2 at any time points after CA4P (Table 2) [17,18]. These results suggest that the vascular targeting agent, CA4P selectively attack the tumor blood vessels with little effect on normal vasculature.

Table 2 Tumor oxygen dynamics assessed by ^{19}F MRI with respect to CA4P treatment

Groups		no. animals	pO_2 (mean ± se torr)						
			Time course						
			baseline	60 min	90 min	2 h	oxygen	24 h base	oxygen
Breast tumor	CA4P (30 mg/kg)	7	23 ± 5	13 ± 5	$9 \pm 3^*$	$2 \pm 2^*$	$5 \pm 3^*$	15 ± 4	$58 \pm 11^+$
	Saline (0.25 ml)	3	31 ± 10	38 ± 16	36 ± 16	35 ± 14	$79 \pm 23^*$	39 ± 15	$108 \pm 26^+$
Normal muscle	CA4P (30 mg/kg)	3	24 ± 1	25 ± 8	25 ± 7	24 ± 5	$79 \pm 18^*$	NA	NA

*$p < 0.05$ from baseline; + $p < 0.05$ from 24 h air (24 h after injection of CA4P); NA: no measurement.

I have also performed extensive studies on tumor blood vessels, perfusion, and hypoxia in the 13762 rat breast tumors. Immunohistochemical studies of tumor hypoxia and vasculature using hypoxic marker pimonidazole and endothelium marker CD31 showed that a higher microvascular density (MVD) and lower labeling index of pimonidazole (Figs 4 and 5).
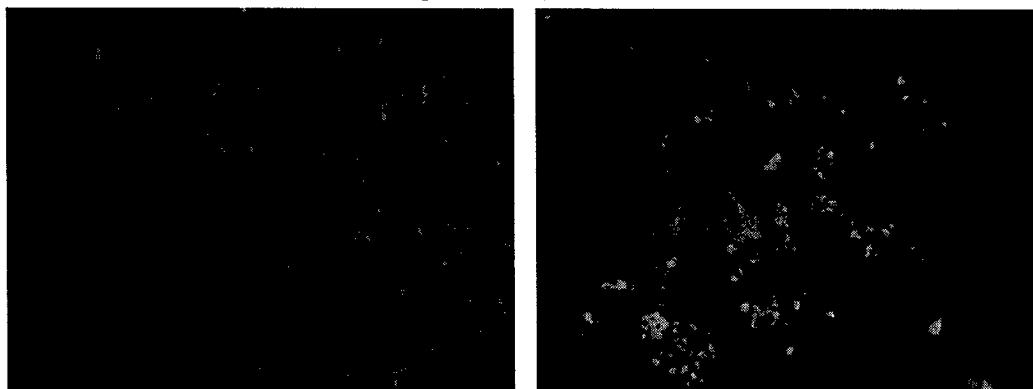

Figure 4 Comparison of pimonidazole and CD31 in a representative tumor. Fluorescent immunostaing for CD31 (left, red) and hypoxia (pimonidazole; right, green) indicated extensive vasculature and disperse hypoxic regions.

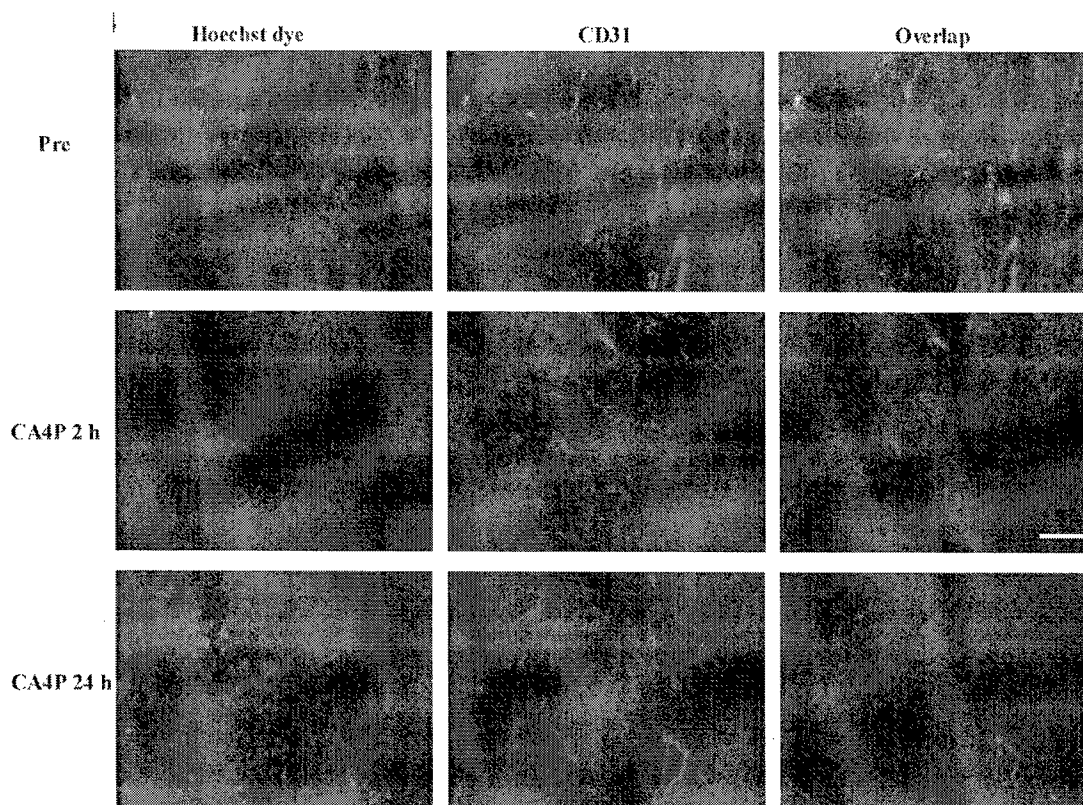**Figure 5** Perfusion marker Hoechst staining pre, 2 h, and 24 h post CA4P (left). Vascular endothelium of the same field was immunostained by anti-CD31 (red, middle). A good match (right) between Hoechst and anti-CD31 stained vascular endothelium was found in the pretreated tumor. Two hours after treatment, significant reduction in perfused vessels was detected, followed by a recovery at 24 h point. Bar = 100 μm.

As proposed time frame, the Task 1 in the Statement of Work is complete. One peer-review paper based on MRI and histological studies of the vascular targeting agent has been published [17].

In accordance with the Statement of Work Task 2, experimental radiation therapy has been designed and initiated based on the MRI oximetry data. Preliminary data of control group (n = 6) and irradiation alone group (n = 6) showed a single dose of 10 Gy significantly inhibited tumor growth (Fig. 6). Studies of combination of radiation and CA4P are underway.
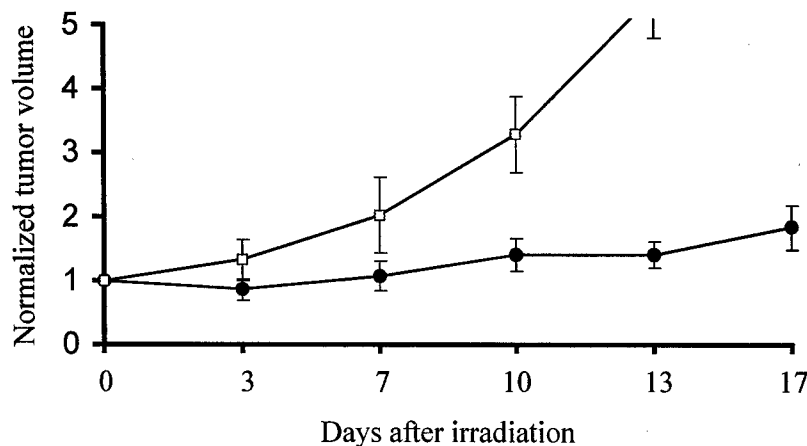

Figure 6. Tumor growth was significantly delayed by a single dose of 10 Gy radiation (●) compared to control tumors (□).

By collaborating with Drs. Hanli Liu and Ralph Mason (Co-investigator), non-invasive interrogation of breast tumor response to CA4P has also been performed using Near-Infrared Spectroscopy (NIRS) and Bioluminescent imaging (BLI) [19]. Consistent and complementary results have been acquired from these studies (Figs. 7 and 8).
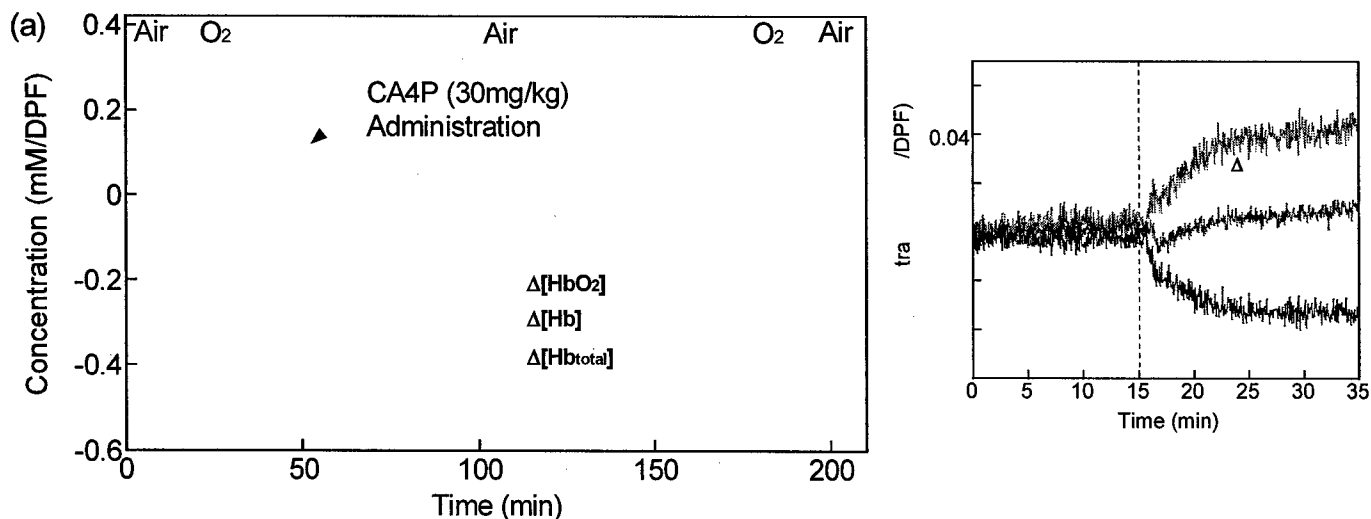
Figure 7 Qualitative NIRS detection of tumor hemodynamic changes before, 2 h (a) and 24 h (b) after CA4P (30 mg/kg; i.p.) administration. Significant decrease in concentration of both oxygenated [HbO$_2$]and total hemoglobin ([Hb]$_{total}$; blood volume) was observed immediately after CA4P. In contrast to pretreated baseline study, there was no response to oxygen inhalation 2 h after treatment. Twenty four hours later, significant increase in [HbO$_2$] was found in response to oxygen, but the extent of increase was about 6 times lower than baseline level.

8

Figure 8 Application of BLI in human breast tumor xenograft. A nude mouse with MDA-MB-231-luc mammary tumor was monitored temporally before and after treatment with the vascular targeting agent combretastatin (CA4P). Significant reduction in signal intensity was observed 2 h after CA4P (Right), compared to pre-treatment (Left).

Based on the above results, one peer reviewed paper, one paper of book section and two abstracts of conference proceeding have been published during this annum. Several other manuscripts are being prepared.
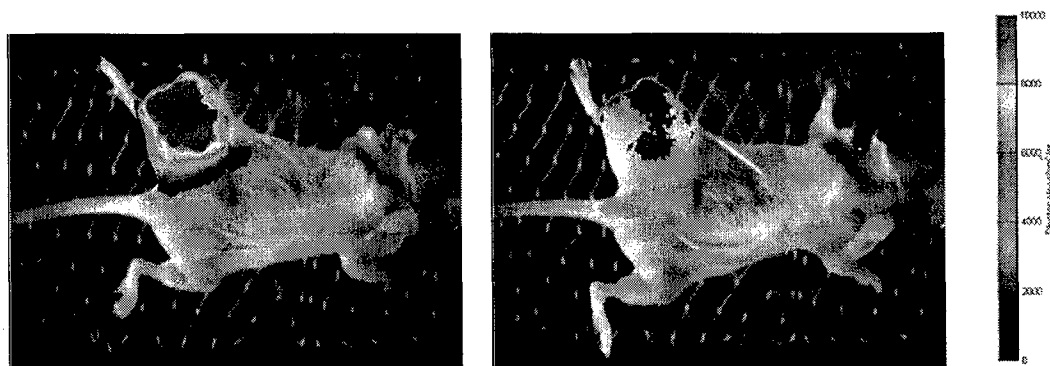
Key Research Accomplishments

- **Assessment of dynamic perfusion and oxygenation in the breast tumors in response to the vascular targeting agent, Combretastatin A4 phosphate, by** *in vivo* **MR approaches**

a. ^{1}H DCE MRI showed significant reduction in tumor perfusion and permeability 2 h after administration of CA4P (30 mg/kg, i.p.), while recovery was found in tumor periphery but not center.

b. ^{19}F *FREDOM* MRI revealed that tumor pO_2 dropped significantly at 90 min and further decreased at 2 h after CA4P.

c. Tumor pO_2 improved 24 h later, but it was still significantly lower than the pretreated baseline pO_2. With respect to oxygen breathing, pO_2 in the periphery improved significantly, while the center remained hypoxic pure oxygen inhalation at this time point.

- **Correlation of MR findings with biological studies**

a. Immunohistochemical studies of tumor hypoxia and vasculature using hypoxic marker pimonidazole and endothelium marker CD31.

b. Consistent with MRI findings, histological study of tumor perfusion using Hoechst dye 33342 showed a significant reduction in perfused vessels at 2hr after CA4P, which recovered 24 h later.

- **Experimental radiation therapy**

a. Irradiation alone on tumor growth has been accomplished.

- **Complementary studies using other non-invasive techniques**

a. Near-Infrared Spectroscopy (NIRS) and Bioluminescent imaging (BLI) approaches have been applied for assessment of tumor response to the vascular targeting agent CA4P. The data is consistent with MRI observation.

<u>**Reportable Outcomes**</u>

Reportable outcomes that have resulted from this research endeavor in this annual period include:

- **Peer Reviewed Publications:**
1. **Zhao, D.**, Jiang, L., Hahn, E.W., and Mason, R.P. Tumor physiological response to combretastatin A4 phosphate assessed by MRI. *Int. J. Radiat. Oncol. Biol. Phys.* 62, 872-80, 2005.

- **Sections of Edited Books:**
1. Kim, J. G., **Zhao, D.**, Mason, R. P., Liu H. Chemotherapeutic (cyclophosphamide) effects on rat breast tumor hemodynamics monitored by multi-channel NIRS. *SPIE*, 5693, 282-92, 2005.

- **Abstracts (Published Conference Proceedings):**
1. **Zhao, D.**, Jiang, L., Adam, A., Hahn, E.W., and Mason, R.P. Tumor physiological response to antivascular agent combretastatin A4 phosphate assessed by magnetic resonance imaging. *96th AACR*, #3799, Anaheim, CA, Apr 2005.
2. **Zhao, D.**, Jiang, L., Adam, A., Hahn, E.W., and Mason, R.P. *In vivo* MRI monitoring of breast tumor response to the vascular targeting agent combretastatin A4 phosphate. Era of Hope Meeting, P67-24, Phaladephia, PA, June 2005.

- **Manuscripts in preparation:**
Peer reviewed papers:
1. **Zhao, D.**, Jiang, L., Hahn, E.W., and Mason, R.P. Evaluation of breast tumor microcirculation and oxygenation using a combination of BOLD, DCE and ^{19}F MRI. *Magn. Reson. Med.*
2. **Zhao, D.**, Harper, A., Richer, E., Liu, Li., Slavine, N., Shay, J. W., Antich, P. P., Mason, R. P. Novel application of bioluminescent imaging: Interrogating acute effects of the vascular targeting agent combretastatin.

- **Employment or research opportunity:**

  Ya Ren, an experienced research technician, has been recently recruited as a Research Assistant by our department. Mrs. Ren will contribute 40% of her effort to this project.

Conclusion:

Results reported here were successful in accordance with the outlined tasks cited in the original proposed statement of work. Five publications have been achieved during the Year 2. More importantly, these results lay foundation for the undergoing combination treatment of vascular targeting agent with irradiation in terms of order and timing. I am confident that the proposed radiation study will be fulfilled by the next term.

References:

[1]   Folkman J (1972). Anti-angiogenesis: new concept for therapy of solid tumors. *Ann Surg* **175,** 409-416.

[2]   Denekamp J (1990). Vascular attack as a therapeutic strategy for cancer. *Cancer Metastasis Rev* **9,** 267-282.

[3]   Pettit GR, Temple C, Jr., Narayanan VL, Varma R, Simpson MJ, Boyd MR, Rener GA and Bansal N (1995). Antineoplastic agents 322. synthesis of combretastatin A-4 prodrugs. *Anticancer Drug Des* **10,** 299-309.

[4]   Davis PD, Dougherty GJ, Blakey DC, Galbraith SM, Tozer GM, Holder AL, Naylor MA, Nolan J, Stratford MR, Chaplin DJ and Hill SA (2002). ZD6126: a novel vascular-targeting agent that causes selective destruction of tumor vasculature. *Cancer Res* **62,** 7247-7253.

[5]   Dark GG, Hill SA, Prise VE, Tozer GM, Pettit GR and Chaplin DJ (1997). Combretastatin A-4, an agent that displays potent and selective toxicity toward tumor vasculature. *Cancer Res* **57,** 1829-1834.

[6]   Siemann DW, Warrington KH and Horsman MR (2000). Targeting tumor blood vessels: an adjuvant strategy for radiation therapy. *Radiother Oncol* **57,** 5-12.

[7]   Thorpe PE, Chaplin DJ and Blakey DC (2003). The first international conference on vascular targeting: meeting overview. *Cancer Res* **63,** 1144-1147.

[8]   Siemann DW and Rojiani AM (2002). Enhancement of radiation therapy by the novel vascular targeting agent ZD6126. *Int J Radiat Oncol Biol Phys* **53,** 164-171.

[9]   Murata R, Siemann DW, Overgaard J and Horsman MR (2001). Interaction between combretastatin A-4 disodium phosphate and radiation in murine tumors. *Radiother Oncol* **60,** 155-161.

[10]   Siemann DW and Rojiani AM (2002). Antitumor efficacy of conventional anticancer drugs is enhanced by the vascular targeting agent ZD6126. *Int J Radiat Oncol Biol Phys* **54,** 1512-1517.

[11]   Tozer GM, Prise VE, Wilson J, Locke RJ, Vojnovic B, Stratford MR, Dennis MF and Chaplin DJ (1999). Combretastatin A-4 phosphate as a tumor vascular-targeting agent: early effects in tumors and normal tissues. *Cancer Res* **59,** 1626-1634.

[12]   Kragh M, Quistorff B, Horsman MR and Kristjansen PE (2002). Acute effects of vascular modifying agents in solid tumors assessed by noninvasive laser Doppler flowmetry and near infrared spectroscopy. *Neoplasia* **4,** 263-267.

[13]   Goertz DE, Yu JL, Kerbel RS, Burns PN and Foster FS (2002). High-frequency Doppler ultrasound monitors the effects of antivascular therapy on tumor blood flow. *Cancer Res* **62,** 6371-6375.

[14]   Rustin GJ, Galbraith SM, Anderson H, Stratford M, Folkes LK, Sena L, Gumbrell L and Price PM (2003). Phase I clinical trial of weekly combretastatin A4 phosphate: clinical and pharmacokinetic results. *J Clin Oncol* **21,** 2815-2822.

[15]   Galbraith SM, Maxwell RJ, Lodge MA, Tozer GM, Wilson J, Taylor NJ, Stirling JJ, Sena L, Padhani AR and Rustin GJ (2003). Combretastatin A4 phosphate has tumor antivascular activity in rat and man as demonstrated by dynamic magnetic resonance imaging. *J Clin Oncol* **21,** 2831-2842.

[16]   Zhao D, Jiang L and Mason RP (2004). Measuring changes in tumor oxygenation. *Methods Enzymol* **386,** 378-418.

[17]   Zhao D, Jiang L, Hahn EW and Mason RP (2005). Tumor physiological response to combretastatin A4 phosphate assessed by MRI. *Int. J. Radiat. Oncol. Biol. Phys.* **62,** 872-880.

[18]   Zhao D, Jiang L, Adam A, Hahn EW and Mason RP (2005). In vivo MRI monitoring of breast tumor response to the vascular targeting agent combretastatin A4 phosphate. In Era of Hope, Phaladephia, PA.

11

[19]   Kim JG, Zhao D, Mason RP and H. Liu (2005). Application of near infrared spectroscopy to detect early effects of cancer therapy. In Era of Hope, Philadelphia, PA.

Appendices

List of publication enclosed:

1. **Zhao, D.**, Jiang, L., and Mason, R.P. Measuring changes in tumor oxygenation. *Methods Enzymol.* 386, 378-418, 2004. (scanned version attached last year)
2. **Zhao, D.**, Jiang, L., Hahn, E.W., and Mason, R.P. Tumor physiological response to combretastatin A4 phosphate assessed by MRI. *Int. J. Radiat. Oncol. Biol. Phys.* 62, 872-80, 2005.
3. Kim, J. G., **Zhao, D.**, Mason, R. P., Liu H. Chemotherapeutic (cyclophosphamide) effects on rat breast tumor hemodynamics monitored by multi-channel NIRS. *SPIE*, 5693, 282-92, 2005.
4. **Zhao, D.**, Jiang, L., Adam, A., Hahn, E.W., and Mason, R.P. Tumor physiological response to antivascular agent combretastatin A4 phosphate assessed by magnetic resonance imaging. *96th AACR*, #3799, Anaheim, CA, Apr 2005.
5. **Zhao, D.**, Jiang, L., Adam, A., Hahn, E.W., and Mason, R.P. *In vivo* MRI monitoring of breast tumor response to the vascular targeting agent combretastatin A4 phosphate. Era of Hope Meeting, P67-24, Phaladephia, PA, June 2005.

results exhibit a linear correlation between ΔHbO and ΔpO_2 of the tumors under hyperoxic gas intervention, suggesting that the NIRS approach could have a good potential value in the clinic. Finally, the newly developed tumor hemodynamic model allows us to reveal tumor heterogeneities at different tumor locations based on the multichannel NIRS results. Through this chapter, we lay a foundation for an NIR imaging technique to be further developed to facilitate investigations of tumor heterogeneity and vascular perfusion. Such a noninvasive imaging approach can enhance our understanding of the dynamics of tumor oxygenation and the mechanism of tumor physiology under baseline and perturbed conditions.

Acknowledgments

[18] Measuring Changes in Tumor Oxygenation

By Dawen Zhao, Lan Jiang, and Ralph P. Mason

Introduction

Significance of pO_2 in Oncology

It has long been appreciated that hypoxic tumor cells are more resistant to radiotherapy.[1] Indeed, a 3-fold increase in radio resistance may occur when cells are irradiated under hypoxic conditions compared with oxygen pressure $pO_2 > 15$ torr for a given single radiation dose. However, recent modeling has indicated that the proportion of cells in the range 0–20 torr may be most significant in terms of surviving a course of fractionated radiotherapy.[2] Certain chemotherapeutic drugs also present differential efficacy, depending on hypoxia.[3,4] Increasingly, there is evidence that hypoxia also

[1] L. Gray, A. Conger *et al.*, *Br. J. Radiol.* **26,** 638 (1953).
[2] B. G. Wouters and J. M. Brown, *Radiat. Res.* **147,** 514 (1997).
[3] B. Teicher, J. Lazo *et al.*, *Cancer Res.* **41,** 73 (1981).
[4] A. C. Sartorelli, *Cancer Res.* **48,** 775 (1988).

influences such critical characteristics as angiogenesis, tumor invasion, and metastasis.[5–8] Moreover, repeated bouts of intermittent hypoxic stress may be important in stimulating tumor progression.[9] Thus the ability to measure pO_2 noninvasively and repeatedly, with respect to acute or chronic interventions, becomes increasingly important.

Early work examined cells *in vitro*, where ambient oxygen concentrations are readily controlled. *In vivo*, hypoxia may be achieved by clamping the blood supply to a tumor,[10] but other levels of oxygenation reflect the interplay of supply and consumption.[11,12] Robust fine-needle polarographic electrodes opened the possibility of measuring pO_2 in tumors *in situ* and *in vivo* to define local pO_2 under baseline conditions or with respect to interventions. In early work, Cater and Silver[13] showed the ability to monitor pO_2 at individual locations in patients' tumors with respect to breathing oxygen. Later, Gatenby *et al.*[14] showed that pO_2 in a tumor was correlated with clinical outcome. Tumor oximetry received its greatest boost with the development of the Eppendorf Histograph polarographic needle electrode system.[15] This computer-controlled device equipped with a stepper motor can reveal distributions of tumor oxygenation and has been applied extensively to clinical trials. Many reports have now shown that tumors are highly heterogeneous and have extensive hypoxia; furthermore, strong correlations have been shown in cervix and head and neck tumors between median pO_2 or hypoxic fraction and survival or disease-free survival.[5,16–20] Extensive hypoxia also has been found in tumors of the prostate and breast.[21–23] Thus tumor oxygenation is now recognized as a strong

[5] E. K. Rofstad, K. Sundfor *et al.*, *Br. J. Cancer* **83**, 354 (2000).

[6] K. De Jaeger, M. C. Kavanagh *et al.*, *Br. J. Cancer* **84**, 1280 (2001).

[7] M. Höckel and P. Vaupel, *J. Natl. Cancer Inst.* **93**, 266 (2001).

[8] H. J. Knowles and A. L. Harris, *Breast Cancer Res.* **3**, 318 (2001).

[9] R. A. Cairns, T. Kalliomaki *et al.*, *Cancer Res.* **61**, 8903 (2001).

[10] J. Moulder and S. Rockwell, *Int. J. Radiat. Oncol. Biol. Phys.* **10**, 695 (1984).

[11] T. W. Secomb, R. Hsu *et al.*, *Adv. Exp. Med. Biol.* **454**, 629 (1998).

[12] M. W. Dewhirst, B. Klitzman *et al.*, *Int. J. Cancer* **90**, 237 (2000).

[13] D. Cater and I. Silver, *Acta Radiol.* **53**, 233 (1960).

[14] R. A. Gatenby, H. B. Kessler *et al.*, *Int. J. Radiat. Oncol. Biol. Phys.* **14**, 831 (1988).

[15] M. Nozue, I. Lee *et al.*, *J. Surg. Oncol.* **66**, 30 (1997).

[16] D. M. Brizel, S. P. Scully *et al.*, *Cancer Res.* **56**, 941 (1996).

[17] M. Höckel, K. Schlenger *et al.*, *Cancer Res.* **56**, 4509 (1996).

[18] M. Nordsmark, M. Overgaard *et al.*, *Radiother. Oncol.* **41**, 31 (1996).

[19] A. W. Fyles, M. Milosevic *et al.*, *Radiother. Oncol.* **48**, 149 (1998).

[20] T. H. Knocke, H. D. Weitmann *et al.*, *Radiother. Oncol.* **53**, 99 (1999).

[21] P. W. Vaupel, K. Schlenger *et al.*, *Cancer Res.* **51**, 3316 (1991).

[22] P. Hohenberger, C. Felger *et al.*, *Breast Cancer Res. Treat.* **48**, 97 (1998).

[23] B. Movsas, J. D. Chapman *et al.*, *Urology* **53**, 11 (1999).

prognostic indicator, and this device has laid a convincing foundation for the value of measuring pO_2 in patients. However, the Histograph is highly invasive, and it is not possible to make repeated measurements at individual locations, precluding dynamic studies to assess the influence of interventions on tumor pO_2.

Given that hypoxic tumors are more resistant to certain therapies, it becomes important to assess tumor oxygenation as part of therapeutic planning. Patients could be stratified according to baseline hypoxia to receive adjuvant interventions designed to modulate pO_2, or more intense therapy as facilitated by intensity modulated radiation therapy (IMRT). Tumors, which do not respond to interventions, may be ideal candidates for hypoxia-selective cytotoxins (e.g., tirapazamine[24]). Noting that any therapy and intervention may have side effects or simply add to clinical costs, it is vital that efficacy be established and therapy be optimized for an individual patient. Whether initially hypoxic regions of a tumor can be modified to become better oxygenated has long been considered a key to improving outcome of irradiation. However, many attempts to improve therapeutic outcome by manipulation of tumor oxygenation have shown only modest success in the clinic,[25] and it is thought that lack of success may have resulted from inability to identify those patients who would benefit from adjuvant interventions.

Although pO_2 determinations could be of great clinical value, they are also vital to many laboratory investigations of new drugs and studies of tumor development. Given the potential importance of measuring pO_2, many diverse techniques have been developed, as reviewed by others previously,[26-29] and here, in the next section.

Methods of Measuring Tumor Oxygenation

Table I lists various techniques that have been reported to provide quantitative estimates of pO_2. Historically, polarographic needle oxygen electrodes have been considered a "gold standard," and they have been applied in the clinic since the 1950s. One or more electrodes may be placed in a tumor, facilitating measurement of baseline pO_2 and dynamic response to

---

[24] J. M. Brown, *Mol. Med. Today* **6**, 157 (2000).

[25] J. Overgaard and M. R. Horsman, *Semin. Radiat. Oncol.* **6**, 10 (1996).

[26] H. B. Stone, J. M. Brown *et al.*, *Radiat. Res.* **136**, 422 (1993).

[27] R. P. Mason, S. Ran *et al.*, *J. Cell. Biochem.* **87S**, (2002).

[28] H. M. Swartz, *Biochem. Soc. Trans.* **30**, 248 (2002).

[29] H. M. Swartz and J. F. Dunn, *in* "Oxygen Transport to Tissue XXIV" (J. F. Dunn and H. M. Swartz, eds.), Vol. 530, p. 1. Kluwer Academic, New York, 2003.

interventions.[13,30–32] Initially, the focus was on generating finer needles, which would be less invasive, and tips as fine as a few microns have been applied to animal tissues.[33] However, such needles are progressively brittle and generate such small current that stray electromagnetic fields can interfere. Stationary electrodes sample limited volumes, and recognizing tumor heterogeneity, the Eppendorf Histograph was developed to generate multiple measurements along tracks in tumors.[15,34,35] Following extensive studies in animals, the Histograph has found widespread application in the clinical setting and has unequivocally revealed hypoxia in many tumor types, for example, head and neck,[36,37] cervix,[19,38] breast,[21,22] and prostate.[23] Moreover, pO_2 distributions have been found to have prognostic value. Disease-free survival is significantly worse for patients with hypoxic tumors, though the optimal prognostic parameter has variously been median pO_2 or percent measurements <5 torr (HF_5).

Although the Eppendorf Histograph uses a large invasive needle (size = 26 G or about 0.35 mm), it has provided great impetus for further investigations. One aspect is the application of less invasive probes. Fiber-optic probes are typically finer and do not consume oxygen during measurement. Typically, only two or four locations are sampled simultaneously, but as with the earlier electrodes, these optical probes facilitate observation of dynamic changes in pO_2 in response to interventions.[39–43] Both the current commercial systems, the OxyLite (http://www.oxford-optronix.com/tissmon/oxylite/oxylite.htm) and FOXY (http://www.oceanoptics.com/Products/foxyfaqs.asp), exploit the fluorescent quenching by oxygen of a ruthenium complex coating. OxyLite measures fluorescent lifetime, whereas FOXY uses a simple intensity integration and is correspondingly much cheaper. Fibers are fragile, and coatings have a limited lifetime.

[30] N. Evans and P. Naylor, Br. J. Radiol. 36, 418 (1963).
[31] C. Song, I. Lee et al., Cancer Res. 47, 442 (1987).
[32] D. Zhao, A. Constantinescu et al., Int. J. Radiat. Oncol. Biol. Phys. 53, 744 (2002).
[33] D. W. Crawford and M. A. Cole, J. Appl. Physiol. 58, 1400 (1985).
[34] F. Kallinowski, R. Zander et al., Int. J. Radiat. Oncol. Biol. Phys. 19, 953 (1990).
[35] P. W. Vaupel, D. K. Kelleher, and M. Günderoth, "Tumor Oxygenation." Gustav Fischer Verlag, Stuttgart, Germany, 1995.
[36] D. M. Brizel, G. S. Sibly et al., Int. J. Radiat. Oncol. Biol. Phys. 38, 285 (1997).
[37] V. Rudat, B. Vanselow et al., Radiother. Oncol. 57, 31 (2000).
[38] C. Aquino-Parsons, A. Green et al., Radiother. Oncol. 57, 45 (2000).
[39] J. R. Griffiths, Br. J. Radiol. 72, 627 (1999).
[40] J. Bussink, J. H. A. M. Kaanders et al., Radiat. Res. 154, 547 (2000).
[41] R. D. Braun, J. L. Lanzen et al., Am. J. Physiol. Heart Circ. Physiol. 280, H2533 (2001).
[42] D. Zhao, A. Constantinescu et al., Am. J. Clin. Oncol. 24, 462 (2001).
[43] Y. Gu, V. Bourke et al., Appl. Opt. 42, 1 (2003).

TABLE I
TUMOR OXIMETRY METHODS

Technique	Reporter	Parameter measured	Invasiveness	Characteristic resolution		References
				Spatial	Temporal	
FREDOM	HFB	R_1	Minimal 32-G needle	Map multiple locations each 8 mm³	6.5 min	Hunjan, Zhao et al.[159]; Zhao, Constantinescu et al.[134]; Song, Constantinescu et al.[135]; Zhao, Constantinescu et al.[32]; Kim, Zhao et al.[106]; Zhao, Constantinescu et al.[136]; Zhao, Ran et al.[137]
¹⁹F MRI	PFC	R_1	IV	Perfused regions	min	Hees and Sotak[153]; Dardzinski and Sotak[117]; McIntyre, McCoy et al.[158]; Fan, River et al.[95]; Wang, Su et al.[88]
¹⁹F MRS	PFC	R_1	IV	Perfused regions	s to min	Hees and Sotak[153]; Mason, Antich et al.[154]; Baldwin and Ng[156]; McIntyre, McCoy et al.[158]; van der Sanden, Heerschap et al.[138]
DCE MRI	Gd-DTPA	Contrast kinetics	IV	Maps	min	Cooper, Carrington et al.[87]; Lyng, Vorren et al.[a]; Wang, Su et al.[88]
ESR/EPR	Charcoal, phthalocyanine	Linewidth	Needle	Single location 23 G IT	seconds	O'Hara, Goda et al.[b]; Goda, Bacic et al.[c]; O'Hara, Goda et al.[59]; Gallez, Jordan et al.[d]

						References
ESR/EPR	Nitroxides	Linewidth	IV	Global or map	s to min	Jordan, Misson et al.[48]; He, Beghein et al.[49]; Jiang, Beghei et al.[50]; O'Hara, Blumenthal et al.[e]; Baudelet and Gallez[94]; Dunn, O'Hara et al.[f]; Jordan, Gregoire et al.[52]; Mahy, De Bast et al.[55]
OMRI	Free radical	Overhauser enhancement	IV	mm³ maps	10 min	Elas, Williams et al.[53]; Krishna, English et al.[60]
Needle electrode	Oxygen	Current	Needle 26 G IT	Single location	~1 s	Cater and Silver[13]; Evans and Naylor[30]; Hasegawa, Rhee et al.[g]; Gatenby, Kessler et al.[14]; Song, Shakil et al.[h]; Zhao, Constantinescu et al.[32]
(Histograph)	Oxygen	Current	Needle 26 G IT	Multiple tracks	1 s per location	Eble, Wenz et al.[i]; Falk, Laurence et al.[j]; Vaupel, Kelleher et al.[35]; Brizel, Scully et al.[16]; Höckel, Schlenger et al.[k]; Nozue, Lee et al.[15]; Fyles, Milosevic et al.[19]; Siemann, Johansen et al.[l]; Mason, Constantinescu et al.[175]; Aquino-Parsons, Green et al.[38]; Jenkins, Evans et al.[75]; Höckel and Vaupel[7]

(continued)

TABLE I (continued)

Technique	Reporter	Parameter measured	Invasiveness	Characteristic resolution		References
				Spatial	Temporal	
Optical probe (OxyLite, FOXY)	Rh complex	Fluorescent lifetime	Needle (26 G)	2–4 locations	Real time	Griffiths[39]; Bussink, Kaanders et al.[40]; Braun, Lanzen et al.[41]; Zhao, Constantinescu et al.[134]; Gu, Bourke et al.[43]; Jordan, Beghein et al.[54]
Phosphorescence	PD complex	Lifetime	IV	Maps	<1 min	Wilson[m]; Vinogradov, Lo et al.[n]; Dewhirst, Ong et al.[o]; Wilson, Vinogradov et al.[63]; Erickson, Braun et al.[p]
Fluorescence	EF5	Fluorescent intensity	IV + biopsy	Maps microscopic	Once	Koch[79]
Mass spectrometry	Oxygen	Atoms	Needle	Single location		Potapov, Sirovskii et al.[q]

[a] H. Lyng, A. O. Vorren et al., J. Magn. Reson. Imaging 14, 750 (2001).
[b] J. A. O'Hara, F. Goda et al., Radiat. Res. 144, 222 (1995).
[c] F. Goda, G. Bacic et al., Cancer Res. 56, 3344 (1996).
[d] B. Gallez, B. F. Jordan et al., Magn. Reson. Med. 42, 627 (1999).
[e] J. A. O'Hara, R. D. Blumenthal et al., Radiat. Res. 155, 466 (2001).
[f] J. F. Dunn, J. A. O'Hara et al., J. Magn. Reson. Imaging 16, 511 (2002).
[g] T. Hasegawa, J. G. Rhee et al., Int. J. Radiat. Oncol. Biol. Phys. 13, 569 (1987).
[h] C. W. Song, A. Shakil et al., Int. J. Hyperthermia 12, 367 (1996).

[i] M. J. Eble, F. Wenz et al., in "Tumor Oxygenation" (P. W. Vaupel, D. K. Kelleher, and M. Günderoth, eds.), p. 95. Gustav Fischer, Stuttgart, Germany, 1995.

[j] S. Falk, V. Laurence et al., in "Tumor Oxygenation" (P. W. Vaupel, D. K. Kelleher, and M. Günderoth, eds.), p. 281. Gustav Fischer, Stuttgart, Germany, 1995.

[k] M. Höckel, K. Schlenger et al., Semin. Radiat. Oncol. 6, 3 (1996).

[l] D. W. Siemann, I. M. Johansen et al., Int. J. Radiat. Oncol. Biol. Phys. 40, 1171 (1998).

[m] D. F. Wilson, in "Oxygen Transport to Tissue XIV" (W. Erdmann and D. F. Bruley, eds.), p. 195. Plenum Press, New York, 1992.

[n] S. A. Vinogradov, L.-W. Lo et al., Biophys. J. 70, 1609 (1996).

[o] M. W. Dewhirst, E. T. Ong et al., Br. J. Cancer 79, 1717 (1999).

[p] K. Erickson, R. D. Braun et al., Cancer Res. 63, 4705 (2003).

[q] A. A. Potapov, E. B. Sirovskii et al., Vopre. Neirokhir. 1, 20 (1979).

Reporter molecules have been developed for use with electron spin resonance (ESR or EPR), where the line width is highly sensitive to oxygen.[28,44-55] Two primary approaches are used: (1) direct intratumoral (IT) injection of char crystals,[49,56] phthalocyanine,[57] or India ink[58] into a tissue or (2) intravenous (IV) infusion of water-soluble agents which disseminate throughout the tumor vasculature.[47,53] Direct IT injection is invasive and has generally been applied as a spectroscopic approach to report pO_2 at single locations only. Nonetheless, significant data have been achieved demonstrating hypoxiation and reoxygenation with respect to irradiation, and the importance of timing successive radiation doses to coincide with reoxygenation.[59] Char particles may be stable in tissue for weeks to years, allowing measurements of chronic changes in tissues (e.g., accompanying tumor growth).[28] The IV approach is noninvasive, but reporter molecules may predominately distribute in the well-perfused vasculature, potentially biasing measurements toward the well-oxygenated tumor regions. Progressive uptake and clearance of agents produces variable concentrations, and some agents degrade in tissue requiring appropriate correction factors.[47] Nonetheless, images of tumor oxygen distribution have been reported, including three-dimensional representations.[53] Spin radicals also may be applied to a combined ESR–NMR (nuclear magnetic resonance) approach, Overhauser-enhanced magnetic resonance imaging (OMRI), exploiting the Overhauser enhancement in the tissue water proton MRI signal that occurs by polarization transfer from free radicals upon electromagnetic irradiation.[60]

[44] H. M. Swartz, S. Boyer et al., Magn. Reson. Med. 20, 333 (1991).

[45] H. M. Swartz, S. Boyer et al., in "Oxygen Transport to Tissue XIV" (W. Erdmann and D. F. Bruley, eds.), p. 221. Plenum Press, New York, 1992.

[46] H. M. Swartz, K. J. Liu et al., Magn. Reson. Med. 31, 229 (1994).

[47] P. Kuppusamy, R. Afeworki et al., Cancer Res. 58, 1562 (1998).

[48] B. F. Jordan, P. Misson et al., Int. J. Radiat. Oncol. Biol. Phys. 48, 565 (2000).

[49] J. He, N. Beghein et al., Magn. Reson. Med. 46, 610 (2001).

[50] H. Jiang, N. Beghei et al., Phys. Med. Biol. 46, 3323 (2001).

[51] P. E. James and H. M. Swartz, Methods Enzymol. 350, 52 (2002).

[52] B. F. Jordan, V. Gregoire et al., Cancer Res. 62, 3555 (2002).

[53] M. Elas, B. B. Williams et al., Magn. Reson. Med. 49, 682 (2003).

[54] B. F. Jordan, N. Beghein et al., Int. J. Cancer 103, 138 (2003).

[55] P. Mahy, M. De Bast et al., Radiother. Oncol. 67, 53 (2003).

[56] N. Vahidi, R. B. Clarkson et al., Magn. Reson. Med. 31, 139 (1994).

[57] J. F. Glockner and H. M. Swartz, in "Oxygen Transport to Tissue XIV" (W. Erdmann and D. F. Bruley, eds.), p. 229. Plenum Press, New York, 1992.

[58] F. Goda, K. Jian Lu et al., Magn. Reson. Med. 33, 237 (1995).

[59] J. A. O'Hara, F. Goda et al., Radiat. Res. 150, 549 (1998).

[60] M. C. Krishna, S. English et al., Proc. Natl. Acad. Sci. USA 99, 2216 (2002).

Vascular oxygenation has been probed by fluorescence or phosphorescence imaging based on reporter complexes delivered IV.[61,62] Historically, the approach was limited to superficial tissues due to limited light penetration. The latest molecules are active in the near-infrared, permitting greater depth of signal penetration.[63]

NMR facilitates interrogation of deep tissues noninvasively, and ^{19}F NMR approaches will be reviewed in detail in the following section. The methods discussed earlier provide direct quantitative measurements of pO_2 based on various physiochemical parameters, such as electric current, fluorescent lifetime, magnetic resonance linewidth, or relaxation. Other approaches are less direct, but can reveal hypoxia or correlates of pO_2.

Specific classes of reporter molecules have been developed to reveal hypoxia[26,64] (e.g., pimonidazole,[65,66] EF5,[67,68] CCl-103F,[69] Cu-ATSM[70,71] galactopyranoside IAZA[72]). Following IV infusion, these agents become reduced in tissues and are trapped. However, in the presence of oxygen they are reoxidized and ultimately clear from the body. Histologic assessment of the distribution of these agents provides microscopic indications of local hypoxia. EF5, pimonidazole, and Cu-ATSM are currently being tested in clinical trials, and correlations have been reported with clinical outcome.[66,67,70] Many variants have been proposed over the past 20 years, and incorporation of radionuclides has facilitated noninvasive investigations using positron emission tomography (PET) or single photon emission computed tomography (SPECT), while ^{19}F labels permitted NMR spectroscopy.[72-74] Generally, only a single time point is investigated, but dynamic variations in hypoxia may be assessed, even in biopsy specimens, by applying pairs of hypoxia reporters in a pulse-chase fashion with respect to an intervention, as shown by Ljungkvist et al.[69]

[61] D. Wilson and G. Cerniglia, Cancer Res. 52, 3988 (1992).
[62] G. Helminger, F. Yuan et al., Nature Med. 3, 177 (1997).
[63] D. F. Wilson, S. A. Vinogradov et al., Comp. Biochem. Physiol., Part A Mol. Integr. Physiol. 132, 153 (2002).
[64] J. R. Ballinger, Semin. Nucl. Med. 31, 321 (2001).
[65] J. A. Raleigh, S. C. Chou et al., Radiat. Res. 151, 580 (1999).
[66] J. H. A. M. Kaanders, K. I. E. M. Wijffels et al., Cancer Res. 62, 7066 (2002).
[67] S. M. Evans, S. Hahn et al., Cancer Res. 60, 2018 (2000).
[68] W. R. Dolbier, Jr., A. R. Li et al., Appl. Radiat. Isotop. 54, 73 (2001).
[69] A. S. E. Ljungkvist, J. Bussink et al., Int. J. Radiat. Oncol. Biol. Phys. 48, 1529 (2000).
[70] F. Dehdashti, P. W. Grigsby et al., Int. J. Radiat. Oncol. Biol. Phys. 55, 1233 (2003).
[71] F. Dehdashti, M. A. Mintun et al., Eur. J. Nucl. Med. Molec. Imaging 30, 844 (2003).
[72] J. D. Chapman, E. L. Engelhardt et al., Radiother. Oncol. 46, 229 (1998).
[73] R. J. Maxwell, P. Workman et al., Int. J. Radiat. Oncol. Biol. Phys. 16, 925 (1989).
[74] R. J. Hodgkiss, Anticancer Drug Des. 13, 687 (1998).

Several studies have shown a lack of correlation between hypoxic marker binding and pO_2 assessed using the Eppendorf Histograph, which may be related to chronic versus acute hypoxia, or the extent of necrosis.[75-77] The ultimate value of the techniques is evidenced by correlations between uptake and outcome.[66,70,71,78] Recent data also indicate that EF5 fluorescence may be correlated with pO_2.[79]

The techniques discussed so far all depend on exogenous reporter molecules or probes. Ideally, oxygenation could be related to endogenous characteristics. Because many biochemical pathways are under oxygen regulation, they can provide an elegant window on hypoxia, for example, induction of hypoxia-inducible factor 1 (HIF-1) and glucose transporter 1 (Glut-1) together with secondary responses, such as increased production of vascular endothelial growth factor (VEGF), NIP3 and tumor-associated macrophage activity.[8] Such molecules indicate hypoxia, though they may be induced by other factors. Intrinsic radiation sensitivity also may be assessed using the Comet assay.[80] These assays each require biopsy. Other markers potentially associated with hypoxia may be found in the plasma or urine and have been correlated with clinical outcome.[81] An attractive alternative is the introduction of transgenes with hypoxic response elements (HREs) as promoter sequences coupled to reporter genes such as GFP (green fluorescent protein)[82,83] or luciferase.[84,85] GFP synthesis is an energetic process, which could be hindered under hypoxia conditions. Likewise, bioluminescence accompanying action of luciferase on luciferin requires adenosine triphosphate (ATP) and O_2, but reports suggest that even under exceedingly low pO_2, sufficient oxygen remains to reveal hypoxia.

Many practical considerations govern clinical application of oximetry methods. Proton MRI is routinely applied for anatomic evaluation of tumors and would provide an ideal conduit for prognostic investigations. Application of contrast agents may reveal tumor boundaries to enhance detectability, and the dynamic contrast enhancement (DCE) changes provide insight into vascular perfusion and surface permeability area.[86]

[75] W. T. Jenkins, S. M. Evans et al., Int. J. Radiat. Oncol. Biol. Phys. 46, 1005 (2000).

[76] P. L. Olive, J. P. Banath et al., Acta Oncol. 40, 917 (2001).

[77] M. Nordsmark, J. Loncaster et al., Radiother. Oncol. 67, 35 (2003).

[78] C. J. Koch, S. M. Hahn et al., Cancer Chemother. Pharmacol. 48, 177 (2001).

[79] C. J. Koch, Methods Enzymol. 352, 3 (2002).

[80] P. L. Olive, P. J. Johnston et al., Nature Med. 4, 103 (1998).

[81] Q. T. Le, P. D. Sutphin et al., Clin. Cancer Res. 9, 59 (2003).

[82] Y. Cao, C. Li et al., "A Study of Hypoxia-Induced Gene Expression in Human Tumors." 48th Annual Meeting of Radiation Research, San Juan, Puerto Rico, 2001.

[83] D. Vordermark, T. Shibata et al., Neoplasia 3, 527 (2001).

[84] T. Shibata, A. J. Giaccia et al., Gene Ther. 7, 493 (2000).

[85] E. Payen, M. Bettan et al., J. Gene Med. 3, 498 (2001).

[86] A. R. Padhani, J. Magn. Reson. Imaging 16, 407 (2002).

Specific studies have shown a correlation between DCE and pO_2,[87] and indeed, a theoretical underpinning has been provided based on the Krogh cylinder model.[88] However, the correlation is unlikely to be widely applicable, since DCE is sensitive to vascular flow, perfusion, and permeability, where pO_2 depends on oxygen consumption as well as delivery.

Blood oxygen level dependent (BOLD) contrast proton NMR facilitates rapid interrogation of vascular oxygenation and is particularly appropriate for examining dynamic responses to interventions.[48,89–91] Deoxyhemoglobin is paramagnetic and induces signal loss in T_2^*-weighted images. However, BOLD does not provide absolute pO_2 values and is confounded by the influence of blood flow, as investigated extensively by Howe et al.,[92] who termed the expression *FLOOD* (flow and oxygen level dependent) contrast. In addition, variation in vascular volume can introduce signal perturbation.[93] Nonetheless, some studies have indicated a correlation with relative pO_2, but poor indication of absolute pO_2.[53,94,95]

Near-infrared spectroscopy (NIRS) offers an alternative approach based on the differential light absorption of the strong chromophores oxyhemoglobin and deoxyhemoglobin. NIRS provides a noninvasive means to monitor global tumor vascular oxygenation in real time based on endogenous molecules. Although many NIRS investigations have been conducted in the brain and breast in both laboratory and clinical settings over the past decade, there have been relatively few reports regarding solid tumors.[43,96–106] Most studies to date have used reflectance mode. By contrast, we have favored transmission mode, so as to interrogate deep tumor regions, and we have presented preliminary studies in rat breast

[87] R. A. Cooper, B. M. Carrington et al., Radiother. Oncol. **57,** 53 (2000).

[88] Z. Wang, M.-Y. Su et al., Technol. Cancer Res. Treat. **1,** 29 (2002).

[89] H. A. Al-Hallaq, J. N. River et al., Int. J. Radiat. Oncol. Biol. Phys. **41,** 151 (1998).

[90] S. P. Robinson, F. A. Howe et al., Semin. Radiat. Oncol. **8,** 198 (1998).

[91] R. Mazurchuk, R. Zhou et al., Magn. Reson. Imaging **17,** 537 (1999).

[92] F. A. Howe, S. P. Robinson et al., Magn. Reson. Imaging **17,** 1307 (1999).

[93] F. A. Howe, S. P. Robinson et al., NMR Biomed. **14,** 497 (2001).

[94] C. Baudelet and G. Gallez, Magn. Reson. Med. **48,** 980 (2002).

[95] X. Fan, J. N. River et al., Int. J. Radiat. Oncol. Biol. Phys. **54,** 1202 (2002).

[96] H. D. Sostman, S. Rockwell et al., Magn. Reson. Med. **20,** 253 (1991).

[97] R. G. Steen, K. Kitagishi et al., J. Neurooncol. **22,** 209 (1994).

[98] F. Steinberg, H. J. Rohrbom et al., Adv. Exp. Med. Biol. **428,** 553 (1997).

[99] E. L. Hull, D. L. Conover et al., Br. J. Cancer **79,** 1709 (1998).

[100] B. J. P. van der Sanden, A. Heerschap et al., Magn. Reson. Med. **42,** 490 (1999).

[101] H. Liu, Y. Song et al., Appl. Op. **39,** 5231 (2000).

[102] M. Kragh, B. Quistorff et al., Eur. J. Cancer **37,** 924 (2001).

[103] G. Gulsen, H. Yu et al., Technol. Cancer Res. Treat. **1,** 497 (2002).

[104] E. L. Heffer and S. Fantini, Appl. Opt. **41,** 3827 (2002).

[105] T. O. McBride, B. W. Pogue et al., J. Biomed. Opt. **7,** 72 (2002).

[106] J. G. Kim, D. Zhao et al., J. Biomed. Optics **8,** 53 (2003).

and prostate tumors with respect to various interventions.[43,101,106] NIR approaches are presented in detail in Chapter 17 of this volume.

Each technique has specific virtues and drawbacks, which must be considered for any given application, particularly the degree of invasiveness, the ability to generate maps of heterogeneity, and the ability to assess dynamic changes. In addition, the location of a measurement (e.g., vascular versus tissue compartments, the precision of measurements, and spatial and temporal resolution) must be considered. For further details of the techniques described earlier, the reader is referred to the references. In the next section, we present ^{19}F NMR approaches in greater detail.

^{19}F NMR Approaches to Measuring pO_2

Nuclear magnetic resonance (NMR) is attractive because it is inherently noninvasive. Liquid-state NMR is characterized by several parameters, including signal amplitude, chemical shift (δ), spin–spin relaxation (T_2), and spin–lattice relaxation (T_1). Oxygen could be quantified using ^{17}O NMR, but this is rather esoteric.[107] Alternatively, it has long been recognized that the oxygen molecule (O_2) is paramagnetic, causing increased spin–lattice relaxation rates ($R_1 = 1/T_1$). Indeed, physical and theoretical chemists must go to great lengths to rigorously remove oxygen from solutions (using freeze–thaw procedures) to achieve inherent relaxation rates for studying nuclear interactions.[108] Proton NMR studies have reported changes in the water relaxation rate as a result of tissue oxygenation,[109] but many other processes (metal ions, cellularity, pH, ionic strength) also cause relaxation, and thus it is not suitable for detecting pO_2, except under rare circumstances, such as with the eye.[110] There is also a substantial temperature response, whereas the relaxivity due to oxygen is only 0.0002 s^{-1}/torr.[110]

However, several investigators showed that the ^{19}F NMR spin–lattice relaxation rates for fluorocarbons are much more sensitive to pO_2.[111,112] Thomas et al.[113] pioneered the application of ^{19}F NMR relaxometry to measure pO_2 in tissues, in vivo, including lung, liver, and spleen; several other investigators demonstrated feasibility and applications,[114–120] as

[107] X. H. Zhu, H. Merkle et al., Magn. Reson. Med. 45, 543 (2001).

[108] M. A. Hamza, G. Serratice et al., J. Magn. Reson. 42, 227 (1981).

[109] E. Tadamura, H. Hatabu et al., J. Magn. Reson. Imaging 7, 220 (1997).

[110] B. A. Berkowitz, C. McDonald et al., Magn. Reson. Med. 46, 412 (2001).

[111] J.-J. Delpuech, M. A. Hamza et al., J. Chem. Phys. 70, 2680 (1979).

[112] M. A. Hamza, G. Serratice et al., J. Am. Chem. Soc. 103, 3733 (1981).

[113] S. R. Thomas, in "Magnetic Resonance Imaging" (C. L. Partain, R. R. Price, J. A. Patton, M. V. Kulkarni, and A. E. J. James, eds.), Vol. 2, p. 1536. W. B. Saunders, London, 1988.

[114] J. E. Fishman, P. M. Joseph et al., Magn. Reson. Imaging 5, 279 (1987).

reviewed some years ago by Mason.[121] The ^{19}F NMR R_1 of perfluorocarbons (PFCs) varies linearly with pO_2,[113,122] and each resonance is sensitive to pO_2, temperature, and magnetic field, but importantly, is essentially unresponsive to pH, CO_2, charged paramagnetic ions, mixing with blood, or emulsification.[123–127]

A particular PFC molecule may have multiple resonances, and each resonance has a characteristic R_1 response to pO_2. This is attributed to steric effects of O_2, as it approaches the molecule,[112] which implies that perfluorinated groups, which are both geometrically and magnetically comparable, should have similar R_1 responses to oxygen tension. At a fixed temperature and magnetic-field strength, the R_1 response to pO_2 of any single resonance obeys the simple formula

$$R_1 = R_{1a} + (R_{1p}X) \tag{1}$$

where X is the mole fraction of O_2 dissolved in the PFC, R_{1a} is the anoxic relaxation rate, and R_{1p} is the relaxation rate due to the paramagnetic contribution of oxygen. According to Henry's law, the dissolved mole fraction is related directly to the partial pressure of oxygen,

$$pO_2 = KX \tag{2}$$

where K represents Henry's constant for a given solution of gas at a specified temperature. By substitution,

$$R_1 = R_{1a} + (R_{1p}/K)pO_2 \tag{3}$$

The slope (R_{1p}/K) indicates the response of a particular resonance to pO_2.

PFCs essentially act as molecular amplifiers, since the solubility of oxygen is greater than in water, but thermodynamics require that the pO_2 in the PFC will rapidly equilibrate with the surrounding medium, and estimates of diffusion suggest the equilibration can occur within seconds.

[115] S. K. Holland, R. P. Kennan et al., Magn. Reson. Med. 29, 446 (1993).

[116] B. R. Barker, R. P. Mason et al., J. Magn. Reson. Imaging 4, 595 (1994).

[117] B. J. Dardzinski and C. H. Sotak, Magn. Reson. Med. 32, 88 (1994).

[118] U. Noth, S. P. Morrissey et al., Magn. Reson. Med. 34, 738 (1995).

[119] H. T. Tran, Q. Guo et al., Acad. Radiol. 2, 756 (1995).

[120] S. Laukemper-Ostendorf, A. Scholz et al., Magn. Reson. Med. 47, 82 (2002).

[121] R. P. Mason, Artif. Cells Blood Substit. Immobil. Biotechnol. 22, 1141 (1994).

[122] P. Parhami and B. N. Fung, J. Phys. Chem. 87, 1928 (1983).

[123] L. C. Clark, Jr., J. Ackerman et al., in "Oxygen Transport to Tissue VI" (D. Bruley, H. I. Bicher, and D. Reneau, eds.), p. 835. Plenum Press, New York,.

[124] C. F. Kong, G. M. Holloway et al., J. Phys. Chem. 88, 6308 (1984).

[125] C.-S. Lai, S. Stair et al., J. Magn. Reson. 57, 447 (1984).

[126] D. Eidelberg, G. Johnson et al., Magn. Reson. Med. 6, 344 (1988).

[127] S. R. Thomas, R. G. Pratt et al., Radiology 18, 159 (1991).

Because relaxation is proportional to oxygen concentration, the effect will be greater at a given pO_2 than for water. Importantly, ions do not enter the hydrophobic PFC phase, and thus do not affect the bulk relaxation. Indeed, PFCs are typically exceedingly hydrophobic and do not mix with the aqueous phases, but rather form droplets or emulsions. Based on these principles, PFCs have been applied to *in vivo* pO_2 measurements. Characteristics of many diverse PFCs are summarized in Table II.

At any given magnetic field (Bo) and temperature (T), sensitivity to changes in pO_2 is given by $R_1 = a + bpO_2$. Thus a greater slope is important, and the ratio $\eta = b/a$ has been proposed as a sensitivity index.[128] Generally, a small "a" value (intercept) represents greater sensitivity, but it also generates longer T_1 values under hypoxic conditions, potentially increasing data acquisition times. Indeed, the T_1 of hexafluorobenzene (HFB) at 4.7 T may reach 12 s, potentially creating long imaging cycles, but this is readily overcome by applying single-shot (echo planar) imaging techniques, as presented in a later section.

Many PFCs, such as perfluorotributylamine (PFTB), perflubron (formerly referred to as perfluorooctyl bromide; PFOB), and Therox (F44-E), have several ^{19}F NMR resonances, which can be exploited to provide additional information in spectroscopic studies, but seriously hamper effective imaging. Multiple resonances can lead to chemical shift artifacts in images, which compromise the integrity of relaxation time measurements, though they can be avoided by selective excitation, or detection, chemical shift imaging, deconvolution, or sophisticated tricks of NMR spin physics.[116,119,129-133] These approaches add to experimental complexity and are generally associated with lost signal to noise ratio (SNR). Thus we strongly favor PFCs with a single resonance, and we will describe the use of HFB,[27,32,42,106,134-137] though some research groups favor 5-crown-5-ether (15C5).[88,117,138,139]

[128] S. R. Thomas, R. G. Pratt *et al.*, *Magn. Reson. Imaging* **14**, 103 (1996).
[129] L. J. Busse, R. G. Pratt *et al.*, *J. Comp. Ast. Tomagr.* **12**, 824 (1988).
[130] R. P. Mason, N. Bansal *et al.*, *Magn. Reson. Imaging* **8**, 729 (1990).
[131] H. K. Lee and O. Nalcioglu, *J. Magn. Reson. Imaging* **2**, 53 (1992).
[132] U. Nöth, R. Deichmann *et al.*, *J. Magn. Reson. B* **105**, 233 (1994).
[133] R. G. Pratt, J. Zheng *et al.*, *Magn. Reson. Med.* **37**, 307 (1997).
[134] D. Zhao, A. Constantinescu *et al.*, *Radiat. Res.* **156**, 510 (2001).
[135] Y. Song, A. Constantinescu *et al.*, *Technol. Cancer Res. Treat.* **1**, 471 (2002).
[136] D. Zhao, A. Constantinescu *et al.*, *Radiat. Res.* **159**, 621 (2003).
[137] D. Zhao, S. Ran *et al.*, *Neoplasia* **5**, 308 (2003).
[138] B. P. J. van der Sanden, A. Heerschap *et al.*, *Int. J. Radiat. Oncol. Biol. Phys.* **44**, 649 (1999).
[139] T. Q. Duong, C. Ladecola *et al.*, *Magn. Reson. Med.* **45**, 61 (2001).

TABLE II

^{19}F NMR Characteristics and Applications of PFCs for Tissue Oximetry

PFC	Sensitivity to $pO_2{}^a$	Temp. sensitivity (torr/°)	Magnetic field $B_0(T)$	Application/comments	References
Hexafluorobenzene (HFB)	A = 0.0835 B = 0.001876	0.13	4.7	Rat breast tumor, prostate tumor, human lymphoma xenograft	Hunjan, Zhao et al.[159]; Zhao, Constantinescu et al.[32,134,136]; Mason, Ran et al.[27]; Song, Constantinescu et al.[135]; Zhao, Ran et al.[137]
HFB	A = 0.074 B = 0.00158		4.7	Rat prostate tumor	Hunjan, Mason et al.[161]; Mason, Constantinescu et al.[175]
HFB	A = 0.093 B = 0.103	1.40	7	Phantom	Mason, Rodbumrung et al.[143]
Perfluoro-15-Crown-5-ether (15C5)	A = 0.345 B = 0.0034	2.94	2.0	Tumor cells	Helmer, Han et al.[157]
15C5	A = 0.333 B = 0.0033	3.98	2.0	Mouse tumor, spleen, liver	Dardzinski and Sotak[117]
15C5	A = 0.44 B = 0.0028		4.3	Human glioma tumor in mice	van der Sanden, Heerschap et al.[100]; van der Sanden, Heerschap et al.[138]
15C5	A = 0.375 B = 0.00198		4.7	Rat breast tumor	Fan, River et al.[95]
15C5	A = 0.362 B = 0.1239		4.7	Rat brain	Duong, Ladecola et al.[139]
Perfluorotributyl-amine (FC-43) PFTB	A = 1.09	4.43	0.14	Pig liver, spleen, lung	Thomas, Pratt et al.[128]
PFTB	B = 0.00623		0.14	Rat liver, spleen, lung	Pratt, Zheng et al.[133]; Thomas, Gradon et al.[163]

TABLE II (continued)

PFC	Sensitivity to pO$_2$[a]	Temp. sensitivity (torr/°)	Magnetic field B$_0$(T)	Application/ comments	References
PFTB	A = 0.684 B = 0.00305		4.7	Rabbit eye	Berkowitz, Wilson et al.[166]; Wilson, Berkowitz et al.[b]
PFTB	A = 0.9072 B = 0.004486		1.5	Human eye	Wilson, Berkowitz et al.[167]
PFTB	A = 0.8848 B = 0.1307	8.17	7	Mouse Meth-A tumor and heart	Mason, Shukla et al.[141]
Perfluorotripropylamine (FTPA)	A = 0.314 B = 0.002760^{-3}		1.9	Rat subcutaneous tumor	Fishman, Joseph et al.[c]
FTPA	A = 0.301 B = 0.00312		1.4	Rat spleen, lung, liver	Fishman, Joseph et al.[114]
FTPA	A = 0.4052 B = 0.0023		2.0	Rat liver, spleen	Holland, Kennan et al.[115]
FTPA			4.4	Cells	Taylor and Deutsch[d]
Bis-perfluoro-butylethylene (F-44E)	A = 0.3421 B = 0.11172		7.05	Rat, alginate capsules	Noth, Grohn et al.[164]
F-44E	A = 0.342 B = 0.1201		7.05	Rat spleen, liver, abdominal aorta, vena cava	Noth, Morrissey et al.[118]
F-44E	A = 0.2525 B = 0.16527	0.59	2.0	Mouse tumor	Hees and Sotak[153]
Perfluorooctyl-bromide (perflubron) (PFOB)	A = 0.517 B = 0.0038		9.4	Rat heart	Shukla, Mason et al.[e]
PFOB	A = 0.2677 B = 0.12259	1.26	4.7	Prostate tumor in rat	Antich et al.[162]

Compound	A, B			Tissue	Reference
PFOB	A = 0.328 B = 0.12137	2.85	7	Phantom	Mason, Shukla et al.[142]
PFOB	A = 0.085 B = 0.0033		2.0	Rat tumor	Sostman, Rockwell et al.[96]
PFOB			1.5	Rabbit liver	Tran, Guo et al.[119]
PFOB			8.5	Pig liver, lung, spleen	Millard and McGoron[f]
PFOB			1.45	Rat lung, Mouse lung	Thomas, Clark, Jr. et al.[g]
PFOB			1.5	Pig lung	Laukemper-Ostendorf, Scholz et al.[120]
Perfluoro-2,2′,2′-tetramethyl-4,4′-bis(1,3-fioxolane) (PTBD)	A = 0.50104 B = 0.1672		2.0	Phantom	Sotak, Hees et al.[h]

Some original papers presented calibration curves in other forms (e.g., including coefficients for temperature dependence). In those cases, equations have been derived assuming 37°. Where a PFC has more than one resonance, the equation presented is either for the most sensitive signal, or the equation used where the signal may have been unresolved.

[a] R_1 (s^{-1}) = A + B × pO$_2$ (torr).
[b] C. A. Wilson, B. A. Berkowitz et al., Exp. Eye Res. 55, 119 (1992).
[c] J. E. Fishman, P. M. Joseph et al., Invest. Radiol. 24, 65 (1989).
[d] J. Taylor and C. J. Deutsch, Biophys. J. 53, 227 (1988).
[e] H. P. Shukla, R. P. Mason et al., Magn. Reson. Med. 35, 827 (1996).
[f] R. W. Millard and A. J. McGoron, Artif. Cells Blood Subst. Immobil. Biotechnol. 22, 1251 (1994).
[g] S. R. Thomas, L. C. Clark, Jr. et al., J. Comput. Assist. Tomogr. 10, 1 (1986).
[h] C. H. Sotak, P. S. Hees et al., Magn. Reson. Med. 29, 188 (1993).

R_1 is sensitive to temperature, although the response varies greatly between PFCs and between individual resonances of each individual PFC. Over small temperature ranges, a linear correction to calibration curves is appropriate, but over larger temperature ranges, the response can be complex, as investigated extensively by Shukla et al.[140] for several PFCs. Differential sensitivity of pairs of resonances to pO_2 and temperature allowed Mason et al.[141] to simultaneously determine both parameters by solving simultaneous equations. However, generally it is preferable for a pO_2 sensor to exhibit minimal response to temperature, since this is not always known precisely in vivo and temperature gradients may occur across tumors. As shown in Table II, even a relatively small error in temperature estimate can introduce a sizable discrepancy into the apparent pO_2; for example, the relative error introduced into a pO_2 determination by a 1° error in temperature estimate ranges from 8 torr/° for PFTB[141] to 3 torr/° for PFOB (perflubron)[142] or 15C5[117] and 0.1 torr/° for HFB,[143] when pO_2 is actually 5 torr. It must be noted that error depends on actual pO_2 and the error varies with magnetic field and temperature. R_1 response does depend on magnetic field, necessitating calibration curves for each type of magnet system (e.g., 1.5, 4.7, or 7 T). Thus comparison of PFC utility for pO_2 measurements is complicated by the field used for specific published investigations, and in Table II, we consider sensitivity as presented.

Choice of PFC may be governed by practical considerations, such as cost and availability, since several products, particularly proprietary emulsions, may be difficult to obtain. HFB and 15C5 offer the immediate advantage of a high symmetry and a single ^{19}F NMR resonance. This offers maximum SNR and simplifies imaging, which may otherwise require frequency selective excitation, deconvolution, or other NMR tricks to avoid chemical shift artifacts.

Route of Administration. The most popular route for the delivery of PFCs is as emulsions injected intravenously. Given the extremely hydrophobic nature of PFCs, they do not dissolve in blood directly, but may be formulated as biocompatible emulsions. Much effort has been applied to formulate stable homogenous emulsions, as reviewed elsewhere.[144] Following IV infusion, the emulsion circulates in the vasculature with a

[140] H. P. Shukla, R. P. Mason et al., J. Magn. Reson. B **106**, 131 (1995).

[141] R. P. Mason, H. P. Shukla et al., Magn. Reson. Med. **29**, 296 (1993).

[142] R. P. Mason, H. P. Shukla et al., Biomater. Artif. Cells Immobilization Biotechnol. **20**, 929 (1992).

[143] R. P. Mason, W. Rodbumrung et al., NMR Biomed. **9**, 125 (1996).

[144] J. G. Riess, Biomater. Artif. Cells Immobilization Biotechnol. **20**, 183 (1992).

typical half-life of 12 h, (depending on the nature of the emulsion) providing substantial clearance within 2 days.[145,146] Primary clearance is by macrophage activity, leading to extensive accumulation in the liver, spleen, and bone marrow.[113,147] Indeed, this is a major shortcoming of IV delivery, since animals may exhibit extensive hepatomegaly or splenomegaly.[148] The emulsions are not toxic, and other than causing swelling, appear not to cause health problems. PFC clearance occurs from the liver with a typical half-life of 60 days for perfluorotripropylamine and 3 days for perflubron, with primary clearance by migration to the lungs and exhalation.[149]

Some investigators have examined pO_2 of tissues, while PFC remained in the blood, providing a vascular pO_2.[114,118,150] Flow can generate artifacts, and correction algorithms have been proposed.[151] Many investigators have measured pO_2 in liver, spleen, and tumors following clearance from the blood, thus providing measurement of tissue pO_2.[95,100,115,117–119,152–157]

Both spectroscopic and imaging approaches have been applied to tissue pO_2 measurements depending on the available SNR. It appears that uptake and distribution efficiency vary with tumor type, but in general, maximum signal is detected from the tumor periphery corresponding with regions of greater perfusion.[100,117,138,154,158,159] Several reports have examined changes in tumor pO_2 in response to acute interventions such as vasoactive drugs and hyperoxic gases.[32,95,100,135–137,153,160] Spectroscopic time resolution has ranged from seconds to minutes,[161,162] whereas imaging often takes longer.[160]

Long tissue retention facilitates chronic studies during tumor development, and progressive tumor hypoxiation has been observed over extended time periods of many days.[154,156] Correlated ^{19}F and proton MRI suggest

[145] M. C. Malet-Martino, D. Betbeder et al., J. Pharm. Pharmacol. 36, 556 (1984).
[146] T. F. Zuck and J. G. Riess, Crit. Rev. Clin. Lab. Sci. 31, 295 (1994).
[147] R. P. Mason, P. P. Antich et al., Magn. Reson. Imaging 7, 475 (1989).
[148] W. I. Rosenblum, M. G. Hadfield et al., Arch. Pathol. Lab. Med. 100, 213 (1976).
[149] R. F. Mattrey and D. C. Long, Invest. Radiol. 23, s298 (1988).
[150] D. Eidelberg, G. Johnson et al., J. Cereb. Blood Flow P. Metab. 8, 276 (1988).
[151] T. Higuchi, S. Naruse et al., in "7th SMRM," p. 435, 1988.
[152] R. P. Mason, R. L. Nunnally et al., Magn. Reson. Med. 18, 71 (1991).
[153] P. S. Hees and C. H. Sotak, Magn. Reson. Med. 29, 303 and erratum 29, 716 (1993).
[154] R. P. Mason, P. P. Antich et al., Int. J. Radiat. Oncol. Biol. Phys. 29, 95 (1994).
[155] S. R. Thomas, R. W. Millard et al., Artif. Cells Blood Subst. Immobil. Biotechnol. 22, 1029 (1994).
[156] N. J. Baldwin and T. C. Ng, Magn. Reson. Imaging 14, 541 (1996).
[157] K. G. Helmer, S. Han et al., NMR Biomed. 11, 120 (1998).
[158] P. P. Antich, R. P. Mason, A. Constantinescu et al., Proc. Soc. Nucl. Med. 35, 216P (1994).
[159] D. J. O. McIntyre, C. L. McCoy et al., Curr. Sci. 76, 753 (1999).
[160] S. Hunjan, D. Zhao et al., Int. J. Radiat. Oncol. Biol. Phys. 49, 1097 (2001).
[161] R. P. Mason, F. M. H. Jeffrey et al., Magn. Reson. Med. 27, 310 (1992).
[162] S. Hunjan, R. P. Mason et al., Int. J. Radiat. Oncol. Biol. Phys. 40, 161 (1998).

that PFC does not redistribute, but remains associated with specific tissues, analogous to tree rings.[154,156] Thus in principle, a whole tumor can be investigated by administering successive doses of PFC emulsion during growth.

PFC emulsions may also be administered intraperitoneally (IP), resulting in similar distribution to IV administration (unpublished observations). Given the volatile nature of many PFCs, they could be inhaled, but although this is a popular route for delivery of anesthetics and blood flow tracers, it does not appear to have been widely exploited for oximetry. Nonetheless, aerosols have been delivered to the lungs by inhalation to facilitate pO_2 measurements.[163]

Two approaches have been applied to circumvent reticuloendothelial uptake. PFC has been incorporated in polyalginate beads for direct implantation at a site of interest.[164,165] We favor direct IT injection of neat PFC, allowing any region of interest in a tumor to be interrogated immediately. Use of a fine needle ensures minimal tissue damage, as described in detail in a later section. Others have used direct injection of emulsions into tumors, but this increases the volume considerably, making it more invasive.[88] Investigators have suggested that emulsification improves retention at the site of injection. Direct injection of neat PFC also has been used to investigate retinal oxygenation[166-168] and cerebral oxygenation in the interstitial and ventricular spaces.[139]

As described in the following section we favor direct intratumoral injection of neat HFB followed by echo planar imaging to generate pO_2 maps in tumors.

FREDOM (Fluorocarbon Relaxometry using Echo Planar Imaging for Dynamic Oxygen Mapping)

Recognizing that tumors are heterogeneous and that pO_2 may fluctuate, we developed a procedure, which allows repeated quantitative maps of regional pO_2 to be achieved with multiple individual locations simultaneously in 6.5 min with a precision of 1–3 torr, when pO_2 is in the

[163] S. R. Thomas, L. Gradon et al., Invest. Radiol. 32, 29 (1997).

[164] U. Nöth, P. Grohn et al., Magn. Reson. Med. 42, 1039 (1999).

[165] U. Zimmermann, U. Noth et al., Artif. Cells Blood Subst. Immobil. Biotechnol. 28, 129 (2000).

[166] B. A. Berkowitz, C. A. Wilson et al., Invest. Ophthalmol. Vis. Sci. 32, 2382 (1991).

[167] C. Wilson, B. Berkowitz et al., Arch. Ophthalmol. 110, 1098 (1992).

[168] W. Zhang, Y. Ito et al., Invest. Ophthalmol. Visual Sci. 44, 3119 (2003).
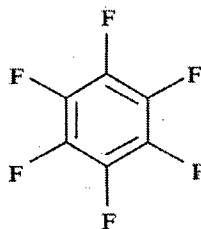
Fig. 1. Hexafluorobenzene (HFB) is a perfluorocarbon (PFC) exhibiting extensive symmetry.

range 0–10 torr.[160] We have applied FREDOM to diverse tumor types and interventions, as reviewed in a later section.

MRI is attractive because it is readily available at many institutions. For small animal work, ^{19}F NMR is widely available at 4.7, 7, and 9.4 T by minor adaptation of routine instrumentation, [e.g., retuning proton radiofrequency (RF) coils]. Within the recent past ^{19}F MRI is also becoming available on clinical systems, facilitating translation of these techniques to patients. ^{19}F NMR is particularly facile because there is essentially no background signal in tissues to interfere with measurements, yet the resonance frequency and sensitivity approach that of proton NMR. The pioneering work of Thomas[113] showed that tissue pO_2 could be imaged in various organs based on the ^{19}F NMR spin–lattice relaxation rate (R_1) of PFC reporter molecules following IV infusion. Prompted by these studies, we surveyed a number of PFCs and identified that HFB (Fig. 1) has many virtues as a pO_2 reporter.[143] Symmetry provides a single narrow ^{19}F NMR signal, and the spin–lattice relaxation rate is highly sensitive to changes in pO_2, yet minimally responsive to temperature (Fig. 2).[143] HFB also has a long spin–spin relaxation time (T_2), which is particularly important for imaging investigations. From a practical perspective, HFB is cheap (<$2/g) and readily available commercially in high purity ($\geq$99%). We obtain supplies from Lancaster Synthesis (Windham, NH), though many other fine chemical supply houses also offer HFB. We do favor bottles over sealed ampoules, since they are easier to handle. HFB is well characterized in terms of lack of toxicity,[169,170] exhibiting no mutagenicity,[171] teratogenicity, or fetotoxicity,[172] and the manufacturer's material

[169] Y. S. Gorsman and T. A. Kapitonenko, *Izv. Estestvennonauchu. Inst. Pevinsk.* **15**, 155 (1973).

[170] I. M. C. M. Rietjens, A. Steensma *et al.*, *Eur. J. Pharmacol.* **293**, 292 (1995).

[171] K. E. Mortelmans and V. F. Simmon, *Gov. Rep. Announce. Index (US)* **81**, 2555 (1981).

[172] K. D. Courtney and J. E. Andrews, *J. Environ. Sci. Health B* **19**, 83 (1984).
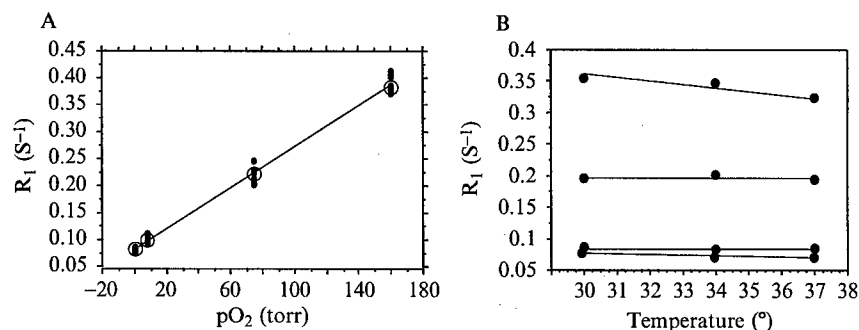
FIG. 2. (A) The ^{19}F NMR spin–lattice relaxation rate (R_1) of HFB shows a linear response to pO_2: at $37°$ and 4.7 T, $R_1 = 0.0835 + 0.001876 \times pO_2$. (B) The ^{19}F NMR R_1 of HFB shows minimal response to temperature in the physiologic range; separate curves are shown at four different pO_2s: 0, 1, 9.8, and 21% O_2.

data safety sheet indicates $LD_{50} > 25$ g/kg (oral—rat) and LC_{50} 95 g/m^3/2 h (inhalation—mouse).

HFB had been proposed as a veterinary anesthetic and has been used in many species, including ponies, sheep, cats, dogs, rats, and mice, but was abandoned because of its high volatility (boiling point $81°$) and low flash point $(10°)$.[173] This presented unacceptable dangers in veterinary suites for inhalation anesthetics. It is not a problem in our studies, where small quantities of liquid (typically, 50 μl) are injected directly into the tumor. HFB requires no special storage, other than a sealed bottle to prevent evaporation. Melting point is 4–$6°$, and density is 1.62 g/ml.

Methodology

Tumor Preparation. We have applied this technique to tumors in rats and mice, but our methodology will focus on our standard application to rats. As for electrode techniques, the tumor must be accessible (e.g., subcutaneous in flank of thigh), though we favor the pedicle model, which provides a tumor remote from the body, analogous to an additional limb.[174] This model is optimal for selective therapy such as local hyperthermia, irradiation, or excision. Noting the increasing interest in orthotopic tumors, the approach is also facile in breast tumors in the mammary fat pad and applicable in the prostate with a little practice.

[173] L. W. Hall, S. R. K. Jackson *et al.*, *in* "Recent Progress in Anaesthesiology and Resuscitation" (A. Arias, R. Llaurado, M. A. Nalda, and J. N. Lunn, eds.), p. 201. Excerpta Medica, Oxford, UK, 1975.

[174] E. W. Hahn, P. Peschke *et al.*, *Magn. Reson. Imaging* **11,** 1007 (1993).

Rats are preanesthetized with ketamine hydrochloride (100 mg/ml) as a relaxant and maintained under general gaseous anesthesia with air (1 dm^3/min) and 1.2% isoflurane [we do note that the appropriate concentration of anesthesia may depend on strain; for example, Copenhagen rats require (and tolerate) higher concentrations than Fisher rats]. In our latest refinement of the procedure, isoflurane may be stopped for a period of minutes during HFB administration, since rats occasionally exhibit respiratory distress, which may be caused by the anesthetic properties of HFB interacting with isoflurane. Within a few minutes, rats are stable and routine isoflurane anesthesia is maintained. In our earlier work we used 0.5% methoxyflurane in 33% oxygen with 66% N$_2$O,[160,175] but isoflurane appears to be a less stressful anesthetic.

HFB is deoxygenated by bubbling nitrogen for 5 min before use. We have previously shown in hypoxic tumor biopsies that use of aerated HFB may introduce a systematic apparent elevation in pO$_2$ ($\sim$2–3 torr). HFB is injected directly into tumors using a gas tight syringe with a custom-made fine sharp needle (32G #7803–04; Hamilton, Reno, NV). Generally, HFB is administered along three to five tracks in the form of a fan in a single central plane of the tumor coronal to the rat's body (Fig. 3A). The needle is inserted manually to penetrate across the whole tumor and withdrawn $\sim$1 mm to reduce pressure, and 3 μl HFB is deposited. The needle is repeatedly withdrawn a further 2–3 mm, and additional HFB is deposited. Typically, HFB is deliberately deposited at about 16 individual locations per tumor, in both the central and peripheral regions of the tumors, to ensure that the interrogated regions are representative of the whole tumor.

The animal is placed on its side in a cradle with a thermal blanket to maintain body temperature. A fiber-optic probe is inserted rectally to monitor core temperature. Temperature measurement is optional, since the R$_1$ is essentially invariant with temperature and does not need correction for pO$_2$ estimates. Of course, temperature regulation and measurement is important to ensure stable tumor physiology. An MR-compatible pulse oximeter equipped with "rat" software (8600V; Nonin, Inc., Plymouth, MN) may be applied to a hind foot to monitor arterial oxygenation (S$_a$O$_2$) and heart rate (optional, but provides additional useful data regarding animal health and physiology).

Most of our MR experiments were performed using an Omega CSI 4.7 horizontal bore magnet system with actively shielded gradients (GE systems, acquired by Bruker Instrument, Inc., Fremont, CA). Recently, our MR system has been upgraded to a Varian Unity INOVA, providing

[175] R. P. Mason, A. Constantinescu et al., Radiat. Res. 152, 239 (1999).
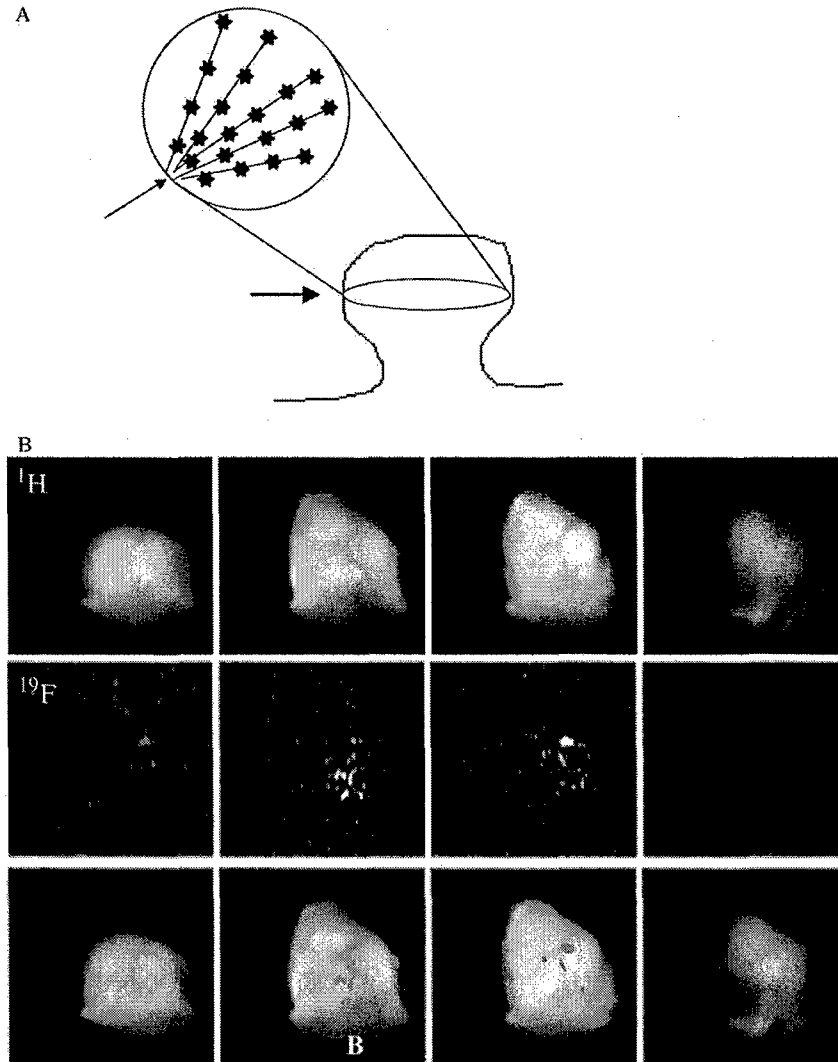
FIG. 3. (A) Recommended pattern of IT injection. Several tracks in the form of a fan in a single plane. (B) Four contiguous MR images (5 mm thick) of a representative Dunning prostate R3327-AT1 tumor (volume $= 1.6$ cm^3). *Top:* ^{1}H MRI; *middle:* corresponding ^{19}F; *bottom:* overlay to show interrogated regions. *B* marks point of attachment of the tumor to back of rat.
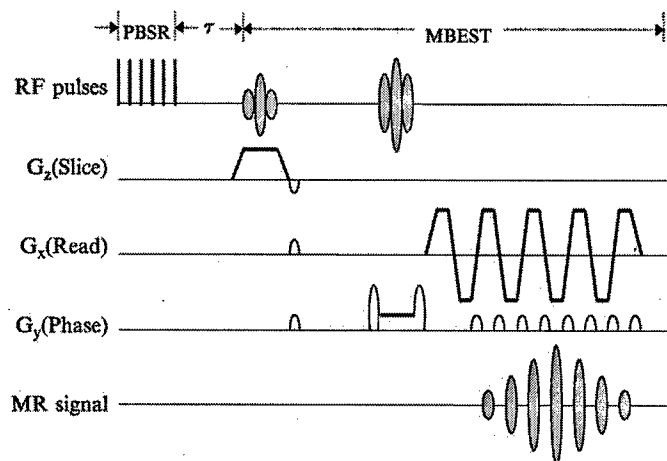
Fig. 4. MRI sequence used to achieve relaxation curves.

enhanced data acquisition and processing software and stronger imaging gradients. A tunable (^{1}H/^{19}F) MR coil, 2 or 3 cm in diameter matched to the tumor size (constructed from a cylindrical copper tube about 2 cm deep and acting as a single-turn solenoid), is placed around the tumor-bearing pedicle. Shimming is performed on the proton water signal to a typical line-width of 60–100 Hz. Proton images are obtained for anatomic reference using a three-dimensional (3D) spin–echo sequence. The coil is then re-tuned in place to 188.27 MHz, and corresponding ^{19}F MR images are obtained. Overlaying the ^{19}F MR images on the corresponding proton images reveals the distribution of HFB (Fig. 3B). Typically, ^{19}F NMR signal is obtained from 6–10% of the total tumor voxels.[136,137,175]

pO$_2$ maps are obtained using our standard MR oximetry protocol.[116,160,176] This applies pulse burst saturation recovery (PBSR) echo planar imaging (EPI) relaxometry using the ARDVARC (*a*lternated *r*elaxation *d*elays with *v*ariable *a*cquisitions to *r*educe *c*learance effects) acquisition protocol to map the tumors (Fig. 4).[175,177] EPI uses a single spin–echo with "blipped" phase encoding (modulus-blipped echo-planar single-pulse technique [MBEST]), although other EPI sequences should be equally applicable. We chose the PBSR approach to T$_1$ relaxation measurements for historical reasons; our earliest work used ^{19}F NMR spectroscopy of tumors with excitation and detection based on surface coils.[152] The PBSR approach is suitable for use with the nonuniform excitation typical of surface

[176] B. R. Barker, R. P. Mason et al., Magn. Reson. Imaging 11, 1165 (1993).
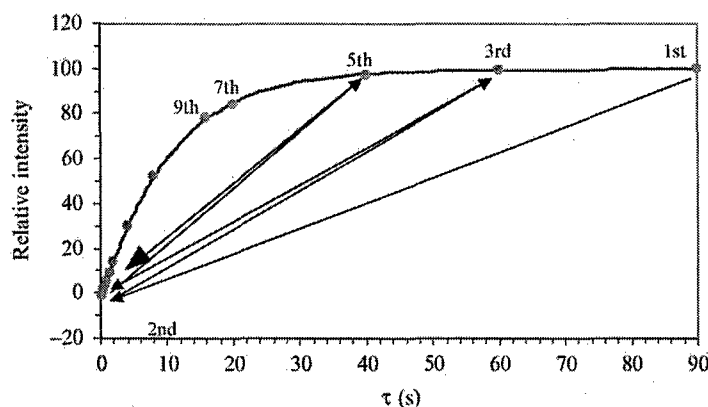[177] D. Le, R. P. Mason et al., Magn. Reson. Imaging 15, 971 (1997).

FIG. 5. Typical relaxation curve showing order of data acquisition. $y = A [1 - (1 + W) \exp(-R_1 \times \tau)]$ and $T_1 = 10.34 \pm 0.16$ s, $A = 99.5$, $W = 0.04$, and hence $pO_2 = 7.0 \pm 0.7$ torr.

coils as presented by Evelhoch and Ackerman.[178] For EPI, we do apply carefully calibrated $\pi/2$ pulses to ensure accurate refocusing of images, but we continue to favor the PBSR approach, since it provides particularly rapid estimation of T_1 by avoiding the need for extended relaxation recovery times between acquisitions. Saturation is achieved by a series of 20 nonspatially selective $\pi/2$ pulses with 50-ms spacing, which is sometimes called a "Comb" format.

Typical FREDOM parameters use 32×32 data points across a field of view of 40×40 mm, providing 1.25 mm in-plane resolution. Recently, we have applied a slice selection gradient, providing 5-mm-thick slices, and hence, 8-μl voxels. However, the deposition of HFB is designed to occur in a plane, and thus the discrete distribution of the reporter molecule itself can be used to define the slice. We apply a PBSR preparation sequence because it is ideally suited for measuring diverse, long T_1 values. Unlike more traditional inversion recovery sequences, there is no need to wait $>5\ T_1$ between successive images. As shown in Fig. 5, we use 14 delays in the order 90 s, 200 ms, 60 s, 400 ms, 40 s, 600 ms, 20 s, 800 ms, 16 s, 1 s, 8 s, 1.5 s, 4 s, and 2 s, selected to cover the whole range of T_1s (viz pO_2 values). Many papers have been published on optimizing relaxation curves and choosing parameters to enhance precision.[179-181] Our experience suggests that our

[178] J. L. Evelhoch and J. J. H. Ackerman, *J. Magn. Reson.* **53**, 52 (1983).

[179] A. P. Crawley and R. M. Henkelman, *Magn. Reson. Med.* **7**, 23 (1988).

[180] S. J. Doran, J. J. Attard *et al.*, *J. Magn. Reson.* **100**, 101 (1992).

[181] F. Franconi, F. Seguin *et al.*, *Medical Phys.* **22**, 1763 (1995).

parameters are appropriate for interrogating a broad range of pO_2 values, though they have not been rigorously or theoretically optimized. More delays could improve curve fitting, but would increase experiment time. We believe fewer delays would degrade quality of the curve fitting.

Traditional T_1 measurement sequences acquire data with delays in monotonic order, whereas we alternate longer and shorter delays to minimize any systematic errors, which would be introduced if the signal amplitude varies during the measurement. We have found that HFB clears from tissue with a typical half-life of 600 min,[162] which would introduce errors into the amplitude. Although the total acquisition time for a T_1 map is 6.5 min, we reduce the time between first and last acquisitions further by applying the longest delay first. Our experience shows that it is important to measure at least two data points on the plateau of the curve (i.e., >5 × T_1, and we choose 60 and 90 s, respectively. The data points with longer recovery times have greater SNR, and we find that a minimum SNR = 10 is required to produce satisfactory T_1 curves and pO_2 estimates. The variation in amplitude between longest and shortest delays approaches 100-fold. The poorest SNR data points (short delay; τ) could compromise the quality of the T_1 curves, and thus we obtain multiple acquisitions at these times to provide enhanced SNR by signal averaging. Because the τ values are short, it adds little to the overall experimental time. We use NA = 12 for $\tau < 1$ s; NA = 8 for $\tau = 1$ s; NA = 4 for $\tau = 1.5, 2$, and 4 s; NA = 2 for $\tau = 8$ s; and 16 s and NA = 1 for the longer delays. Signal amplitudes are corrected for the additional acquisitions, and a 2-d Fourier transform (FT) is applied to each image. Curve fitting is then applied on a voxel-by-voxel basis to each image set. Data quality could probably be enhanced by application of apodization and filtering functions, such as Fermi and Hanning filters, though we have not yet implemented these approaches. The acquisition protocol is not part of the standard software supplied by the manufacturer, but we can assist interested investigators.

Data are transferred to a personal computer (PC) for further analysis using a program created in our laboratory (T_1map [Fig. 6], PASCAL by Dennis Le). T_1map recognizes issues in data analysis and provides filters, clustering algorithms, and temporospatial correlation to assist in effective data reduction. At top right of Fig. 6 is a map, which may be toggled to display signal amplitude, T_1, T_1 error ($T_{1\ err}$), or pO_2 (Fig. 7). Blank pixels indicate that no curve fit could be achieved. Gray pixels indicate a successful curve fit and potential pO_2 value, but with errors beyond the specified range. In this example, thresholds were set as $T_{1\ err} < 2.5$ s and the ratio $T_{1\ err}/T_1 < 50\%$. Tightening these thresholds can produce higher-quality data, but eliminates more data. Colored pixels report measurements satisfying the threshold criteria, and these are tabulated in the form of a

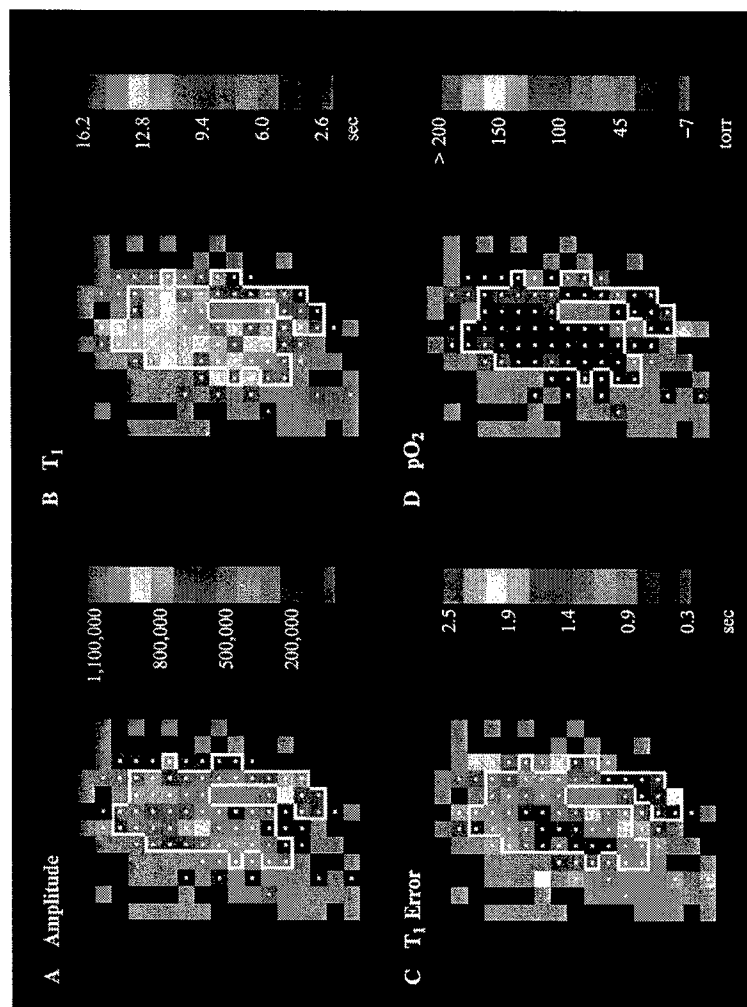FIG. 6. Example T_1map used for data filtering, clustering, and analysis.

Fig. 7. (continued)

histogram (center), which can be plotted with selected data bins and ranges of interest. At bottom right of Fig. 6 are data for each pixel, including coordinate and fitted parameters. In the box on the left are shown the number of fitted data points, number of accepted data points, and statistics such as mean T_1, pO_2, and corresponding amplitude-weighted values.

pO_2 is calculated on the basis of a curve fit to exponential data. Any curve fitting is associated with uncertainty, and indeed our procedure determines $T_{1\ err}$ values. Although the concept of negative pO_2 values may appear impossible, it is perfectly reasonable, provided that error bars and uncertainties are considered. Thus a value of -2 torr $\pm$ 3 torr legitimately indicates an actual pO_2 very close to zero. Some oximetry approaches ignore negative values or bin them all as zero. We accept any value providing that the error estimated for T_1 is within a specified range.

The most powerful aspect of FREDOM is the ability to follow the fate of individual voxels, and thus we usually acquire at least three baseline pO_2 maps, followed by further maps accompanying interventions, such as hyperoxic gas breathing. Even under baseline conditions, fluctuations in T_1 are apparent. These may arise from uncertainty in T_1, which may be reflected in $T_{1\ err}$ or transient fluctuations in pO_2.

T_1 map allows us to investigate sequential maps and select only those pixels that consistently show small $T_{1\ err}$s, for example, white regions of interest (ROI). In subsequent maps we may include only these regions, which satisfy the inclusion criteria for every map. This allows us to follow population dynamics based on specific tumor regions, avoiding potential anomalies due to varying numbers of "good quality" pixels in sequential images. Typically, 50–150 pixels provide high-quality data in any given map, but generally 20–80 pixels may be followed for a series of 23 maps associated with interventions.

The ROI tool also facilitates clustering, for example, selection of only those tumor regions, which consistently have $pO_2 < 10$ torr throughout the baseline period (these may be considered as chronically hypoxic, as opposed to regions, which fluctuate and may only be <10 torr in some

FIG. 7. Maps showing (A) ^{19}F NMR signal intensity, (B) spin–lattice relaxation times (T_1), (C) estimated errors in T_1, and (D) pO_2 values. Black squares show regions where signal to noise or data quality was so poor as to not provide a T_1 curve fit. Gray voxels show regions that provided a curve fit, but where the uncertainty in the data exceeded the threshold criteria (i.e., $T_{1\ err} > 2.5$ s or $T_{1\ err}/T_1 > 50\%$). All colored voxels ($n = 100$) provided a curve fit within the acceptance criteria in this map, but only those 56 voxels within the white regions of interest (ROI) provided consistently high-quality data throughout the sequence of eight maps acquired during baseline and with oxygen breathing. Data were obtained using the FREDOM approach from a representative Dunning prostate R3327-AT1 tumor (2 cm^3).

baseline maps). The ability to follow groups of pixels with particular base-
line characteristics has revealed heterogeneity in response to many inter-
ventions—often those regions initially well oxygenated show rapid and
large response to hyperoxic gas breathing, whereas those that are initially
poorly oxygenated show little and sluggish response (e.g., Fig. 8). This ap-
proach can also reveal phenomena such as the "steal" effect, whereby ini-
tially well-oxygenated regions decrease in pO_2, while others increase,
which might appear as "no change," when histogram-based population
statistics are used.

Figure 9 shows that the data quality is strongly related to signal ampli-
tude. Although these data represent 56 voxels from a single tumor, we have
previously shown similar data for the alternate PFC perflubron.[116] Given the
high solubility of O_2 in PFCs, there could be a concern that PFCs act as
reservoirs, perturbing local pO_2. Fig. 9B shows that there is no correlation
($r^2 < 0.05$) between signal amplitude (viz. HFB concentration) and pO_2.

As with any measurement, sampling is a critical issue. FREDOM is
analogous to the Eppendorf Histograph in that it samples multiple loca-
tions, which appear to reflect interstitial pO_2. Histograph data suggest that
a minimum of 100–140 data points[182] along five tracks[183] are required to ac-
curately represent the pO_2 distribution of a tumor, though such criteria do
depend on tumor size and heterogeneity. We applied Monte Carlo simula-
tion to assess the data requirements for FREDOM. A data set was
selected, which provided 120 high-quality data points, and these data points
were accessed in random order with continuous calculation of mean pO_2 to
assess the asymptotic trend lines toward the actual mean pO_2 (Fig. 10). It
appears that about 50 data points are required to well represent the pO_2
distribution of the tumor, which is generally achievable in any individual
pO_2 map. However, the unique ability to observe dynamic changes in
pO_2 at multiple locations simultaneously is the greatest strength of FRE-
DOM. Detection of heterogeneous responses is useful even if fewer data
points are examined, since each location serves as its own control.

Validation of Measurements. The spin–lattice relaxation rate (R_1) is de-
termined for each voxel using a three-parameter fit of signal intensities to

$$y_i = A[1 - (1 + W) \exp(-R_1 \times \tau)] \tag{4}$$

using the Levenberg–Marquardt least squares fitting protocol.[116] Typically,
~100–300 voxels provide an R_1 fit and potential pO_2 value. Because noise

[182] K. A. Yeh, S. Biade *et al.*, *Int. J. Radiat. Oncol. Biol. Phys.* **33**, 111 (1995).
[183] O. Thews, D. K. Kelleher *et al.*, *in* "Tumor Oxygenation" (P. W. Vaupel, D. K. Kelleher,
and Günderoth, eds.), Vol. 24, p. 39. Gustav Fischer Verlag, Stuttgart, Germany, 1995.
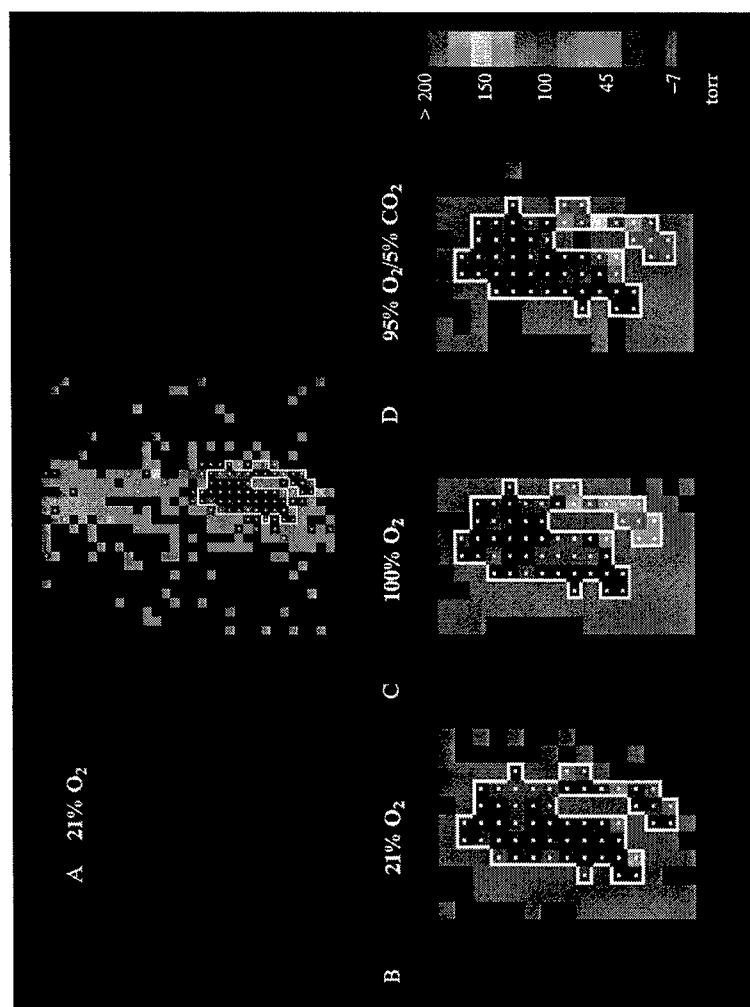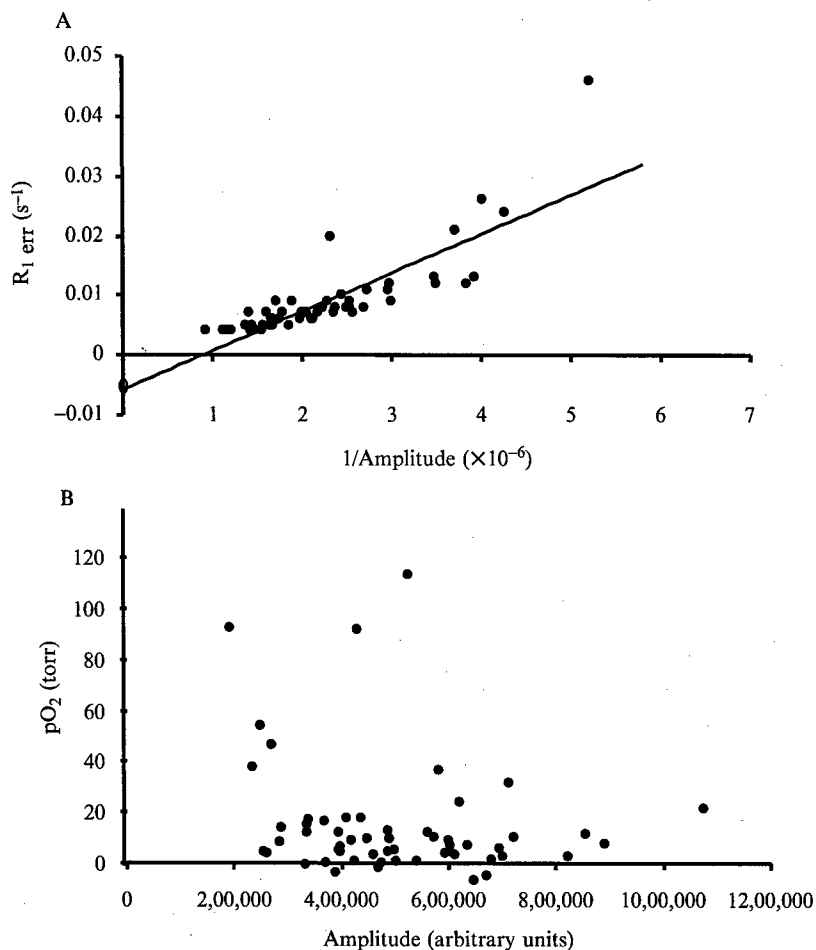
FIG. 9. (A) Relationship of $R_{1\ err}$ with signal amplitude showing strong correlation ($r^2 >$ 0.69). (B) Relationship of pO_2 and signal amplitude showing lack of correlation ($r^2 < 0.05$).

FIG. 8. PO_2 maps obtained using the FREDOM approach from the tumor shown in Fig. 3. (A) Under baseline conditions, those voxels ($n = 56$) within the white region provided consistently reliable data during repeated measurements. (B) Baseline map (breathing air: $FO_2 = 21\%$): mean $pO_2 = 7.2 \pm 2.6$ (SE) torr, median $pO_2 = 1.3$ torr (range -7–88 torr). (C) Breathing oxygen ($FO_2 = 100\%$): fourth map obtained 24–32 min after switching from air: mean $pO_2 = 47.2 \pm 10.7$ torr ($p < 0.0001$ compared with baseline), median $pO_2 = 8.3$ torr (range -3–204 torr). (D) Breathing carbogen ($FO_2 = 95\%$): fifth map after switching to carbogen: mean $pO_2 = 43.1 \pm 9.2$ torr ($p < 0.0001$ compared with baseline), median $pO_2 = 5.6$ torr (range -10–216 torr).

Fig. 10. Monte Carlo simulation of tumor oxygenation. Asymptotic behavior shows that tumor may be characterized by about 50 data points. For this large AT1 tumor in a rat breathing oxygen, all estimates converge on the mean $pO_2 = 31.7 + 1.0$ (SE) torr.
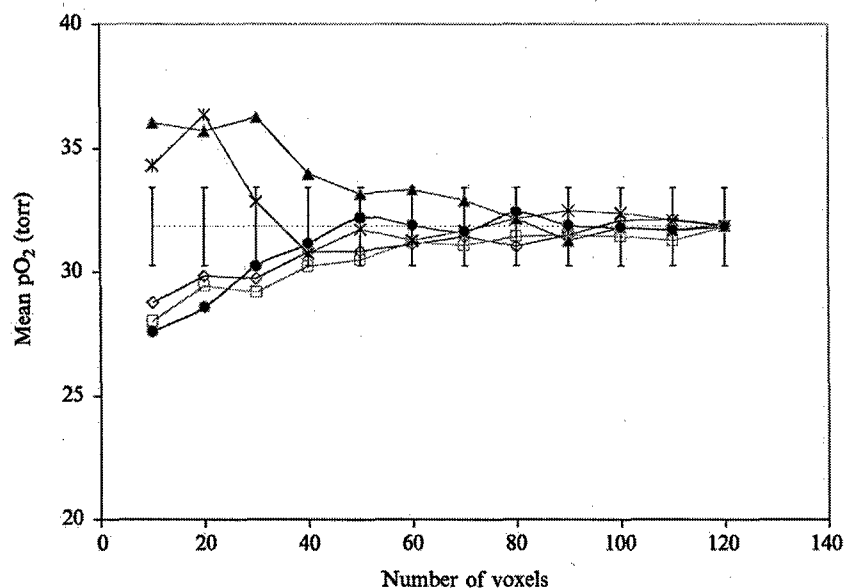
itself may give an apparent relaxation curve (R_1) fit, data are selected within a region of interest, having $T_{1\ err} < 2.5$ s and the ratio $T_{1\ err}/T_1 <$ 50%. With respect to respiratory interventions, only those voxels that provided consistently reliable data throughout the measurements are included for further analysis. At 37° and 4.7 T

$$pO_2(torr) = [R_1(s^{-1}) - 0.0835]/0.001876 \tag{5}$$

Equation (5) provides pO_2 in units of torr. The literature can be complicated by use of various units, and it may be instructive to provide conversion factors. We favor torr (1 torr = 1 mmHg), since radiobiologic hypoxia develops in the range 0–15 torr and this is the traditional unit favored by radiation biologists and oncologists. Further, 760 torr = 1 standard atmosphere (atm.), and gases are often quoted in %atm. For SI units, 101, 325 Pa (or N/m^2) = 1.01325 × 10^6 dynes/cm^2 = 1 atm. Some investigators quote oxygen concentrations in μM, often assuming that the solubility of oxygen in water at 37° is 1.35 μM/torr.[29] Quoting concentrations can be confusing because the solubility of oxygen is highly variable in solutions. FREDOM calibration is based on pO_2 values, and as shown by Eqs. 1–3,

these are directly related to the solubility of oxygen in HFB. However, partitioning of oxygen between the aqueous and PFC phases depends on pO_2, not concentrations. Thus the pO_2 determined by FREDOM will accurately reflect the ambient tissue pO_2 and if the solubility of oxygen can be estimated in the particular milieu, then $[O_2]$ could be calculated.

Both systematic and random errors may interfere. Random errors may be diminished by performing multiple repeat measurements (provided that the biologic system is stable). Systematic errors are more complex and could arise *inter alia* from erroneous calibrations, inappropriate curve fitting, and temperature changes. Appropriate curve fitting may be the greatest problem in relaxation analysis. Provided signal/noise > 10 for the most intense signals, we generally obtain excellent curve fits. Each voxel (or ROI) will comprise HFB at a range of pO_2 values, creating a multiexponential curve. However, modeling shows that the fit provides an "average" value. For population data, we sometimes determine error-weighted means $[\Sigma(x/\sigma^2)]/[\Sigma(1/\sigma^2)]$ in order to exploit as much available data as possible.

In terms of absolute pO_2 values, the most critical aspect is effective calibration curves. Over the years we have achieved pO_2-dependent ^{19}F NMR relaxation curves for many PFCs[116,141–143,160] and encountered potential pitfalls. The calibration curve we recommend at 4.7 T and 37° is given by Eq. (5) which was originally presented by Hunjan *et al.*[160] Briefly, 125 μl HFB was added to each of four gas-tight NMR tubes together with 0.5 ml water and saturated at 37° by bubbling with carbon dioxide, 1% O_2 (balance N_2), 9.8% O_2 (balance N_2), or air, respectively. Tubes were sealed, and the phantom was maintained at 37° in a water bath within a coil in the magnet. FREDOM was applied using the parameters described earlier, and the spin–lattice relaxation rates were estimated on a voxel-by-voxel basis using three-parameter fit. Equation (5) was established using linear regression analysis of amplitude squared weighted mean values for each gas.[159]

Although the relationship $R_1 = f(pO_2)$ is theoretically expected to be linear and empirically found to be so, we believe that it is important to use calibration gases in the range of physiologic pO_2. We recommend purchase of rigorously calibrated gases. We bubble gases for 30 min and use gas-tight Wilmad NMR tubes, which may be sealed with ground glass joints. Samples are used within hours of saturation. As desired, multiple tubes may be prepared at given pO_2, but since a linear relationship is expected, it may be equally appropriate to use additional gases. T_1 may be determined multiple times for each sample, and we recommend using the pulse sequence to be applied for *in vivo* investigations. In 1997, we published a calibration curve

$$R_1(s^{-1}) = 0.074(\pm 0.003) + 0.012(\pm 0.0002)pO_2(\% atm.) \qquad (6)$$

for HFB at 37° and 4.7 T.[177] Considering temperature sensitivity gave

$$R_1(s^{-1}) = 0.77(\pm 0.03) - (0.00009 \pm 0.001)T(°C)$$
$$+ (0.018 \pm 0.003)P(\% atm.) - (0.00017 \pm 0.00008)TP(°C\% \ atm.)$$
$$(7)$$

More recently, we achieved Eq. (5) as a new calibration curve at 37° and 4.7 T using the ARDVARC approach.[160] This calibration curve is based on higher-quality data and provides superior pO_2 estimates. In particular, when tissue is expected to be hypoxic (excised tissue), we find fewer apparently negative pO_2 values.

A major strength of the FREDOM approach is that calibration curves remain valid between samples and across experimental platforms. Calibration curves obtained *in vitro* are valid *in vivo*. Thus we believe other investigators can apply Eq. (5) without the need to establish their own calibrations, provided that studies are undertaken at about 4.7 T and in the range 30–45°. As discussed in an earlier section and Table II, a 1° error in temperature estimates will only introduce a 0.13-torr error in pO_2 estimate, when pO_2 is about 5 torr. We also note that the calibration curves for HFB are relatively insensitive to magnetic field.[111,143]

We have previously investigated microbiodistribution of HFB based on Oil Red O stain, which indicated that HFB occurs as microscopic droplets (1–20 μm) widely distributed across tumor tissue.[175] Significantly, there was no evidence for formation of films, which could act as conduction conduits, causing oxygen equilibration. Occasionally, an animal (viz. tumor) will move slightly during a long time series of measurements. In this case the requirement of consistently high-quality curve fits throughout the data set for individual voxels fails because the tissues have moved relative to the voxel grid. Such motion is immediately apparent when examining the images. There is a choice of eliminating such a data set or relaxing the acceptance criteria and examining pO_2 population distribution without spatial continuity. It is important to recognize that all methods include a degree of sampling. In some approaches, this involves the selective placement and tracking of electrodes; in others, the choice of locations for biopsy and the number of microscopic fields of view. Sampling can be avoided by obtaining global measurements, as commonly acquired using near-infrared approaches, but this may itself mask the fundamental tumor heterogeneity[101] (see Chapter 17 in this volume).

We have previously shown that HFB shows little macroscopic redistribution over a period of hours.[177] It does clear from the tumors with a

typical half-life of HFB of about 600 min, though some tumors show essentially no detectable clearance over a period of 6 h.[143,162] Clearance of HFB precludes long-term studies of chronic oxygenation, unless further doses of HFB are administered.

Comparison of pO_2 distributions using FREDOM or the Eppendorf Histograph has shown close similarity in both small and large tumors.[175] Dynamic studies in several tumor types have shown equivalent behavior when assessed using polarographic oxygen electrodes or OxyLite or FOXY optical probes.[32,43,134] Relative hypoxia has been compared with the histologic reporter pimonidazole, revealing similar trends across tumor types.[137]

Applications of FREDOM

FREDOM has been applied to investigations of diverse tumor types (syngeneic rat prostate and breast tumors and xenograft human lymphomas) with respect to growth and acute interventions.[27,32,134–137,160] Perhaps the greatest strength is the ability to investigate regional dynamic changes in pO_2 accompanying acute interventions. Figure 8 shows changes in regional pO_2 in an AT1 tumor accompanying hyperoxic gas breathing. As published previously,[137,160,162] the areas that were initially better oxygenated responded with elevated pO_2, whereas those relatively hypoxic regions showed little response. Data also may be presented as histograms (Fig. 11), revealing significant differences between mean and median pO_2 and hypoxic fractions between small and large tumors, and between the slow- and fast-growing sublines H and AT1 of the Dunning prostate R3327. Figure 12 shows variation in global mean pO_2 accompanying respiratory challenge with oxygen or carbogen and return to baseline following the intervention. Because individual tumor regions may be observed, local response may be compared at identical locations, efficiently comparing the efficacy of interventions (Fig. 13). Figure 14 shows the differential behavior of regions in undifferentiated Dunning prostate R3327-AT1 tumors versus highly differentiated H tumors. In each tumor type there are both well and poorly oxygenated regions under baseline conditions (see Fig. 11). In response to hyperoxic gas breathing, well-oxygenated regions in both tumor types show a rapid and significant elevation in pO_2, which is reversible when inhaled gas is returned to air (Fig. 14). Poorly oxygenated regions in H tumors respond slowly, but ultimately rise above the range of radiobiologic hypoxia, whereas corresponding regions in AT1 tumors do not. We also have investigated vasoactive drugs[42] and vascular targeting agents,[27] and the short-term changes in pO_2 following irradiation also have been examined.[184] Perhaps the most significant results to date
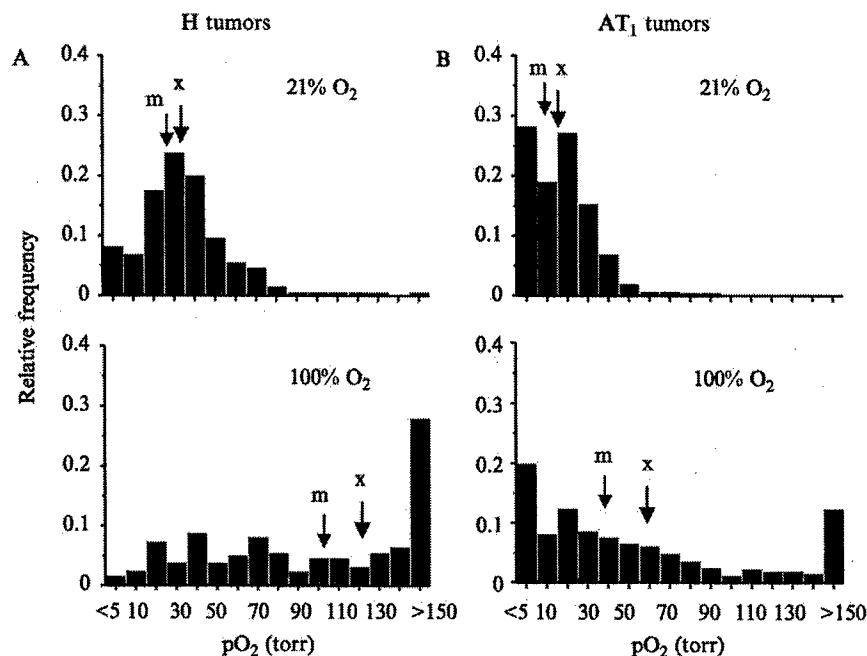
Fig. 11. Histograms of tumor oxygenation pooled for six H (A) and seven AT1 (B) small Dunning prostate R3327 rat tumors. The H tumors (219 voxels) showed significantly higher baseline pO_2 (mean $= 31 \pm 2$ torr, median $= 27$ torr) than the size-matched AT1 tumors (338 voxels; mean $= 14 \pm 1$ torr, median $= 11$ torr; $p < 0.0001$). With respect to oxygen challenge (bottom), mean pO_2 in both groups increased significantly (mean $= 122 \pm 7$ in the H versus, mean $= 58 \pm 4$ in the AT1; $p < 0.0001$). Arrows indicate mean (x) and median (m) pO_2, respectively.

show that pO_2 measurements and detection of changes in pO_2 accompanying interventions correlate with the efficacy of tumor irradiation.[136]

Future

   Ultimately, the value of a technique depends on its robustness, ease of use, and widespread implementation. To date, few laboratories had adopted the FREDOM approach because efficient investigation of HFB requires an unusual NMR pulse sequence. With the recent upgrade of our own instrumentation to the Varian Unity INOVA, the software is

[184] R. P. Mason, S. Hunjan et al., Int. J. Radiat. Oncol. Biol. Phys. 42, 747 (1998).
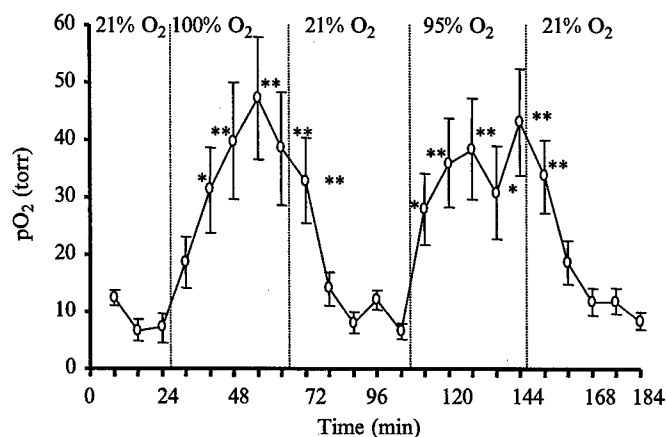
FIG. 12. Dynamic pO_2 (mean ± SE) obtained from sequential maps of the AT1 tumor shown in Fig. 8 with respect to respiratory challenge. *, $p < 0.001$; **, $p < 0.0001$ versus baseline.
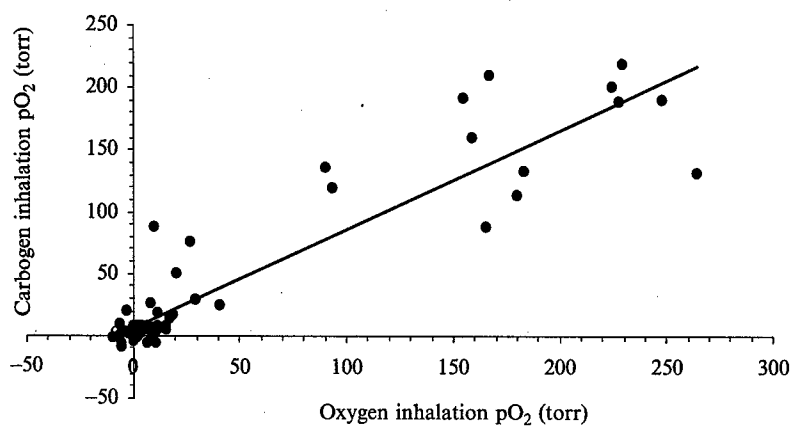
FIG. 13. Correlation between maximum pO_2 detected in each of 56 voxels from the AT1 tumor shown in Fig. 8, when the rat breathed oxygen versus carbogen ($r^2 > 0.85$).

now available on this popular platform, facilitating ready implementation elsewhere. In terms of research applications, it is known that tumor tissue pO_2 varies rapidly in response to many acute interventions, ranging from irradiation to photodynamic therapy, and various chemotherapies. We foresee FREDOM as a valuable tool for assessing the dynamic time course
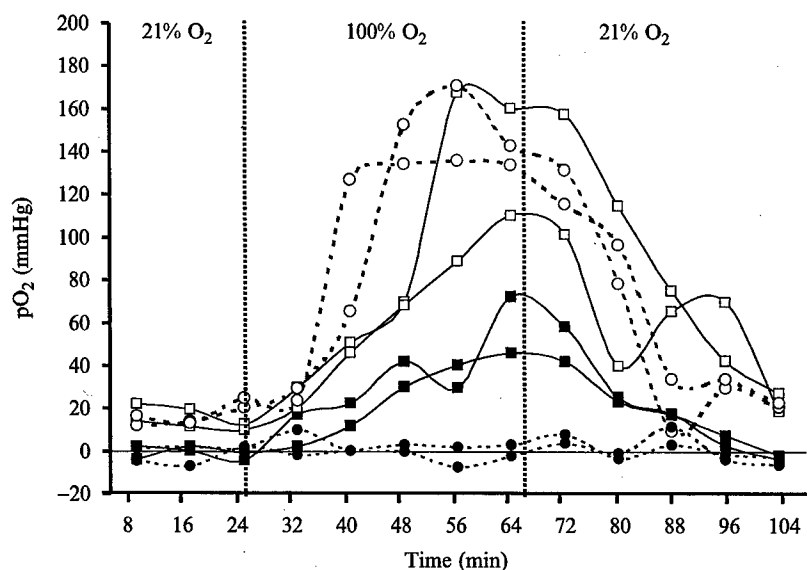
FIG. 14. Variation in pO_2 with respiratory challenge for individual regions chosen as initially well oxygenated ($pO_2 > 10$ torr) or hypoxic ($pO_2 < 5$ torr) from an AT1 (dotted lines) and H (solid lines) tumor, respectively. All the well-oxygenated regions in the two sublines increased significantly in pO_2 in response to oxygen breathing ($p < 0.01$). The hypoxic regions from the H tumor increased, whereas those in the AT1 tumor did not.

of such interventions to provide clear insight into the mode of action of therapeutic approaches and aid in the high-throughput screening of new drugs, such as vascular targeting and antiangiogenic agents.

Acknowledgments

ELSEVIER

BIOLOGY CONTRIBUTION

TUMOR PHYSIOLOGIC RESPONSE TO COMBRETASTATIN A4 PHOSPHATE ASSESSED BY MRI

DAWEN ZHAO, M.D., PH.D., LAN JIANG, M.S., ERIC W. HAHN, PH.D., AND RALPH P. MASON, PH.D.

Department of Radiology, University of Texas Southwestern Medical Center, Dallas, TX

Purpose: To evaluate the effect of the vascular targeting agent, combretastatin A4 phosphate, on tumor oxygenation compared with vascular perfusion/permeability.

Methods and Materials: ^{19}F MRI oximetry and dynamic contrast-enhanced (DCE)-MRI were used to monitor tumor oxygenation and perfusion/permeability in syngeneic 13762NF rat breast carcinoma.

Results: A significant drop was found in the mean tumor pO_2 (23 to 9 mm Hg, $p < 0.05$) within 90 min after treatment (30 mg/kg of combretastatin A4 phosphate) and a further decrease was observed at 2 h (mean 2 mm Hg; $p < 0.01$). The initial changes in pO_2 in the central and peripheral regions were parallel, but by 24 h after treatment, a significant difference was apparent: the pO_2 in the periphery had improved significantly, and the center remained hypoxic. These data are consistent with DCE-MRI, which revealed an ~70% decrease in perfusion/permeability (initial area under signal-intensity curve) at 2 h ($p < 0.001$). The initial area under signal-intensity curve recovered fully after 24 h in a thin peripheral region, but not in the tumor center.

Conclusion: The response observed by DCE-MRI, indicating vascular shutdown, paralleled the pO_2 measurements as expected, but quantitative pO_2 measurements are potentially important for optimizing the therapeutic combination of vascular targeting agents with radiotherapy.   © 2005 Elsevier Inc.

MRI, Vascular targeting agent, Vasculature, Oxygenation, Breast tumor.

INTRODUCTION

Tumor growth, survival, and metastasis depend critically on the development of new blood vessels (1). Therefore, extensive research has focused on developing strategies to attack the tumor vasculature (1, 2). Tubulin-binding agents (e.g., combretastatin A4 phosphate [CA4P] and ZD6126) represent one kind of vascular targeting agent (VTA) (3, 4). Promising preclinical studies have shown that such agents selectively cause tumor vascular shutdown and subsequently trigger a cascade of tumor cell death in experimental tumors (4, 5). Although massive necrosis can be induced, tumors usually regrow from a thin viable rim. Thus, a combination of VTAs with additional conventional therapeutic approaches will be required (6, 7). Several studies involving the combination of VTAs with radiotherapy (8–11) or chemotherapeutic agents (12) have shown enhanced tumor response.

To better understand the mode of action, and hence, optimize such combinations, *in vivo* imaging approaches have been initiated to monitor the physiologic changes resulting from VTA administration (13–15). Dynamic contrast-enhanced (DCE)-MRI based on the transport properties of gadolinium-diethylenetriamine pentaacetic acid (Gd-DTPA) is the most commonly used imaging approach to study tumor vascular perfusion and permeability. DCE-MRI was included as part of the Phase I clinical trials of CA4P (16, 17). The results of preclinical and clinical DCE-MRI studies have shown a reversible change in vascular perfusion in the tumor periphery after a single dose of VTA (18–21). For combination with radiotherapy, measurement of tumor oxygen dynamics will be especially important, because reduced perfusion can induce hypoxia, potentially modulating the radiation response. A number of studies have reported an improved response when administering VTAs after radiotherapy, with the enhancement reduced or lost, if VTAs were administered before radiotherapy, implying increased hypoxia induced by VTAs (8, 10). Direct measurements of tissue pO_2 using the Eppendorf electrode, conducted by Horsman *et al.* (22, 23), found increased hypoxia 3 h after CA4P or ZD6126 administration. We have

developed a method for measuring tumor oxygenation and dynamics based on ^{19}F nuclear magnetic resonance echo planar imaging after direct intratumoral injection of the reporter molecule hexafluorobenzene (HFB) called "fluorocarbon relaxometry using echo planar imaging for dynamic oxygen mapping" (FREDOM) (24, 25). This technique provides pO$_2$ measurements at multiple specific locations simultaneously within a tumor and reveals the dynamic changes at individual locations with respect to interventions. We have previously evaluated the tumor oxygen response to varying interventions such as hyperoxic gas breathing (26, 27). We also had an anecdotal example of pO$_2$ response to a tumor-selective infarcting agent (28). We have now applied both DCE-MRI and FREDOM to evaluate tumor perfusion/permeability and oxygen dynamics in response to CA4P in conjunction with confirmatory histologic examination.

METHODS AND MATERIALS

Tumor model

Rat mammary carcinoma 13762NF was implanted syngeneically in a skin pedicle surgically created on the fore back of Fisher 344 adult female rats ($n = 25$, ~150 g, Harlan), as previously described in detail (29). Of the 25 rats, 9 were used for DCE-MRI, 10 for FREDOM, and 6 for histologic study. The Institutional Animal Care and Use Committee approved the investigations.

Drug preparation and dosing

CA4P was provided by OXiGENE (Waltham, MA). CA4P was dissolved in 0.9% saline at a concentration of 30 mg/mL before each experiment. A single dose of 30 mg/kg CA4P was chosen for this study, because it is considered a clinically relevant dose (18).

MRI experiments

When tumors reached ~1 cm diameter (~0.6 cm^3), MRI was performed using a 4.7 T horizontal bore magnet with a Varian Unity Inova system. Each rat was given intraperitoneal ketamine hydrochloride (120 μL; 100 mg/mL, Aveco, Fort Dodge, IA) as a relaxant and maintained under general anesthesia (air and 1% isoflurane, Baxter International, Deerfield, IL). A 27-gauge butterfly catheter (Abbott Laboratories, Abbott Park, IL) was placed intraperitoneally for infusion of CA4P or saline alone. For DCE-MRI, a tail vein was catheterized using a second 27-gauge butterfly catheter for contrast agent administration. For oximetry, hexafluorobenzene (50 μL, Lancaster, Gainesville, FL) was injected directly into the tumor along two or three tracks in a single central plane of the tumor, coronal to the rat's body using a Hamilton syringe (Reno, NV) with a custom-made, fine, sharp needle (32-gauge), as previously described in detail (25). A tunable (^{1}H/^{19}F) volume radiofrequency (RF) coil was placed around the tumor-bearing pedicle. Each animal was placed on its side in the magnet with no change in position during the whole study, so that individual regions could be tracked. A thermal blanket was used to maintain body temperature.

^{1}H DCE-MRI

Nine tumor-bearing rats were studied before CA4P injection ($n = 6$) or saline alone ($n = 3$) and 2 and 24 h after treatment. On each occasion, a series of T$_1$-weighted spin echo images (TR 160 ms, TE 16 ms, field of view 40 × 40 mm, matrix 128 × 128, voxel size 2.0 × 0.3 × 0.3 mm, total time for 3 slices 23 s) was acquired before and after a bolus injection of Gd-DTPA-BMA (injection within 1 s; 0.1 mmol/kg, Omniscan, Amersham Health, Princeton, NJ) on three 2-mm-thick cross-sections parallel to the animal. Data were processed on a voxel-by-voxel basis using software written by us using Interactive Data Language (IDL), version 5.3/5.4 (Research Systems, Boulder, CO). For each slice, the tumor was separated into central and peripheral regions. The tumor periphery was taken to be a 1–2-mm-thick rim aligned around the whole tumor. Signal intensity vs. time curves were plotted and relative signal intensity changes (ΔSI) of each tumor voxel were analyzed using the equation: $(\Delta SI) = (SI_E - SI_b)/SI_b$, where SI_E refers to the enhanced signal intensity in the voxel and SI_b is defined as the average of the baseline images. The area under the normalized signal intensity-time curve (IAUC) for the first 1.5 min after Gd-DTPA-BMA injection was integrated.

^{19}F tumor oximetry—FREDOM

A separate cohort of 10 tumors (7 treated and 3 controls) was used for pO$_2$ measurement. A single 4-mm slice parallel to the rat body containing the strongest fluorine signal was chosen for the ^{19}F MRI pO$_2$ studies. ^{1}H and ^{19}F MR images were acquired using a spin-echo sequence. Overlaying the ^{19}F MR image on the corresponding ^{1}H image revealed the distribution of HFB. After conventional MRI, tumor oxygenation was estimated on the basis of ^{19}F pulse burst saturation recovery echo planar imaging relaxometry of the HFB, as previously described (24). This approach provided pO$_2$ maps with 1.25 mm in plane resolution and 6-μL voxel size in 6.5 min. The spin-lattice relaxation rate [R1 (s^{-1}) = 1/T1] was estimated on a voxel-by-voxel basis using a three-parameter monoexponential function. pO$_2$ was estimated using the relationship pO$_2$ mm Hg = (R1 − 0.0835)/0.001876 (24). The data are presented in bins of 5 mm Hg, except for the highest and lowest bins, which were open ended. Before CA4P or saline injection, a series of pO$_2$ maps was acquired with respect to respiratory challenge with oxygen: typically, two baseline measurements, three with oxygen and four on return to air. Immediately after the last (fourth) air measurement, CA4P (30 mg/kg) or saline (0.15 mL) was injected intraperitoneally. An additional series of pO$_2$ maps was acquired after 10, 30, 60, 90, and 120 min, and finally another three maps while breathing oxygen. The 24 h follow-up study comprised two measurements with air and four with oxygen. The oxygen challenge was included to evaluate vascular function.

Markers of vascular perfusion and endothelium

Six animals were used to study the total blood vessels and perfused vessels before ($n = 2$), 2 h ($n = 2$), and 24 h ($n = 2$) after CA4P. The blue fluorescent dye Hoechst 33342 (Molecular Probes, Eugene, OR) was injected into the tail vein of the anesthetized rats at a concentration of 10 mg/kg in 0.9% saline (0.1 mL), and the tumors were excised 1 min later. Tumor specimens were immediately immersed in liquid nitrogen and then stored at −80°C. Immediately after cryostat sectioning (6 μm thick), the slices were imaged for Hoechst 33342 under ultraviolet wavelength (330–380 nm). Perfused vessels were determined by counting the total number of structures stained by Hoechst 33342 in four fields per section selected to show high perfusion and calculating

the mean number of vessels per millimeter squared. On the following day, the same slices, as well as their adjacent slices, were immunostained for the endothelial marker, CD31. A primary mouse anti-rat CD31 monoclonal antibody (1:20 dilution, Serotec, Raleigh, NC) was added and incubated for 2 h at 37°C in a humid box. The slides were incubated with Cy3-conjugated goat anti-mouse secondary antibody (1:100 dilution, Jackson Immunoresearch Laboratories, West Grove, PA) for 1 h at 37°C. After mounting with Vectorshield medium (Vector Laboratories, Burlingame, CA), the slides were observed under red fluorescence (530–550 nm excitation) to detect anti-CD31 and then the corresponding Hoechst 33342 again under ultraviolet light. Image analysis was performed using Metaview software (Universal Imaging, West Chester, PA).

Statistical analysis

Statistical significance was assessed using analysis of variance on the basis of Fisher's Protected Least Significant Difference (StatView, SAS Institute, Cary, NC) or Student's t tests.

RESULTS

DCE-MRI findings

Baseline ^{1}H MRI showed stable signal throughout the tumor (not shown). Immediately after a bolus injection of Gd-DTPA-BMA, the signal intensity increased significantly, reaching a peak after 23–69 s, and then gradually decreasing toward baseline. The maximal signal enhancement averaged over the whole tumor in all three slices ranged from ~52% to 85% for the nine tumors.

A single dose of CA4P 30 mg/kg caused a dramatic decrease in signal enhancement at the 2 h point, and a 24 h follow-up image showed signal recovery in a thin tumor rim, as shown for a representative tumor (Fig. 1). Distribution of the IAUC values showed a distinct shift to the left at both 2 and 24 h after treatment (Fig. 1b). The highly enhancing fraction (IAUC >1.5) at 24 h after CA4P reached the pretreatment level, indicating complete recovery in the tumor periphery (Fig. 1b). For all six tumors treated with
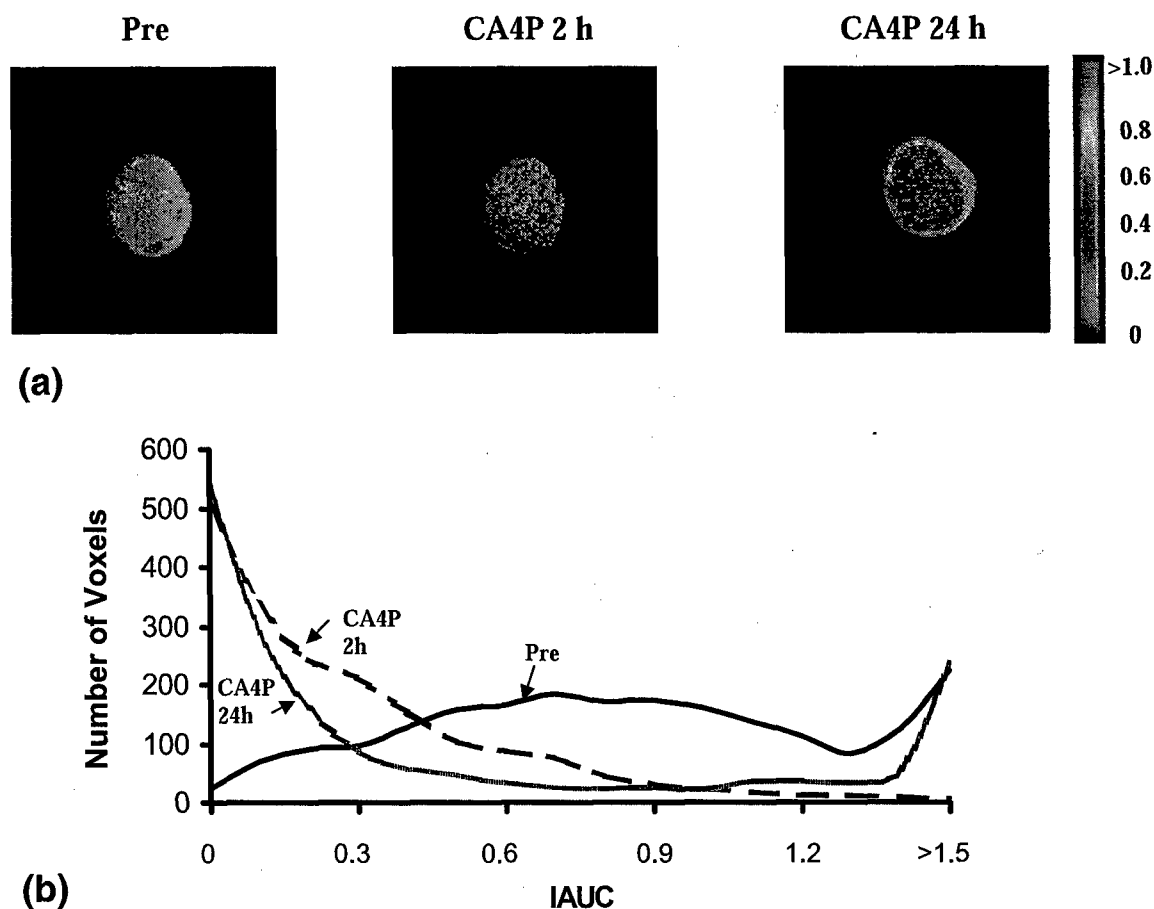
Fig. 1. Dynamic contrast-enhanced-magnetic resonance imaging (DCE-MRI) performed before, 2 h, and 24 h after treatment with CA4P (30 mg/kg). Series of T_1-weighted contrast-enhanced images acquired at these times with respect to infusion of bolus injection of contrast agent. (a) Normalized images of signal enhancement 23 s after contrast agent administration shown for representative tumor. Significantly less signal enhancement was observed for whole tumor region 2 h after treatment. Full recovery is apparent in tumor rim 24 h after treatment. (b) Based on serial images obtained with respect to contrast agent infusion, Initial area under signal-intensity curve (IAUC) was calculated on voxel-by-voxel basis. Frequency distribution of IAUC values is shown. Distributions at 2 and 24 h showed significant increases in number of voxels with no signal enhancement (IAUC <0.05). However, frequency of highly enhancing voxels (IAUC >1.5) at 24 h recovered to pretreatment level.

CA4P, a significant decrease in IAUC was observed for the whole tumor region at 2 h: the tumor peripheral and central region was reduced by 65% and 70%, respectively (p <0.05; Table 1). A complete recovery in IAUC for the tumor periphery was seen 24 h after treatment, but the tumor center remained low (Table 1). IAUC frequency data from these six tumors also showed a significant increase in the number of nonenhancing voxels (IAUC <0.05), and the percentage of voxels with IAUC >0.5 decreased from 55% to 5% 2 h after administration of CA4P (p <0.05, Table 2). In control tumors treated with saline, the IAUC was similar at all points (Tables 1 and 2).

Tumor oximetry—FREDOM

Overlay of ^{19}F on ^{1}H image (Fig. 2a) confirmed that HFB was distributed in both peripheral and central regions of a central plane of the tumor. In the series of echo planar imaging relaxation data sets, typically ~40–100 voxels provided an R1 fit, and potential pO_2 value. Because noise may give an apparent relaxation curve (R1) fit, data were selected by applying thresholds of T1 error <2.5 s and T1 error/T1 ratio <50%. Only those voxels, which provided consistently reliable data throughout the time course, were included for additional analysis. As an example (Fig. 2b), 25 voxels qualified for all these prerequisites and could be followed through the 17 measurements from baseline to 2 h after CA4P. At 24 h, 31 voxels were traceable through the six measurements with respiratory challenge. As expected, on the basis of the distribution of HFB (Fig. 2a), each pO_2 map (Fig. 2b) comprised two distinct groups of voxels, representing the peripheral and central location of HFB, respectively. Variations in the mean pO_2 with respect to intervention for these two groups of voxels are presented separately in Fig. 2c. Before CA4P administration, the mean pO_2 was 45 mm Hg in the tumor periphery and 36 mm Hg in the center during air breathing. Both regions responded significantly to oxygen breathing (p <0.05), and this was reversed on return to air breathing. A significant decrease in pO_2 was detected as early as 30 min after CA4P administration in the tumor periphery and by 60 min in the center (p

<0.05). The decline continued with the lowest pO_2 values (13 mm Hg and 10 mm Hg) at the 2-h point. At this time, oxygen challenge no longer produced an increase in pO_2 for either region. At 24 h later, the peripheral pO_2 had increased significantly (24 mm Hg), but was still significantly lower than the pretreatment value (p <0.05). After 24 h, pO_2 again responded significantly to breathing oxygen in the tumor periphery (p <0.01). However, pO_2 in the central regions (4 mm Hg) was even lower at 24 h than at 2 h and did not respond to oxygen breathing. Histograms of pooled voxels assessed for the seven tumors showed significantly decreased pO_2 at 1, 2, and 24 h after treatment (p <0.01). The hypoxic fraction <5 mm Hg (HF_5) increased significantly from a pretreatment value of 21% to 36% at 1 h and 68% at 2 h, but was only 34% at 24 h (Fig. 3). For the seven treated tumors, two tumors showed a significant decrease in pO_2 as early as 30 min after treatment (p <0.05). A significant decrease in the mean pO_2 for the group was found at 90 min after CA4P (23 ± 5 vs. 9 ± 3 mm Hg; p <0.05) and a further decrease at 2 h (2 ± 2 mm Hg; Table 3). The mean pO_2 increased significantly to 15 ± 4 mm Hg at 24 h compared with 2 h (p <0.05). For the control tumors, no significant differences in pO_2 were found among any of the measurements (before and 2 or 24 h after).

Histologic examination and immunohistochemistry

On the basis of the perfusion assessed by distribution of Hoechst 33342, a significant decrease in the number of perfused vessels was evident at 2 h (21 ± 6/mm^2 vs. 145 ± 23/mm^2 pre-CA4P, p <0.01), followed by recovered perfusion at 24 h (114 ± 19/mm^2). Comparisons of perfused vessels marked by Hoechst 33342 and with the total vessels labeled by anti-CD31 before and 2 and 24 h after CA4P are shown in Fig. 4.

DISCUSSION

In common with previous reports in the literature (15, 18), CA4P caused a significant reduction in tumor perfusion within 2 h. DCE-MRI showed that the IAUC in the tumor

Table 1. Normalized IAUC by DCE-MRI

	Mean IAUC		
Group	Baseline	2 h	24 h
CA4P (n = 6) (30 mg/kg)			
Periphery	0.88 ± 0.06	0.31 ± 0.08‡	0.86 ± 0.06
Center	0.44 ± 0.11†	0.13 ± 0.08‡	0.12 ± 0.05*†‡
Control (n = 3) (saline)			
Periphery	1.09 ± 0.04	0.93 ± 0.13	0.86 ± 0.05
Center	0.52 ± 0.19†	0.46 ± 0.05†	0.44 ± 0.03†

Abbreviations: IAUC = initial area under signal-intensity curve; DCE = dynamic contrast enhanced; CA4P = combretastatin A4 phosphate.

* p <0.05 from baseline.

† p <0.05 from periphery.

‡ p <0.05 from control.

Table 2. Comparison of weakly (IAUC <0.05) and strongly (IAUC >0.05) responding voxels with respect to DCE-MRI and drug administration

Group	IAUC	Total voxels (%)		
		Baseline	2 h	24 h
CA4P (n = 6) (30 mg/kg)	<0.05	16	54*†	41*†
	>0.5	55	5*†	32*†
Control (n = 3) (saline)	<0.05	14	15	19
	>0.5	62	58	51

Individual voxels (total = 10,508 in CA4P vs. 5376 in control) categorized according to IAUC.

Abbreviations as in Table 1.

* p <0.01 from baseline.

† p <0.05 from control.

periphery was reduced 70% 2 h after a single dose of CA4P (30 mg/kg), followed by a full recovery by 24 h. However, the drop in the IAUC of the tumor center was not reversible (Table 1). The IAUC reflects tumor blood flow, vascular permeability, and a fraction of interstitial space. Histologic data using the perfusion marker, Hoechst 33342, confirmed a significant decrease in perfused vessels 2 h after CA4P, with recovery evident at 24 h (Fig. 4).

Vascular shutdown induced by VTA is expected to decrease tumor pO_2. Horsman et al. (23) recently reported that tumor pO_2, measured by Eppendorf electrode, was significantly decreased 3 h after ZD6126. In line with that study, ^{19}F MRI oximetry showed that CA4P caused a significant decrease in pO_2 within 90 min and a further reduction within 2 h. As for perfusion, pO_2 recovered toward pretreatment levels after 24 h in the tumor periphery (Fig. 2C).

Although VTAs cause vascular shutdown and lead to extensive hemorrhagic tumor necrosis, rapid tumor regrowth occurs from the surviving rim. Many preclinical studies have shown that a single dose of VTA is associated with very little tumor growth delay (4, 5, 23). Thus, a combination with other therapeutic modalities (e.g., radiotherapy and conventional chemotherapy) will be needed to achieve complete control. The rationale for such combinations is that VTAs target the poorly perfused and relatively hypoxic regions of the central tumor, and conventional therapy is applied to attack the relatively better oxygenated, highly proliferating rim. A critical issue regarding such combinations is the timing and sequencing of the agents. Thus, a primary goal of this study was to monitor longitudinal pO_2 changes after CA4P to facilitate and potentially optimize such combinations. Others have demonstrated enhanced therapeutic efficacy by combining CA4P, ZD6126, or 5,6-dimethylxanthenone-4-acetic acid (DMXAA) with radiotherapy (8–11), radioimmunotherapy (30), or chemotherapy (12). In the study of combined ZD6126 with radiotherapy, Siemann and Rojiani (8) reported increased tumor cell kill by administering drug immediately (30 min to 1 h) after a single radiation dose compared with administering the drug 24 h or 1 h before. This observation coincides with our present findings that tumor pO_2 declined 1 h after drug

administration and had not recovered fully at 24 h (Figs. 2C and 3).

Oxygen challenge before and after treatment was used to compare vascular function in this study. In common with our previous observations (31, 32), oxygen breathing significantly increased tumor oxygenation in mammary carcinoma 13762NF under control conditions (Fig. 2 and Table 3). The pO_2 response to CA4P was equally effective in the peripheral and central regions through 2 h after administration (Fig. 2C). pO_2 decreased in both regions within 30 min and continued to decrease for 2 h. Differential behavior with respect to oxygen challenge between the peripheral and central tumor regions was observed only after 24 h. At 24 h, pO_2 in the tumor center was even lower than the pretreatment baseline or the 2-h level and showed no response to oxygen inhalation (Fig. 2). However, oxygen breathing produced a significant increase in pO_2 of the peripheral region, even though the pO_2 was significantly lower than before treatment (Fig. 2). These observations provide further evidence that CA4P at 30 mg/kg induces irreversible vascular damage in the tumor center, and peripheral vessels survived and were functional by 24 h. One would expect that hypoxia modifiers (e.g., oxygen breathing), if given 24 h after CA4P, might improve tumor radiosensitivity.

Hypoxia in solid tumors has been widely recognized as a potent factor that leads to resistance to radiotherapy and some anticancer drugs (33). Recently, increasing evidence has shown that tumor malignant progression may be associated with a hypoxic microenvironment (34, 35). Given the importance of oxygen, many techniques for monitoring pO_2 have been developed (25, 36). Although each method has specific attributes, many are highly invasive and impractical for longitudinal studies of specific regions of interest. The Eppendorf has been considered the gold standard for pO_2 measurement, but it is not suitable for a longitudinal study of the type reported here. In vivo, proton MRI (e.g., DCE-MRI and blood oxygen level-dependent MRI) provides a noninvasive approach to assess tumor vasculature, particularly useful in response to interventions, but neither DCE nor blood oxygen level-dependent MRI provides a straightforward correlation with pO_2 (37, 38). FREDOM not only provides pO_2 values simultaneously at multiple specific locations within a tumor, but also reveals dynamic changes at individual locations with respect to interventions.

Central necrosis develops in 13762NF tumors even at a small size and becomes substantial when tumors become bigger, which has been confirmed previously by histologic examination (32). In some of the tumors used in this study, a low-intensity central region was observed in T_1-weighted images, in which little enhancement was noted after infusion of the contrast agent. After treatment with CA4P, the area of these regions of low-signal intensity increased slightly (data not shown). A similar observation was reported by Beauregard et al. (39) in human colon carcinoma xenograft. In common with our previous study of 13762NF tumors (31, 32), we found considerable intratumoral heterogeneity in the distribution of pO_2 values, ranging from
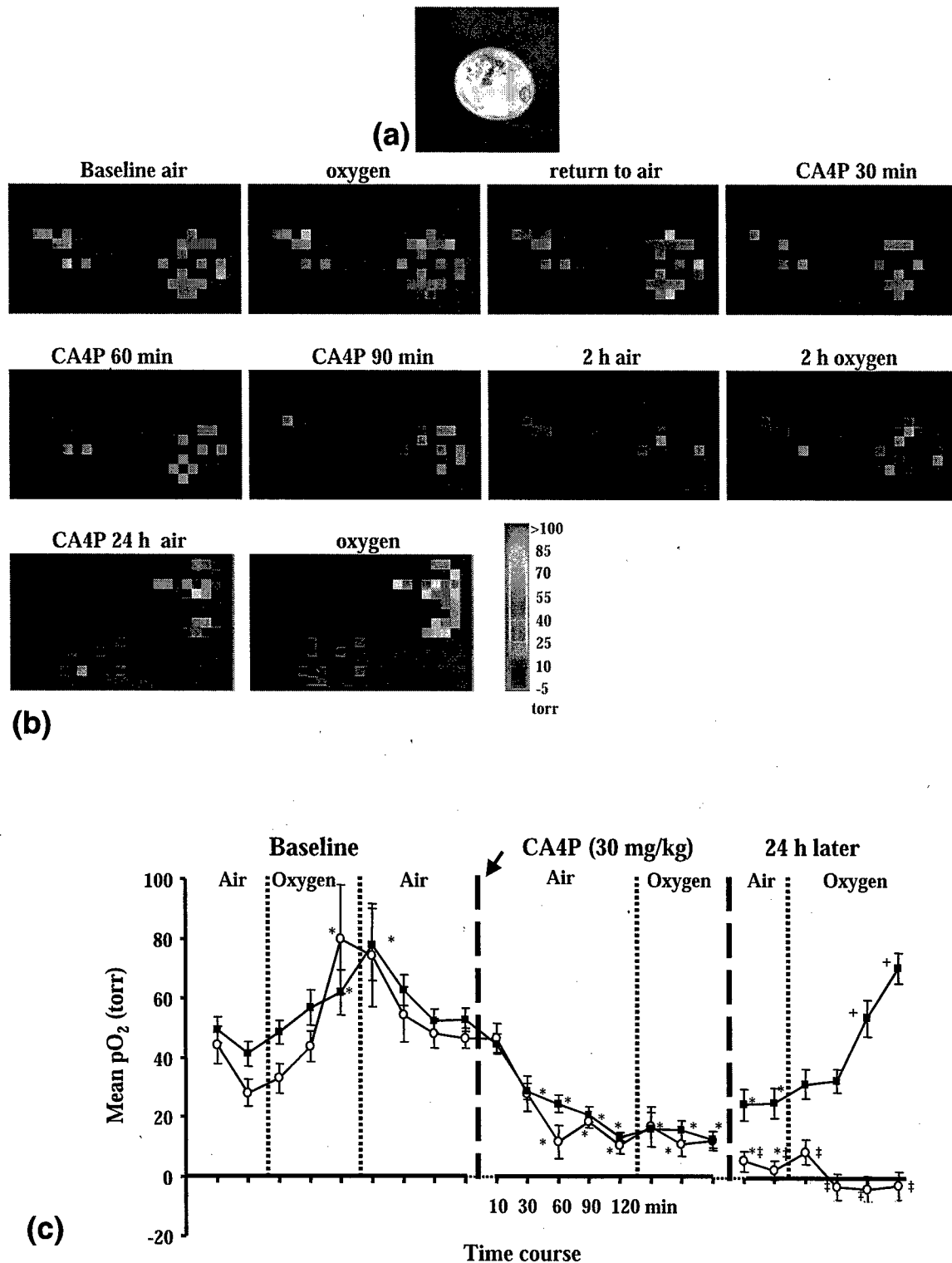
Fig. 2. (a) Distribution of hexafluorobenzene (HFB) in representative tumor (No. 4 in Table 3). Overlay of ^{19}F signal density on anatomic image indicates HFB in both peripheral and central regions. (b) pO_2 maps obtained from same tumor comprise two separated groups of voxels that correspond to locations of HFB on anatomic image; 25 individual voxels were traceable from pretreated baseline to 2 h after CA4P with oxygen breathing; and 31 voxels could be followed 24 h after treatment. Significant decrease in pO_2 was evident for all individual voxels after CA4P. pO_2 did not respond to oxygen inhalation after 2 h; 24-h maps showed improved pO_2 and significant response to oxygen breathing in peripheral region (right), but not in central region (left). (c) Mean pO_2 curves shown for peripheral (black squares) and central (white circles) voxels of tumor. $*p < 0.05$ from baseline air, $^+p < 0.05$ from 24-h air, $^‡p < 0.05$ from periphery.
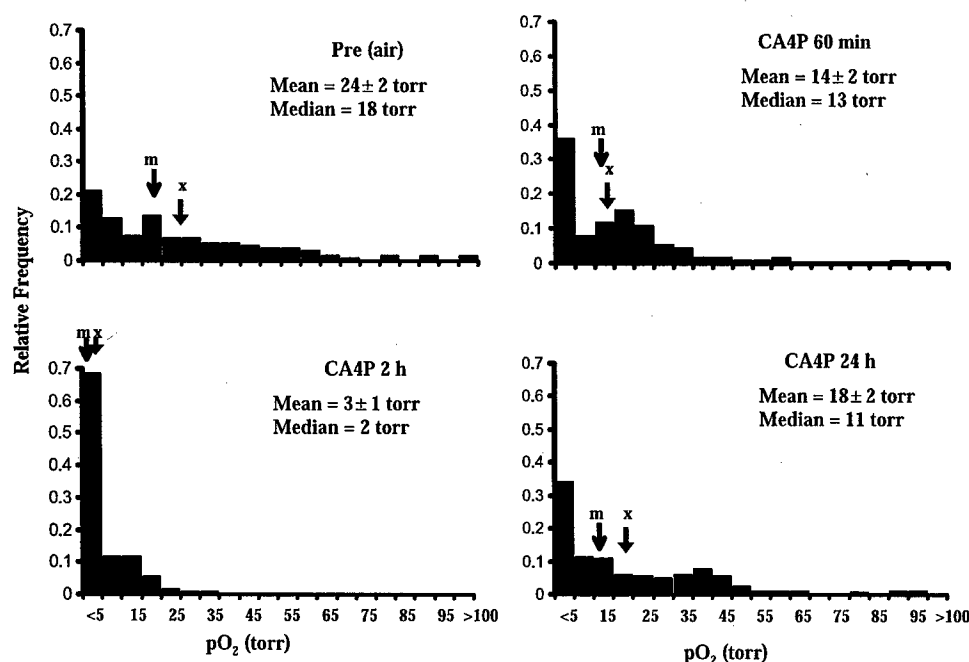
Fig. 3. pO_2 histograms based on relative numbers of voxels in seven tumors showing left shift after CA4P. Ordinate ranges (e.g., 15 refers to 10 mm Hg $\leq pO_2 <$ 15 mm Hg). x = mean; m = median.

hypoxic to well oxygenated. Compared with our previous data on 13762NF tumors, we found the average baseline pO_2 values were lower in the present study (mean 25 mm Hg vs. 63 mm Hg). This difference likely resulted from an altered anesthesia protocol, because we now use a baseline of air/isoflurane, instead of 33% oxygen in nitrous oxide with metafane (32). However, oxygen challenge produced a remarkably similar extent of increase in pO_2 values observed in both studies (72 mm Hg vs. 73 mm Hg).

Previous studies showed little macroscopic redistribution

of HFB during a period of hours (40), but it did clear from the tumors with a typical half-life about 600 min (41). The clearance of HFB normally precludes chronic long-term studies of oxygenation, unless additional doses of HFB are administered. For all three control tumors in this study, additional HFB (50 μL) was required for the 24-h follow-up study. However, no additional HFB was required for studies 24 h after CA4P, presumably owing to vascular shutdown.

These results provide the first insight into regional tumor oxygen dynamics in response to CA4P in a syngeneic rat

Table 3. Tumor oxygen dynamics assessed by ^{19}F MRI with respect to CA4P treatment

| Group	Case No.	Size (cm³)	Baseline air	Time course post CA4P						
				30 min	60 min	90 min	2 h	Oxygen	24 h base	Oxygen
CA4P (30 mg/kg)	1	2.0	36 ± 1	NA	NA	NA	2 ± 3*	5 ± 2*	NA	NA
(n = 7)	2	0.9	12 ± 2	NA	NA	NA	−3 ± 2*	−3 ± 2*	NA	NA
	3	1.2	13 ± 0	35 ± 11	11 ± 3	9 ± 4	1 ± 2*	2 ± 2*	5 ± 0*	30 ± 6†
	4	0.7	43 ± 5	29 ± 3*	21 ± 3*	20 ± 2*	13 ± 1*	16 ± 5*	20 ± 2*	48 ± 7†
	5	0.4	12 ± 2	5 ± 3*	9 ± 3	4 ± 2*	2 ± 1*	7 ± 3*	NA	NA
	6	0.7	15 ± 1	19 ± 3	9 ± 2*	4 ± 2*	1 ± 2*	0 ± 3*	12 ± 1	73 ± 12†
	7	0.3	28 ± 6	29 ± 2	16 ± 4	6 ± 2*	1 ± 1*	7 ± 2*	23 ± 2*	79 ± 6†
	Mean	0.9 ± 0.2	23 ± 5	23 ± 13	13 ± 5	9 ± 3*	2 ± 2*	5 ± 3*	15 ± 4	58 ± 11†
Saline (n = 3)	8	0.6	34 ± 2	47 ± 5	40 ± 5	36 ± 10	31 ± 8	88 ± 10*	37 ± 0	86 ± 5†
	9	0.2	47 ± 2	62 ± 8	65 ± 6	64 ± 5	61 ± 4	114 ± 8*	67 ± 1	159 ± 7†
	10	0.6	13 ± 1	16 ± 6	10 ± 4	9 ± 4	12 ± 6	35 ± 10*	14 ± 1	78 ± 15†
	Mean	0.5 ± 0.1	31 ± 10	42 ± 14	38 ± 16	36 ± 16	35 ± 14	79 ± 23*	39 ± 15	108 ± 26†

Abbreviations: NA = no measurement; other abbreviations as in Table 1.
Data presented as mean ± SE.
* p <0.05 from baseline.
† p <0.05 from 24 h air (24 h after injection of CA4P).
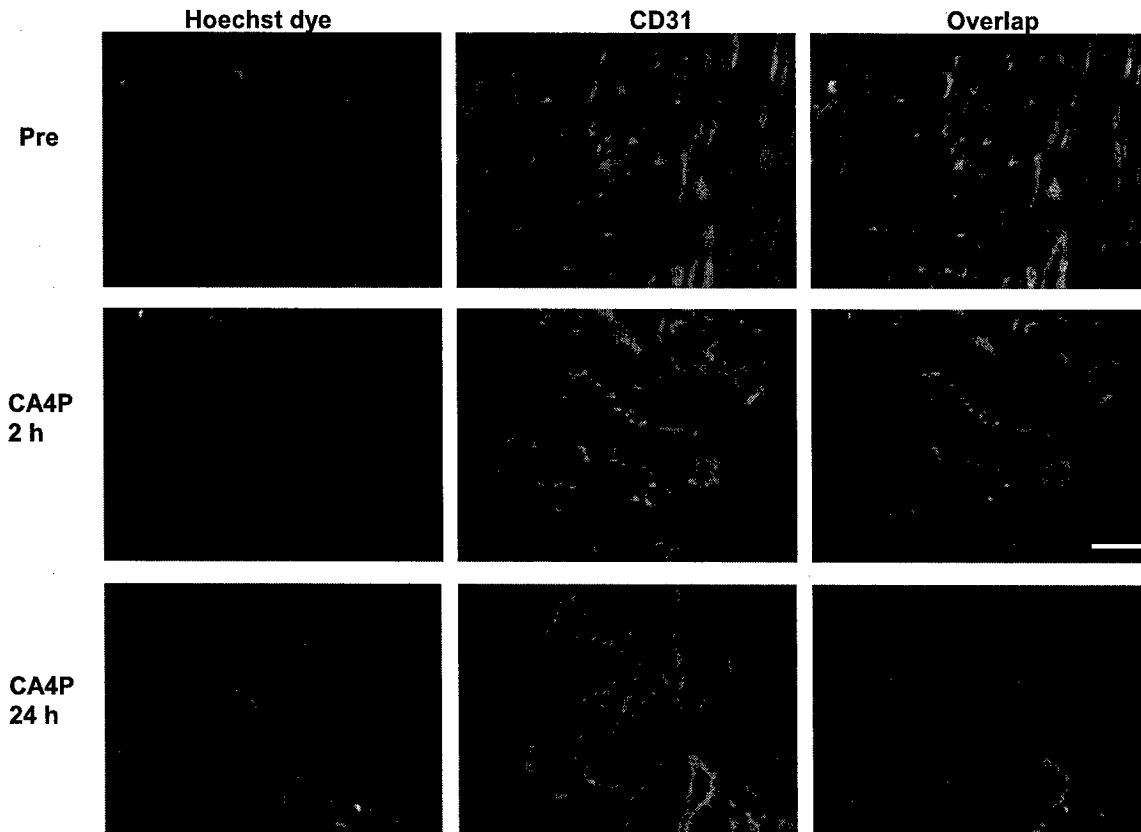
Hoechst dye	CD31	Overlap

Fig. 4. Perfusion marker Hoechst staining before, 2 h, and 24 h after CA4P (left). Vascular endothelium of same field immunostained by anti-CD31 (red, middle). Good match (right) between Hoechst and anti-CD31–stained vascular endothelium found in pretreated tumor. Significant reduction in perfused vessels detected 2 h after treatment followed by a recovery at 24 h. Bar = 100 μm.

tumor. A distinct similarity was noted between the results of the pO_2 measurements and the more traditional DCE, but the quantitative pO_2 values provide the potential for exploiting synergy with other oxygen-dependent therapies. The observations also demonstrate the value of FREDOM in assessing dynamic changes in regional tumor pO_2 *in vivo* in

response to intervention. We believe that dynamic measurements are particularly valuable for understanding the mode of action of therapeutic response to VTAs. Most significantly, these measurements lay a foundation to optimize the timing of combination therapy involving fractionated radiotherapy and multiple doses of VTAs.

REFERENCES

1. Folkman J. Anti-angiogenesis: New concept for therapy of solid tumors. *Ann Surg* 1972;175:409–416.
2. Denekamp J. Vascular attack as a therapeutic strategy for cancer. *Cancer Metastasis Rev* 1990;9:267–282.
3. Pettit GR, Temple C Jr, Narayanan VL, *et al.* Antineoplastic agents 322. synthesis of combretastatin A-4 prodrugs. *Anticancer Drug Des* 1995;10:299–309.
4. Davis PD, Dougherty GJ, Blakey DC, *et al.* ZD6126: A novel vascular-targeting agent that causes selective destruction of tumor vasculature. *Cancer Res* 2002;62:7247–7253.
5. Dark GG, Hill SA, Prise VE, *et al.* Combretastatin A-4, an agent that displays potent and selective toxicity toward tumor vasculature. *Cancer Res* 1997;57:1829–1834.
6. Siemann DW, Warrington KH, Horsman MR. Targeting tumor blood vessels: An adjuvant strategy for radiation therapy. *Radiother Oncol* 2000;57:5–12.
7. Thorpe PE, Chaplin DJ, Blakey DC. The first international conference on vascular targeting: Meeting overview. *Cancer Res* 2003;63:1144–1147.

8. Siemann DW, Rojiani AM. Enhancement of radiation therapy by the novel vascular targeting agent ZD6126. *Int J Radiat Oncol Biol Phys* 2002;53:164–171.
9. Murata R, Siemann DW, Overgaard J, *et al.* Interaction between combretastatin A-4 disodium phosphate and radiation in murine tumors. *Radiother Oncol* 2001;60:155–161.
10. Murata R, Siemann DW, Overgaard J, *et al.* Improved tumor response by combining radiation and the vascular-damaging drug 5,6-dimethylxanthenone-4-acetic acid. *Radiat Res* 2001; 156:503–509.
11. Li L, Rojiani AM, Siemann DW. Preclinical evaluations of therapies combining the vascular targeting agent combretastatin A-4 disodium phosphate and conventional anticancer therapies in the treatment of Kaposi's sarcoma. *Acta Oncol* 2002; 41:91–97.
12. Siemann DW, Rojiani AM. Antitumor efficacy of conventional anticancer drugs is enhanced by the vascular targeting agent ZD6126. *Int J Radiat Oncol Biol Phys* 2002;54:1512–1517.

13. Tozer GM, Prise VE, Wilson J, et al. Combretastatin A-4 phosphate as a tumor vascular-targeting agent: Early effects in tumors and normal tissues. Cancer Res 1999;59:1626–1634.

14. Kragh M, Quistorff B, Horsman MR, et al. Acute effects of vascular modifying agents in solid tumors assessed by noninvasive laser Doppler flowmetry and near infrared spectroscopy. Neoplasia 2002;4:263–267.

15. Goertz DE, Yu JL, Kerbel RS, et al. High-frequency Doppler ultrasound monitors the effects of antivascular therapy on tumor blood flow. Cancer Res 2002;62:6371–6375.

16. Rustin GJ, Galbraith SM, Anderson H, et al. Phase I clinical trial of weekly combretastatin A4 phosphate: Clinical and pharmacokinetic results. J Clin Oncol 2003;21:2815–2822.

17. Galbraith SM, Maxwell RJ, Lodge MA, et al. Combretastatin A4 phosphate has tumor antivascular activity in rat and man as demonstrated by dynamic magnetic resonance imaging. J Clin Oncol 2003;21:2831–2842.

18. Prise VE, Honess DJ, Stratford MR, et al. The vascular response of tumor and normal tissues in the rat to the vascular targeting agent, combretastatin A-4-phosphate, at clinically relevant doses. Int J Oncol 2002;21:717–726.

19. Robinson SP, McIntyre DJ, Checkley D, et al. Tumour dose response to the antivascular agent ZD6126 assessed by magnetic resonance imaging. Br J Cancer 2003;88:1592–1597.

20. McIntyre DJ, Robinson SP, Howe FA, et al. Single dose of the antivascular agent, ZD6126 (N-acetylcolchinol-O-phosphate), reduces perfusion for at least 96 hours in the GH3 prolactinoma rat tumor model. Neoplasia 2004;6:150–157.

21. Padhani AR. MRI for assessing antivascular cancer treatments. Br J Radiol 2003;76(Spec No 1):S60–S80.

22. Horsman MR, Ehrnrooth E, Ladekarl M, et al. The effect of combretastatin A-4 disodium phosphate in a C3H mouse mammary carcinoma and a variety of murine spontaneous tumors. Int J Radiat Oncol Biol Phys 1998;42:895–898.

23. Horsman MR, Murata R. Vascular targeting effects of ZD6126 in a C3H mouse mammary carcinoma and the enhancement of radiation response. Int J Radiat Oncol Biol Phys 2003;57:1047–1055.

24. Hunjan S, Zhao D, Constantinescu A, et al. Tumor oximetry: Demonstration of an enhanced dynamic mapping procedure using fluorine-19 echo planar magnetic resonance imaging in the Dunning prostate R3327-AT1 rat tumor. Int J Radiat Oncol Biol Phys 2001;49:1097–1108.

25. Zhao D, Jiang L, Mason RP. Measuring changes in tumor oxygenation. Methods Enzymol 2004;386:378–418.

26. Zhao D, Constantinescu A, Hahn EW, et al. Differential oxygen dynamics in two diverse Dunning prostate R3327 rat tumor sublines (MAT-Lu and HI) with respect to growth and respiratory challenge. Int J Radiat Oncol Biol Phys 2002; 53:744–756.

27. Zhao D, Constantinescu A, Hahn EW, et al. Tumor oxygen dynamics with respect to growth and respiratory challenge: Investigation of the Dunning prostate R3327-HI tumor. Radiat Res 2001;156:510–520.

28. Mason RP, Ran S, Thorpe PE. Quantitative assessment of tumor oxygen dynamics: Molecular imaging for prognostic radiology. J Cell Biochem 2002;87:45–53.

29. Hahn EW, Peschke P, Mason RP, et al. Isolated tumor growth in a surgically formed skin pedicle in the rat: A new tumor model for NMR studies. Magn Reson Imaging 1993;11:1007–1017.

30. Pedley RB, Hill SA, Boxer GM, et al. Eradication of colorectal xenografts by combined radioimmunotherapy and combretastatin a-4 3-O-phosphate. Cancer Res 2001;61:4716–4722.

31. Song Y, Worden KL, Jiang X, et al. Tumor oxygen dynamics: Comparison of ^{19}F MR EPI and frequency domain NIR spectroscopy. Adv Exp Med Biol 2003;530:225–236.

32. Song Y, Constantinescu A, Mason RP. Dynamic breast tumor oximetry: The development of prognostic radiology. Technol Cancer Res Treat 2002;1:1–8.

33. Brown JM. The hypoxic cell: A target for selective cancer therapy—Eighteenth Bruce F. Cain memorial award lecture. Cancer Res 1999;59:5863–5870.

34. Höckel M, Schlenger K, Aral B, et al. Association between tumor hypoxia and malignant progression in advanced cancer of the uterine cervix. Cancer Res 1996;56:4509–4515.

35. Brizel DM, Scully SP, Harrelson JM, et al. Tumor oxygenation predicts for the likelihood of distant metastases in human soft tissue sarcoma. Cancer Res 1996;56:941–943.

36. Höckel M, Vaupel P. Tumor hypoxia: Definitions and current clinical, biologic, and molecular aspects. J Natl Cancer Inst 2001;93:266–276.

37. Baudelet C, Gallez B. How does blood oxygen level-dependent (BOLD) contrast correlate with oxygen partial pressure (pO$_2$) inside tumors? Magn Reson Med 2002;48:980–986.

38. Zhao D, Jiang L, Constantinescu A, et al. Evaluation of breast tumor microcirculation and oxygenation using a combination of BOLD, DCE and ^{19}F MRI [Abstract]. Proc Int Soc Magn Reson Med 2004;1:222.

39. Beauregard DA, Pedley RB, Hill SA, et al. Differential sensitivity of two adenocarcinoma xenografts to the anti-vascular drugs combretastatin A4 phosphate and 5,6-dimethylxanthenone-4-acetic acid, assessed using MRI and MRS. NMR Biomed 2002;15:99–105.

40. Le D, Mason RP, Hunjan S, et al. Regional tumor oxygen dynamics: ^{19}F PBSR EPI of hexafluorobenzene. Magn Reson Imaging 1997;15:971–981.

41. Mason RP, Rodbumrung W, Antich PP. Hexafluorobenzene: A sensitive ^{19}F NMR indicator of tumor oxygenation. NMR Biomed 1996;9:125–134.

Chemotherapeutic (Cyclophosphamide) Effects on Rat Breast Tumor Hemodynamics Monitored by Multi-Channel NIRS.

Jae G. Kim[a], Dawen Zhao[b], Ralph P. Mason[b], Hanli Liu*[a]

[a]Joint Graduate Program of Biomedical Engineering,
University of Texas Southwestern Medical Center at Dallas/ University of Texas at Arlington
Arlington, TX 76019

[b]Advanced Radiological Sciences, Department of Radiology
University of Texas Southwestern Medical Center at Dallas
Dallas, TX 75390

ABSTRACT

We previously suggested that the two time constants quantified from the increase of tumor oxyhemoglobin concentration, $\Delta[HbO_2]$, during hyperoxic gas intervention are associated with two blood flow/perfusion rates in well perfused and poorly perfused regions of tumors. In this study, our hypothesis is that when cancer therapy is applied to a tumor, changes in blood perfusion will occur and be detected by the NIRS. For experiments, systemic chemotherapy, cyclophosphamide (CTX), was applied to two groups of rats bearing syngeneic 13762NF mammary adenocarcinomas: one group received a single high dose i. p. (200 mg/kg CTX) and the other group continuous low doses (20 mg/kg CTX i. p. for 10 days). Time courses of changes in tumor $\Delta[HbO_2]$ were measured at four different locations on the breast tumors non-invasively with an inhaled gas sequence of air-oxygen-air before and after CTX administration. Both rat body weight and tumor volume decreased after administration of high dose CTX, but continuous low doses showed decrease of tumor volume only. Baselines (without any therapy) intra- and inter-tumor heterogeneity of vascular oxygenation during oxygen inhalation were similar to our previous observations. After CTX treatment, significant changes in vascular hemodynamic response to oxygen inhalation were observed from both groups. By fitting the increase of $\Delta[HbO_2]$ during oxygen inhalation, we have obtained changes of vascular structure ratio and also of perfusion rate ratio before and after chemotherapy. The preliminary results suggest that cyclophosphamide has greatest effect on the well perfused tumor vasculature. Overall, our study supports our earlier hypothesis, proving that the effects of chemotherapy in tumor may be monitored non-invasively by using NIRS to detect changes of hemodynamics induced with respiratory challenges.

Keywords: Breast Cancer, Cyclophosphamide, Hemodynamics, NIR Spectroscopy, Tumor vascular oxygenation

1. INTRODUCTION

In addition to surgical resection, many other types of cancer therapy are available for patients including radiotherapy, photodynamic therapy and chemotherapy. Chemotherapy plays an important role to treat cancers even though it has some side effects. Currently, the effect of chemotherapy is monitored by MRI or CT that can measure the tumor volume changes during cancer treatment. However, it can take up to 3 weeks to detect such changes, and this is considerably late for clinicians to decide whether initial therapeutic strategy should be continued or modified. This delay in detection of chemotherapy effect can reduce the quality of a patient's life and ineffective therapy is costly. Therefore, many researchers are trying to develop tools that can detect the early response to cancer treatment. For example, Li *et al.* have used ^{31}P nuclear magnetic resonance spectroscopy (NMRS) to measure the effectiveness of cyclophosphamide (CTX) treatment in radiation-induced fibrosarcoma (RIF).[1] They found that the ratio of inorganic phosphate to other phosphate metabolites in CTX treated group was significantly decreased during the tumor growth delay period compared to age-matched controls. Poptani *et al.* studied the effects of CTX treatment in RIF-1 tumors in terms of tumor oxygenation

and glycolytic rate changes by utilizing ^{13}C MRS, Eppendorf electrode, and Redox scanning.[2] They observed that CTX treatment caused reduction in glycolytic rate, a significant decrease in tumor tissue pO_2, and also an increase of NADH levels 24 hours after the treatment while tumor volume did not show any significant difference between the CTX-treated and control groups. Zhao *et al.* have reported significant changes in rat breast tumor perfusion following either single dose CTX or continuous low dose "metronomic" therapy.[3]

In the last decade, near infrared spectroscopy (NIRS) has been developed to examine tissue oxygenation and has been widely applied to investigate hemoglobin oxygenations of muscles,[4,5,6] the brain,[7,8,9] and animal tumors.[10,11,12,13,20] Since tumors have higher vascular density and also higher metabolism than normal tissues, total hemoglobin concentration ([Hb_{total}]), oxyhemoglobin concentration ([HbO_2]), and reduced scattering coefficient (μs') were used as markers to identify tumors from the human breast by using NIRS.[14,15,16] In addition, an NIR spectrometer is a low-cost, portable, and real-time display instrument. Therefore, NIRS has a good potential to be used as a monitoring tool for tumor treatment planning and tumor prognosis.

We have previously studied breast tumor oxygenation under gas intervention using NIRS and found that oxyhemoglobin concentration changes ($\Delta[HbO_2]$) during gas intervention can be fitted by a two-exponential equation containing two time constants.[12] Based on the model, we formed a hypothesis that changes in oxygenated hemoglobin concentration result from well perfused and poorly perfused regions of an animal tumor to explain why there are two different time constants in the $\Delta[HbO_2]$ data. The model further allows us to associate the signal amplitudes and time constants to the ratio of vascular density and the ratio of the perfusion rates in the two different regions, respectively.
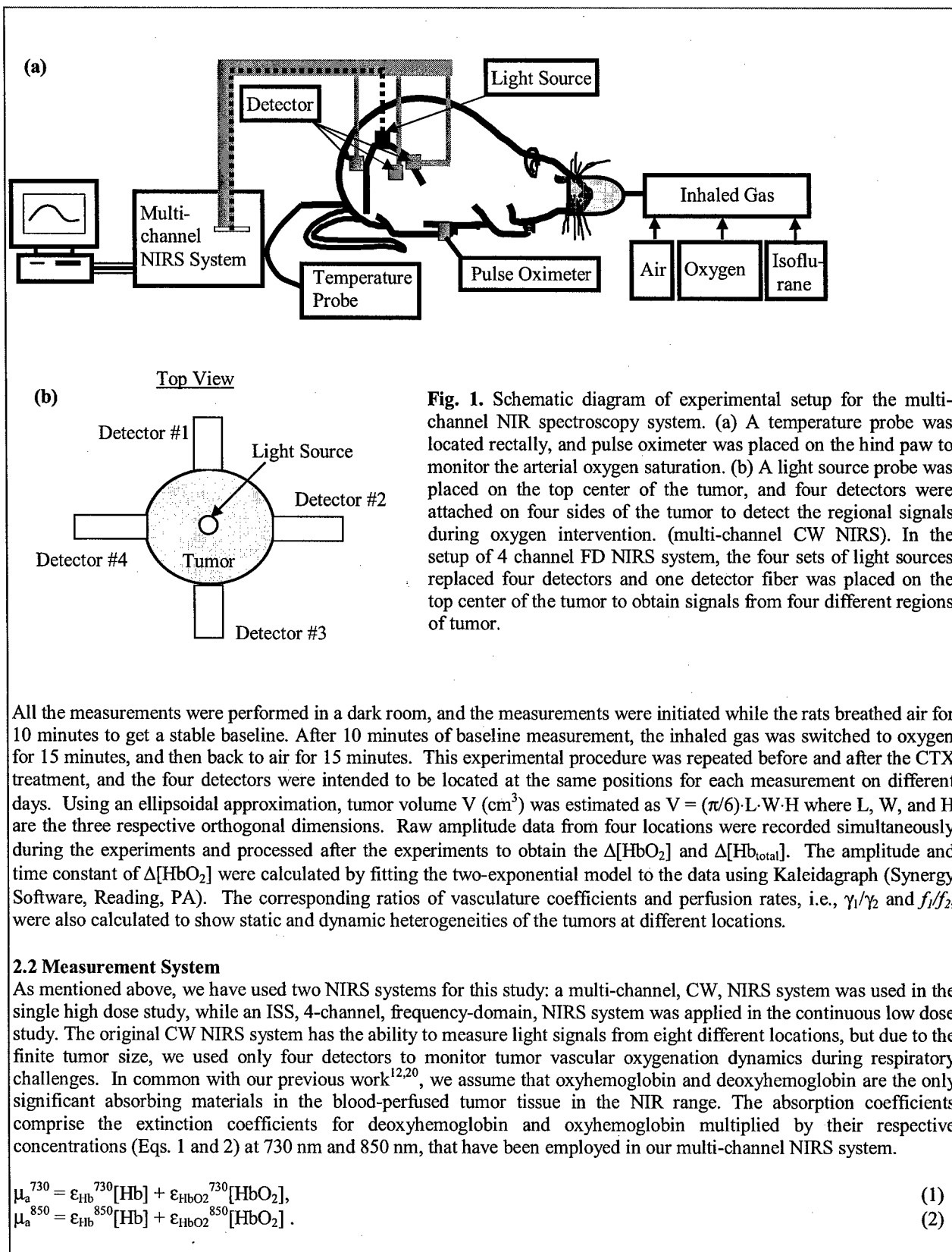
In this study, we applied the NIRS system to monitor the tumor oxygenation changes during oxygen intervention before and after CTX administration. The purpose for this study is to explore the NIRS as a possible tool for monitoring tumor responses to chemotherapy. This work is based on the following hypothesis: when tumor is treated with chemotherapy, changes in blood perfusion and vascular density in the tumor will occur and will be seen as changes of the two fitted parameters from the NIRS measurements. In addition, by developing a non-invasive tool for monitoring cancer therapy, we are not only monitoring the reduction of tumor size, but also detecting the changes of tumor physiological conditions, which are essential for tumor treatment planning and tumor prognosis.

2. MATERIALS AND METHODS

2.1 Tumor Model and Experimental Procedure

Rats were divided into three groups for this study. Two groups were treated with CTX at different doses, and the other group was administered saline instead of CTX as a control group. Cyclophosphamide was chosen as a chemotherapeutic agent for this study since our tumor line is highly responsive to alkylating agents and platinum chemotherapeutic agents.[17] CTX is an antineoplastic alkylating agent, and it has been used to treat lymphomas, cancers of the ovary, breast and bladder, and chronic lymphocytic leukaemia.[18,19] The tumor line was rat mammary adenocarcinomas 13762NF (cells originally provided by the Division of Cancer Therapeutics, NCI), and the tumors were implanted in the hind limb of adult female Fisher 344 rats (~200 g).

The rats were anesthetized with 0.2 ml ketamine HCl (100 mg/ml; Aveco, Fort Dodge, IA) when the tumors reached approximately 1 cm in diameter and maintained under general gaseous anesthesia using a small animal anesthesia unit with air (1 dm^3/min) and 1% isoflurane through a mask placed over the mouth and nose. During the experiments, the rat was placed on a warm blanket to maintain body temperature, which was monitored with a rectally inserted thermal probe connected to a digital thermometer (Digi-Sense, model 91100-50, Cole-Parmer Instrument Company, Vernon Hills, IL). Tumors were shaved before measurements to improve optical contact for transmitting light. A pulse oximeter (model: 8600V, Nonin, Inc.) was placed on the hind foot to monitor arterial oxygenation (S_aO_2) and heart rate. For the single high dose group (n=5), a light source and four detectors from a multi-channel, CW (continuous wave) NIRS (NIM, Inc, Philadelphia, PA) were attached to the tumor using posts and swivel post clamps (see Figure 1(a)). For the multi low dose (n=3) and control (n=3) groups, we have used four-channel, frequency domain (FD), NIRS (ISS, Champaign, IL). In the latter case, the four sets of light sources replaced four detectors shown in Figure 1(b), and one detector fiber was placed on the top center of the tumor to obtain signals from four different regions of tumor.

(a)

(b)

Top View

Fig. 1. Schematic diagram of experimental setup for the multi-channel NIR spectroscopy system. (a) A temperature probe was located rectally, and pulse oximeter was placed on the hind paw to monitor the arterial oxygen saturation. (b) A light source probe was placed on the top center of the tumor, and four detectors were attached on four sides of the tumor to detect the regional signals during oxygen intervention. (multi-channel CW NIRS). In the setup of 4 channel FD NIRS system, the four sets of light sources replaced four detectors and one detector fiber was placed on the top center of the tumor to obtain signals from four different regions of tumor.

All the measurements were performed in a dark room, and the measurements were initiated while the rats breathed air for 10 minutes to get a stable baseline. After 10 minutes of baseline measurement, the inhaled gas was switched to oxygen for 15 minutes, and then back to air for 15 minutes. This experimental procedure was repeated before and after the CTX treatment, and the four detectors were intended to be located at the same positions for each measurement on different days. Using an ellipsoidal approximation, tumor volume V (cm^3) was estimated as V = $(\pi/6) \cdot L \cdot W \cdot H$ where L, W, and H are the three respective orthogonal dimensions. Raw amplitude data from four locations were recorded simultaneously during the experiments and processed after the experiments to obtain the $\Delta[HbO_2]$ and $\Delta[Hb_{total}]$. The amplitude and time constant of $\Delta[HbO_2]$ were calculated by fitting the two-exponential model to the data using Kaleidagraph (Synergy Software, Reading, PA). The corresponding ratios of vasculature coefficients and perfusion rates, i.e., γ_1/γ_2 and f_1/f_2, were also calculated to show static and dynamic heterogeneities of the tumors at different locations.

2.2 Measurement System

As mentioned above, we have used two NIRS systems for this study: a multi-channel, CW, NIRS system was used in the single high dose study, while an ISS, 4-channel, frequency-domain, NIRS system was applied in the continuous low dose study. The original CW NIRS system has the ability to measure light signals from eight different locations, but due to the finite tumor size, we used only four detectors to monitor tumor vascular oxygenation dynamics during respiratory challenges. In common with our previous work[12,20], we assume that oxyhemoglobin and deoxyhemoglobin are the only significant absorbing materials in the blood-perfused tumor tissue in the NIR range. The absorption coefficients comprise the extinction coefficients for deoxyhemoglobin and oxyhemoglobin multiplied by their respective concentrations (Eqs. 1 and 2) at 730 nm and 850 nm, that have been employed in our multi-channel NIRS system.

$$\mu_a^{730} = \varepsilon_{Hb}^{730}[Hb] + \varepsilon_{HbO2}^{730}[HbO_2], \tag{1}$$

$$\mu_a^{850} = \varepsilon_{Hb}^{850}[Hb] + \varepsilon_{HbO2}^{850}[HbO_2] . \tag{2}$$

Based on modified Beer-Lambert's law, the data presented in this paper were analyzed using amplitude values to find the changes in absorption (Eq. 3). By manipulating Equations 1-3, changes in oxygenated hemoglobin, deoxygenated hemoglobin and total hemoglobin concentrations were calculated from the transmitted amplitude of the light through the tumor (Eqs. 4, 5 and 6).

$$\mu_{aB} - \mu_{aT} = \log (A_B/A_T) / L, \tag{3}$$

$$\Delta[HbO_2] = [-0.674*\log (A_B/A_T)^{730} + 1.117*\log (A_B/A_T)^{850}] / L, \tag{4}$$

$$\Delta[Hb] = [0.994*\log (A_B/A_T)^{730} - 0.376*\log (A_B/A_T)^{850}] / L, \tag{5}$$

$$\Delta[Hb_{total}] = \Delta[Hb] + \Delta[HbO_2] = [0.32*\log (A_B/A_T)^{730} + 0.741*\log (A_B/A_T)^{850}] / L, \tag{6}$$

where A_B = baseline amplitude; A_T = transition amplitude; L = optical pathlength between source/detector. The constants contained in these equations were computed with the extinction coefficients for oxy and deoxyhemoglobin at the two wavelengths used.[21] Notice that these coefficients have accounted for four hemes per hemoglobin molecule. In principle, L should be equal to the source–detector separation, d, multiplied by a differential pathlength factor (DPF), i.e., L=d*DPF. Little is known about DPF for tumors, although a DPF value of 2.5 has been used by others.[10] Since our focus is on dynamic changes and relative values of tumor [HbO_2] in response to oxygen intervention, we have taken the approach of including the DPF in the unit, and eq. (4) becomes as follows:

$$\Delta[HbO_2] = [-0.674*\log (A_B/A_T)^{730} + 1.117*\log (A_B/A_T)^{850}] / d, \tag{7}$$

where d is the direct source-detector separation in cm, and the unit of $\Delta[HbO_2]$ in Eq. (7) is mM/DPF.

Since the wavelengths of light sources from the ISS, frequency-domain system were 750 nm and 830 nm, the corresponding equations for $\Delta[HbO_2]$, $\Delta[Hb]$, and $\Delta[Hb_{total}]$ are modified as follows.

$$\Delta[HbO_2] = [-0.709*\log (A_B/A_T)^{750} + 1.404*\log (A_B/A_T)^{830}] / d, \tag{8}$$

$$\Delta[Hb] = [0.9546*\log (A_B/A_T)^{750} - 0.4992*\log (A_B/A_T)^{830}] / d, \tag{9}$$

$$\Delta[Hb_{total}] = \Delta[Hb] + \Delta[HbO_2] = [0.2456*\log (A_B/A_T)^{750} + 0.9048*\log (A_B/A_T)^{830}] / d. \tag{10}$$

2.3 Bi-exponential Model of Tumor Vascular Oxygenation

In our previous report,[12] we followed an approach used to measure regional cerebral blood flow (rCBF) with diffusible radiotracers, as originally developed by Kety[22] in the 1950's. By applying Fick's principle and defining γ as the ratio of HbO_2 concentration changes in the vascular bed to that in veins, we arrived at Eq. (11):

$$\Delta HbO_2^{vasculature}(t) = \gamma H_o[1-\exp(-ft/\gamma)] = A_1[1-\exp(-t/\tau)] \tag{11}$$

where γ is the vasculature coefficient of the tumor, H_o is the arterial oxygenation input and f is the blood perfusion rate.

If a tumor has two distinct perfusion regions, and the measured signal results from both of the regions (Figure 2), then it is reasonable to include two different blood perfusion rates, f_1 and f_2, and two different vasculature coefficients, γ_1 and γ_2, in the model. Therefore, Eq. (11) can be modified to count for the double exponential feature observed in the experiments:

$$\Delta HbO_2^{vasculature}(t) = \gamma_1 H_o[1-\exp(-f_1 t/\gamma_1)] + \gamma_2 H_o[1-\exp(-f_2 t/\gamma_2)]$$
$$= A_1[1-\exp(-t/\tau_1)] + A_2[1-\exp(-t/\tau_2)] \tag{12}$$

where f_1 and γ_1 are the blood perfusion rate and vasculature coefficient in region 1 for the well perfused region, respectively; f_2 and γ_2 have the same respective meanings in region 2 for the poorly perfused region, and $A_1 = \gamma_1 H_o$, $A_2 =$

$\frac{1}{2}H_o$, $\tau_1 = \gamma_1/f_1$, $\tau_2 = \gamma_2/f_2$. Then, if A_1, A_2, τ_1, and τ_2 are determined by fitting the measurements with the model, we can obtain the ratios of two vasculature coefficients and the two blood perfusion rates:

$$\frac{\gamma_1}{\gamma_2} = \frac{A_1}{A_2}, \qquad \frac{f_1}{f_2} = \frac{A_1/A_2}{\tau_1/\tau_2}. \tag{13}$$

With these two ratios, we are able to understand more about tumor physiology, such as tumor vasculature and blood perfusion.

3. RESULTS

3.1 Body weight and tumor volume changes during chemotherapy

Body weight and tumor volume were monitored before and after the CTX treatments to see the tumor responses and side effects from chemotherapy. In the single high dose treatment group, body weight decreased until 6 days after the treatment, but later increased for the rest of days of observation. Two rats among five in this group failed to survive at day 6 due to the toxicity from the high dose CTX treatment. Therefore, the data shown at day 8 and 10 represent the smaller group of rats which survived during the high dose treatment. Tumor volume did not further decreased after day 4. (Fig. 2(b)) In comparison, rats in the continuous low dose group initially lost weight after a low dose of CTX administration, but gradually gained the weight during the treatment, presenting low toxicity from the treatment. This group also showed a significant reduction in tumor volume during the treatment. For a control group, saline was injected into the rats instead of CTX, and a gradual decrease of body weight was observed, while their tumor volumes increased exponentially. Changes in rat body weight and tumor volume were normalized to day 0 (before CTX or saline administration). (Figures 2(a) and (b)) Solid circles represent the data from a control group, and open squares and open diamonds represent the continuous low dose group and single high dose group, respectively.
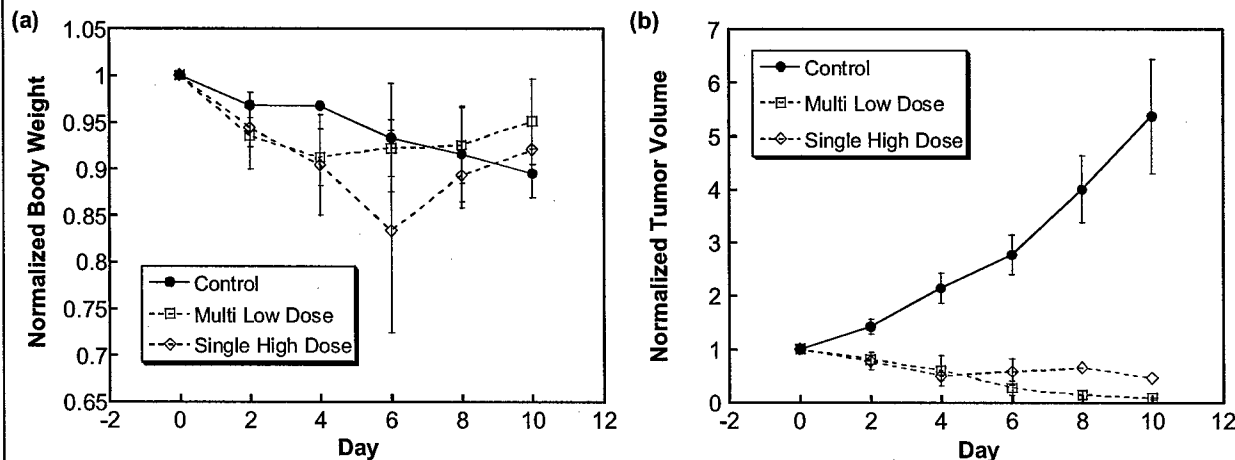

Fig. 2. Normalized changes in rat body weight (a) and tumor volume (b) during the saline and CTX treatments.

3.2 Intratumoral heterogeneity of vascular oxygenation observed by the multi-channel NIRS

In our experiment, we have utilized either one light source and four detectors and from the CW system (NIM, Inc) or four light sources and one detector from the FD system (ISS, Inc.) for the rat breast tumor measurements, and the setups (Fig. 1). After 10 minutes of baseline measurement with air breathing, gas was switched to pure oxygen, causing a rapid increase in tumor [HbO$_2$]. These changes were measured simultaneously from four locations of the tumor. Figure 3 shows a representative set of data before the CTX treatment, with the DC NIRS system. Open circles show the raw data

SPIE USE: _____ DB Check, _____ Prod Check, Notes:

measured by multi-channel NIRS, and the solid black lines represent the fitted curves using our bi-exponential model for hemodynamics during oxygen intervention.[12] It is apparent that the data from each location differs though there are similar trends of $\Delta[HbO_2]$.
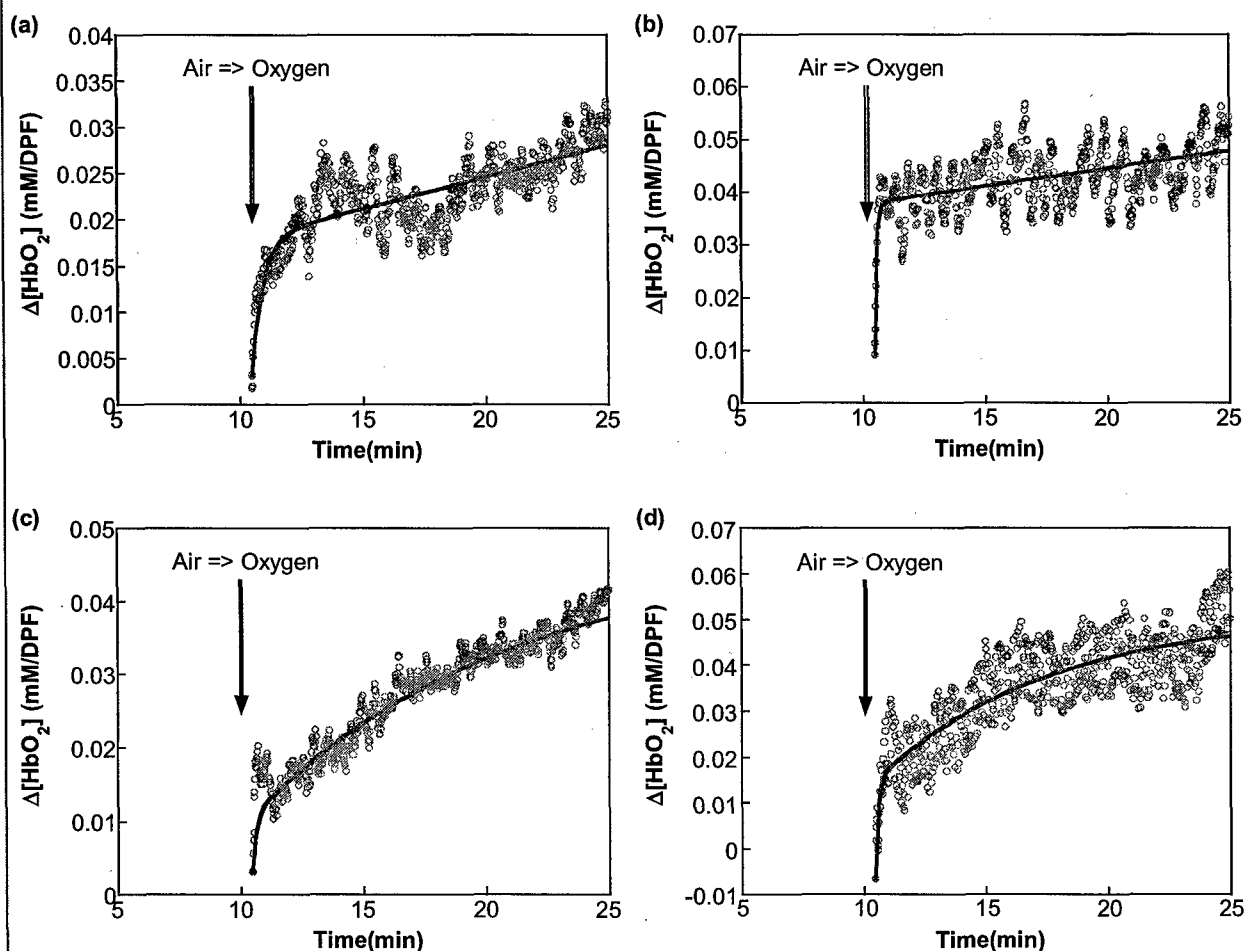

Fig. 3. Dynamic changes of tumor $[HbO_2]$ from four locations in a rat breast tumor. The rising parts of $\Delta[HbO_2]$ from the four locations were fitted using a double-exponential expression. Figures 3(a)-3(d) were taken from locations #1-#4, respectively. In this case, the tumor was not treated yet.

Table 1. Summary of vascular oxygen dynamics determined at the four detectors from tumor shown in the Fig. 3.

Location	A_1	A_2	τ_1	τ_2	A_1/A_2 ($=\gamma_1/\gamma_2$)	τ_1/τ_2	f_1/f_2
1 (Fig. 3a)	0.013	0.027	0.48	24.3	0.48	0.02	24
2 (Fig. 3b)	0.029	0.026	0.09	29.8	1.12	0.003	373
3 (Fig. 3c)	0.008	0.036	0.15	10.6	0.22	0.014	16
4 (Fig. 3d)	0.021	0.037	0.12	7.25	0.57	0.017	34

To compare the data taken from four locations of the tumor more clearly, the time constants and amplitudes from the four fitted curves are summarized in Table 1. The ratios of γ_1/γ_2 and f_1/f_2 characterize tumor vascular structure and blood

SPIE USE: _____ DB Check, _____ Prod Check, Notes:

perfusion within the volume of tumor interrogated by light.[12] In principle, when γ_1/γ_2 is close to 1, it implies that the measured optical signal results equally from both regions 1 (*i.e.*, well perfused region) and 2 (i.e., poorly perfused region); if $\gamma_1/\gamma_2 < 1$, the measured signal results more from region 2 than region 1 [Figures 3(a), 3(c) and 3(d)]. As Table 1 demonstrates, only location #2 has a ratio of γ_1/γ_2 slightly higher than 1, and the readings from locations #1, #3 and #4 have the ratios of γ_1/γ_2 less than 1. This may suggest that the tumor volume that was optically interrogated from location #2 was dominated by well perfused regions, while most of other tumor volumes detected from locations #1, #3 and #4 are composed of more poorly perfused regions. Furthermore, all the ratios of f_1/f_2 from four locations of the tumor shown in Fig. 3 are much greater than 1, indicating that the blood perfusion rate in well perfused region is much greater than that in poorly perfused region. Especially, f_1/f_2 from location #2 is 10 to 20 times higher than those from locations #1, #3, and #4, showing a high level of intratumoral heterogeneity in dynamic vascular structure.

3.3 Monitoring vascular hemodynamics of breast tumors before and after chemotherapy

The tumor hemodynamics during oxygen intervention were measured before and after administration of CTX and saline. The representative data from the control group and continuous low dose group are shown in Figs. 4(a) and 4(b), respectively. Similar to Figure 3, open symbols are the raw data from measurements, and solid lines are the fitted curves using our double exponential model. As mentioned before, there were 4 light sources placed on the surface of tumor. Figure 4 shows the acute and then gradual changes of [HbO₂] after switching the breathing gas from air to oxygen, and the data were observed at the same (or nearly the same) location of tumor from day 0 to day 6. From Figure 4(a), we can see different tumor hemodynamics at different days, but having similar trends and maximum Δ[HbO₂] for the control group. However, the data taken from the continuous low dose group show quite different hemodynamics throughout the treatment days (Fig. 4(b)). Especially, we notice that the fast increase part became much smaller at Days 2 and 6 compared to Day 0, implying a significant decrease in signal from the well perfused region.
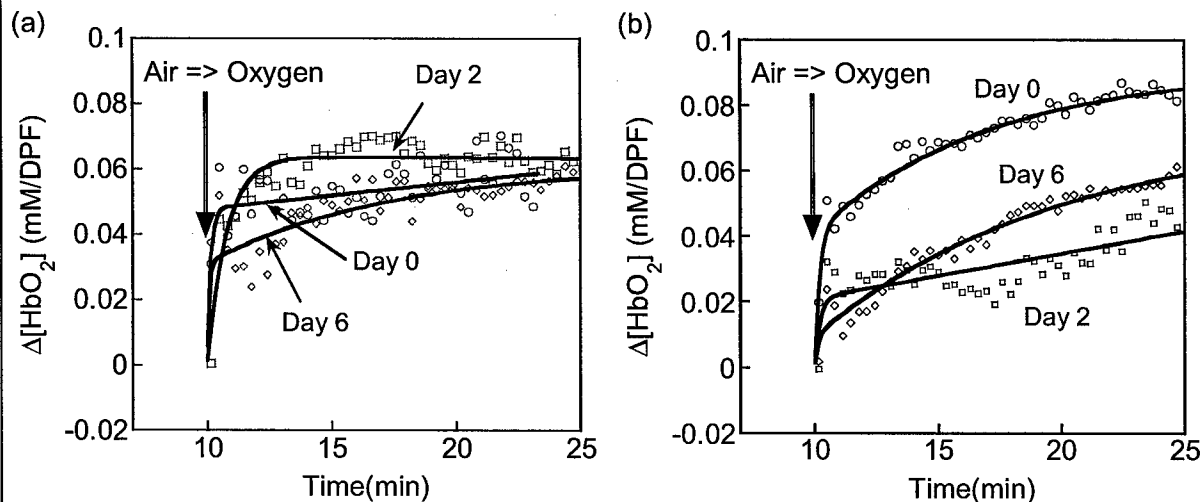

Fig. 4. Dynamic changes of Δ??[HbO₂] taken at location #1 from a rat breast tumor before and after administration of (a) saline and (b) continuous low dose of CTX (20 mg/kg for 10 days). The rising part of Δ[HbO₂] from location #1 was fitted using the double-exponential expression.

Figure 5 also shows the changes of tumor hemodynamics during oxygen intervention, before and after a single high dose of CTX treatment, measured by the CW NIRS. This figure clearly demonstrates that we can observe significant changes in tumor hemodynamics after chemotherapy by using respiratory challenge as a mediator. The fitted parameters from our mathematical model are summarized in Table 2 to compare the changes in hemodynamic parameters before and after administration of CTX. The rising part of Δ[HbO₂] from location #1 was fitted using either a single- or double-exponential expression.

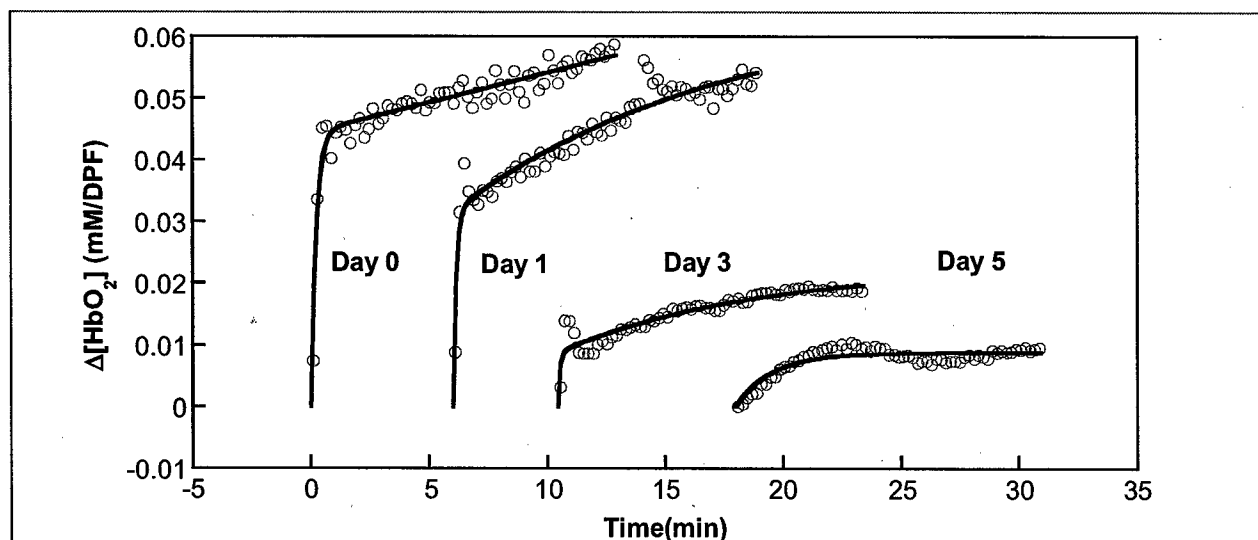SPIE USE: _____ DB Check, _____ Prod Check, Notes:

Fig. 5. Dynamic changes of [HbO$_2$] taken at location #1 from a rat breast tumor before and after a single high dose of CTX treatments (200mg/kg). The rising part of Δ[HbO$_2$] from location #1 was fitted using either a single- or double-exponential expression.

Table 2. Summary of vascular oxygen dynamics determined at location #1 from the tumor shown in Fig. 5 before and after CTX treatment.

Day	A$_1$	A$_2$	τ_1	τ_2	A$_1$/A$_2$ (=γ_1/γ_2)	τ_1/ τ_2	f_1/f_2
0	0.044	0.031	0.23	25.21	1.42	0.0091	156
1	0.032	0.033	0.13	11.36	0.97	0.0114	85
3	0.0087	0.014	0.089	8.36	0.62	0.0106	58
5	0.0087		1.27				

4. DISCUSSION

Changes of rat body weight and tumor volume clearly show that CTX treatment is effective for the tumor type that we have used in this study. For the control group, the average rat body weight gradually decreased during the entire course of treatment, which implies the sickness of rats possibly due to the tumor growth (cachexia). (At Day 10, the tumor volume was ~5 times larger than that at Day 0.) It is clear that there is a different effectiveness of CTX treatment between the single high dose group (200mg/kg) and continuous low dose group (20mg/kg for 10 days). Both of the CTX treatments delayed the tumor growth and even further reduced the tumor volume. However, a single high dose of CTX treatment caused the death of two rats, and the tumor volume was not decreased further 4 days after the treatment, while the continuous low dose CTX treatment continued to provide tumor regression without causing severe sickness. From this observation, it is obvious that continuous low dose of CTX treatment is working much better than a single high dose of CTX treatment for a rat mammary adenocarcinomas 13762NF tumor.

NIRS is a portable, low cost, and real time measurement system that can monitor changes of vascular oxygen levels by using two wavelengths. We have previously used a single-channel NIRS system with one light source and one detector for global measurements of Δ[HbO$_2$] and Δ[Hb$_{total}$] in tumors during respiratory challenges.[12,20] Through those experiments, we have found that most tumors have a bi-phasic behavior in Δ[HbO$_2$] increase (i.e., a rapid increase followed by a slow and gradual increase) after switching the gas from air to carbogen/oxygen. To explain this bi-phasic behavior, we developed a mathematical model and formed a hypothesis that the bi-phasic behavior of Δ[HbO$_2$] during carbogen/oxygen inhalation results from two different vascular regions in tumor with two blood perfusion rates and vascular structures.[12]

By giving an oxygen intervention, tumor blood vessels are acutely subject to an increase of $[HbO_2]$ due to higher supply of oxygenated blood from artery compared to that from air breathing. However, due to the irregular vascular structure in tumor, the well perfused regions in tumor may have an increase in $[HbO_2]$ much faster than other parts of tumor that are poorly perfused. Therefore, two time constants obtained from tumor hemodynamic measurements during oxygen intervention are able to reveal two blood flow/perfusion rates in tumor, more precisely, two speeds of blood flow within the tumor blood vessels. More recently, we have shown that the bi-phasic increase in optical density changes occurs when there exist two different flow rates in tumor vascular phantom.[23] The bi-phasic model is a basis of our current study where we wish to detect any changes in vascular structures, hemodynamic features, or perfusion rate within a tumor after CTX treatment.

The amplitude and time constants obtained from $\Delta[HbO_2]$ increase (Fig. 5) are summarized in Table 2. At day 0, we can see that γ_1/γ_2 is higher than 1, indicating that the measured signal results more from the well perfused region than poorly perfused region. However, this ratio becomes less than 1 after injection of cyclophosphamide (Day 1 and 3). This may be explained by destruction of vascular structure in tumor after chemotherapy. We expect that after a single high dose administration of CTX, the drug circulates in the blood vessels and is delivered to the tumor cells more in the well perfused region than in the poorly perfused region. This will lead to death of tumor cells in the well perfused region more effectively than that in the poorly perfused region, eventually resulting in decreases in tumor volume in the well perfused region more than in the poorly perfused region. Then, the tumor volume containing the well perfused regions will consequently decrease, so will the contribution of detected NIR signals from the well perfused region. In other words, a decrease in γ_1/γ_2 may indicate deceases in well perfused regions in tumor volume, after the administration of CTX.

As shown in Table 2, moreover, the perfusion rate ratio, f_1/f_2, was also decreased after a single high dose of CTX administration. At Day 0, f_1/f_2 was very high, meaning that there was a big difference of perfusion rate between the well perfused and poorly perfused region in tumor. However, this ratio significantly decreased at Day 1 and 3 after CTX treatment, representing that the perfusion rate gap between the well perfused region and poorly perfused region became much smaller than that at day 0. At Day 5, changes in $[HbO_2]$ during oxygen intervention do not show any bi-phasic behavior anymore, and it was fitted by a single-exponential model. This may indicate that most of tumor cells and/or tumor vasculature in the well perfused region are possibly destroyed by the effect of CTX, resulting in quite different hemodynamic behavior.

5. CONCLUSION

In conclusion, we have conducted this study to show the possibility of using NIRS to monitor tumor hemodynamics in response to chemotherapy by comparing the changes in tumor vascular oxygenation before and after CTX treatment. The heterogeneity of tumor vasculature was easily observed by quantifying the blood perfusion rate and vascular coefficients at four different locations of the tumor. Tumor hemodynamics has been significantly changed before and after CTX treatment compared to the saline-treated control group, showing high possibility of the NIRS system to be used as a monitoring tool for cancer treatments. Our future studies will include the development of NIR imaging systems to obtain a map of tumor hemodynamic changes from whole tumor, allowing us to predict the efficacy of tumor treatment.

ACKNOWLEDGEMENTS

REFERENCES

1. S. Li, J. P. Wehrle, S. S. Rajan, R. G. Steen, J. D. Glickson, and J. Hilton, "Response of radiation-induced fibrosarcoma-1 in mice to cyclophosphamide monitored by in vivo ^{31}P nuclear magnetic resonance spectroscopy," *Cancer Research*, **48**, 4736-4742, 1988.

2. H. Poptani, N. Bansal, W. T. Jenkins, D. Blessington, A. Mancuso, D. S. Nelson, M. Feldman, E. J. Delikatny, B. Chance, and J. D. Glickson, "Cyclophosphamide treatment modifies tumor oxygenation and glycolytic rates of RIF-1 tumors: 13C magnetic resonance spectroscopy, Eppendorf electrode, and Redox scanning," *Cancer Research*, **63**, 8813-8820, 2003.

3. D. Zhao, A. Constantinescu, E. W. Hahn, and R. P. Mason, "*In vivo* evaluation of metronomic chemotherapy on prostate tumors by MRI," CaPCure, New York, NY, November 2003.

4. B. Chance, S. Nioka, J. Kent, K. McCully, M. Fountain, R. Greenfield, and G. Holtom, "Time resolved spectroscopy of hemoglobin and myoglobin in resting and ischemic muscle", *Anal. Biochem.*, **174**,698-707, 1988.

5. S. Homma, T. Fukunaga,, and A. Kagaya, "Influence of adipose tissue thickness on near infrared spectroscopic signals in the measurement of human muscle", *J. Biomed. Opt.*, **1**(4), 418-424, 1996.

6. M. Ferrari, Q. Wei, L. Carraresi, R. A. De Blasi, and G. Zaccanti, "Time-resolved spectroscopy of the human forearm", *J. Photochem. Photobiol. B: Biol.*, **16**,141-153, 1992.

7. B. Chance, E. Anday, S. Nioka, S. Zhou, L. Hong, K. Worden, C. Li, T. Murray, Y. Ovetsky, D. Pidikiti, and R. Thomas, "A novel method for fast imaging of brain function non-invasively with light", *Optics Express*, **2**(10), 411-423 1998.

8. R. Wenzel, H. Obrig, J. Ruben, K. Villringer, A. Thiel, J. Bernarding, U. Dirnagl, and A. Villringer, "Cerebral blood oxygenation changes induced by visual stimulation in humans", *J. Biomed. Opt.*, **1**(4),399-404, 1996.

9. M. Cope, and D. T. Delpy, "A system for long term measurement of cerebral blood and tissue oxygenation in newborn infants by near infrared transillumination", *Med. Biol. Eng. Comp.*, **26**, 289-294, 1988.

10. R. G. Steen, K. Kitagishi, and K. Morgan, "In vivo measurement of tumor blood oxygenation by near-infrared spectroscopy: immediate effects of pentobarbital overdose or carmustine treatment", *J. Neuro-Oncol.*, **22**, 209-220, 1994.

11. H. D. Sostman, S. Rockwell, A. L. Sylvia, D. Madwed, G. Cofer, H. C. Charles, R. Negro-Vilar, and D. Moore, "Evaluation of BA1112 rhabdomyosarcoma oxygenation with microelectrodes, optical spectrophotometry, radiosensitivity, and magnetic resonance spectroscopy", *Magn. Reson. Med.*, **20**, 253-267, 1991.

12. H. Liu, Y. Song, K. L. Worden, X. Jiang, A. Constantinescu, and R. P. Mason, "Noninvasive Investigation of Blood Oxygenation Dynamics of Tumors by Near-Infrared Spectroscopy", *Applied Optics*, **39**(28), 5231-5243, 2000.

13. H. Liu, Y. Gu, J.G. Kim, and R. P. Mason, "Near infrared spectroscopy and imaging of tumor vascular oxygenation", *Methods Enzymol.*, **386**, 349-378, 2004

14. S. Nioka, M. Miwa, S. Orel, M. Shnall, M. Haida, S. Zhao, B. Chance, "Optical imaging of human breast cancer," *Adv. Exp. Med. Biol.*, **361**, 171-179, 1994.

15. J. B. Fishkin, O. Coquoz, E. R. Anderson, M. Brenner, B. J. Tromberg, "Frequency-domain photon migration measurements of normal and malignant tissue optical properties in a human subject,"*Applied Optics*, **36**(1), 10-20, 1997.

16. B. Pogue, S. Jiang, S. Srinivasan, X. Song, H. Dehghani, K. Paulsen, T. Tosteson, C. Kogel, S. Soho, S. P. Poplack, "Near-infrared scattering spectrum differences between benign and malignant breast tumors measured in vivo with diffuse tomography," in Biomedical Topical Meetings on CD-ROM (The Optical Society of America, Washington, DC) 2004. ThB1.

17. D. B. S., Hoon, "Circlulating immune complexes in rats bearing 6-thioguanine-resistant variants of the 13762 mammary adenocarcinoma," *Cancer Res.*, **44**, 2406-2409 (1984).

18. A.R. Ahmed, S.M. Hombal, "Cyclophosphamide (Cytoxan). A review on relevant pharmacology and clinical uses," *J. Am. Acad. Dermatol.*, **11**(6), 1115-1126, 1984.

19. P. Calabresi, B. A. Chabner, "Antineoplastic agents", In: A.F. Gilman, T. W. Rall, A.S. Niss, and P. Taylor (Editors), The Pharmacological Basis of Therapeutics, 8th ed. MacGraw-Hill, Singapore. 1992.

20. J. G. Kim, D. Zhao, Y. Song, A. Constantinescu, R. P. Mason, and H. Liu, "Interplay of tumor vascular oxygenation and tumor pO_2 observed using near-infrared spectroscopy, an oxygen needle electrode, and ^{19}F MR pO_2 mapping", *J. Biomed. Opt.*, **8**(1), 53-62, 2003.

21. M. Cope, "The application of near infrared spectroscopy to non invasive monitoring of cerebral oxygenation in the newborn infant", PhD dissertation, Appendix A, University College London, 1991.

22. S. S. Kety, "The theory and applications of the exchange of inert gas at the lungs and tissue," *Pharmacol. Rev.,* **3**, 1-41, 1951.

23. J. G. Kim, and H. Liu, "Investigation of breast tumor hemodynamics using tumor vascular phantoms and FEM simulations", in Biomedical Topical Meetings on CD-ROM (The Optical Society of America, Washington, DC, 2004), WF16.

American Association for Cancer Research

3799 Tumor physiological response to antivascular agent combretastatin A4 phosphate assessed by magnetic resonance imaging

Dawen Zhao, Lan Jiang, Ammar Adam, Eric W. Hahn, Ralph P. Mason. *UT Southwestern Medical Ctr., Dallas, TX.*

Tumor oxygenation has been widely recognized as a potent factor, which influences tumor response to chemo- and radio-therapy. The vascular targeting agent, combretastatin A-4-phosphate (CA4P) causes tumor vascular shutdown and a combination of CA4P with radiotherapy has shown enhanced tumor response. We have recently established a novel magnetic resonance approach to measuring regional tumor oxygen tension *FREDOM* (Fluorocarbon Relaxometry using Echo planar imaging for Dynamic Oxygen Mapping) with hexafluorobenzene, as a reporter molecule. Here, the effect of CA4P on real-time tumor oxygenation and perfusion/permeability was monitored *in vivo* in NF13762 rat breast carcinomas by ^{19}F *FREDOM* and ^{1}H dynamic contrast enhanced (DCE) magnetic resonance imaging (MRI). Syngeneic NF13762 rat breast carcinomas were implanted in a skin pedicle on the foreback of Fisher 344 adult female rats. When tumors reached ~ 1 cm diameter (~ 0.6 cm^3) MRI was performed using a 4.7 T horizontal bore magnet with a Varian Unity Inova system. A series of pO_2 maps acquired at 10, 30, 60, 90, and 120 minutes after i.p. CA4P (30 mg/kg; OXiGENE, Inc. Waltham, MA) showed a significant decrease in pO_2 of some tumors as early as 30 min post injection. For all tumors there was a significant drop in tumor pO_2 within 90 min after treatment (mean baseline pO_2 = 23 torr to 9 torr, p < 0.05) and a further decrease was observed at 2 h (mean = 2 torr; p < 0.01). Intriguingly, the initial changes in pO_2 in central and peripheral regions were parallel, but by 24 h post treatment significant difference was apparent: the pO_2 in periphery improved significantly, while center remained hypoxic. These data are consistent with DCE MRI, which revealed a ~70% decrease in perfusion/permeability (initial area under signal-intensity curve (IAUC)) at 2 h after 30 mg/kg CA4P (p < 0.001). IAUC fully recovered in a thin peripheral region, but not the tumor center 24 h post-treatment. Vascular perfusion marker Hoechst 33342 staining confirmed that the number of perfused vessels decreased significantly at 2 h, and then recovered at 24 h. We conclude that magnetic resonance imaging can monitor *in vivo* dynamic changes in tumor vasculature and oxygenation following VTA administration. These results provide the first insight into regional tumor oxygen dynamics in response to CA4P in a syngeneic rat tumor. While dynamic contrast MRI indicates vascular shut down, the critical pO_2 measurements are potentially more important for optimizing therapeutic combination of VTAs with conventional therapy, in particular, irradiation. Supported by DOD Breast Cancer IDEA Award (DAMD 170310363), in conjunction with NCI RO1 CA79515/EB002762 and the Cancer Imaging Program, a P20 Pre-ICMIC CA86354.

96th Annual Meeting, Anaheim, CA   -   April 16-20, 2005

IN VIVO MRI MONITORING OF BREAST TUMOR RESPONSE TO THE VASCULAR TARGETING AGENT COMBRETASTATIN A4 PHOSPHATE

Dawen Zhao, Lan Jiang, Ammar Adam, Eric W. Hahn, Ralph P. Mason
Department of Radiology, UT Southwestern Medical Center at Dallas
primary author's e-mail address: dawen.zhao@utsouthwestern.edu

Hypoxic cells in tumors has long been recognized as a significant factor influencing tumor response to chemo- and radio-therapy. The vascular targeting agent, combretastatin A-4-phosphate (CA4P) causes tumor vascular shutdown and a combination of CA4P with radiotherapy has shown enhanced tumor response. For the potential combination with radiotherapy, measurement of tumor oxygen dynamics will be especially important. Here, we applied a novel magnetic resonance imaging (MRI) approach to measuring regional tumor oxygen tension: FREDOM (Fluorocarbon Relaxometry using Echo planar imaging for Dynamic Oxygen Mapping) with hexafluorobenzene, as a reporter molecule. FREDOM allowed us to quantitatively determine the in situ, in vivo dynamic action of CA4P on real-time tumor oxygenation.

Syngeneic NF13762 rat breast carcinomas were implanted in a skin pedicle on the foreback of Fisher 344 adult female rats. When tumors reached ~ 1 cm diameter (~ 0.6 cm3) MRI was performed using a 4.7 T horizontal bore magnet with a Varian Unity Inova system. A series of pO2 maps acquired at 10, 30, 60, 90, and 120 minutes after i.p. CA4P (30 mg/kg; OXiGENE, Inc. Waltham, MA) showed a significant decrease in pO2 of some tumors as early as 30 min post injection. For all tumors there was a significant drop in tumor pO2 within 90 min after treatment (mean baseline pO2 = 23 torr to 9 torr, $p < 0.05$) and a further decrease was observed at 2 h (mean = 2 torr; $p < 0.01$). Intriguingly, the initial changes in pO2 in central and peripheral regions were parallel, but by 24 h post treatment significant difference was apparent: the pO2 in periphery improved significantly, while center remained hypoxic. In contrast to tumor behavior, there was no significant change in pO2 of thigh muscles of rat at any time point after CA4P. These data are consistent with dynamic contrast enhanced (DCE) MRI, which revealed a ~70% decrease in perfusion/permeability (initial area under signal-intensity curve (IAUC)) at 2 h after 30 mg/kg CA4P ($p < 0.001$). IAUC fully recovered in a thin peripheral region, but not the tumor center 24 h post-treatment. Vascular perfusion marker Hoechst 33342 staining confirmed that the number of perfused vessels decreased significantly at 2 h, and then recovered at 24 h.

These results provide the first insight into regional tumor oxygen dynamics in response to CA4P in a syngeneic rat tumor. While dynamic contrast enhanced MRI will reveal vascular changes, dynamic pO2 measurements are potentially more important for optimizing combinations of VTAs with conventional anti-cancer therapies against breast cancers.